Dynamic model of a gun drive system for a battle tank

This book was bound by
Badminton Press
18 Half Croft, Syston, Leicester, LE7 8LD
Telephone: Leicester (0533) 602918.

DYNAMIC MODEL OF A GUN DRIVE SYSTEM FOR A BATTLE TANK

by

C. W. BARLOW

ABSTRACT

Mathematical models are presented for both the traverse and elevation gun drive systems of a modern main battle tank. The models are based upon the generation of torque, through the gun drive gearboxes, arising from collision engagement of the mating gears, and included a full description of the non-linear effects of both backlash and friction.

Digital simulation studies, based upon the mathematical models, showed that under open-loop conditions, the initial backlash was predominant in controlling the torque generation, the angular velocity and displacement error, at each mesh.

The representation of the gun dynamics as a lumped stiffness and inertia excluded barrel frequencies higher than the fundamental, which resulted in low frequency gun vibrations as a result of its relatively low natural frequency (5 Hz).

The results from the digital simulation of the closed-loop traverse gun drive system showed that backlash was not significant to pointing accuracy,. providing that there was no non-linear friction in the system. The inclusion of the non-linear friction components resulted in a steady-state pointing error of the system. The pointing accuracy of the system decreased with increased Coulomb friction.

DYNAMIC MODEL OF A GUN DRIVE SYSTEM FOR A BATTLE TANK

by

C.W. Barlow , B-Tech.

A Master's Dissertation
Submitted in partial fulfillment of the requirements
for the award of
the degree of M.phil of the Loughborough University of Technology.

June, 1985.

PREFACE

This dissertation is a report of research carried out by the author in the Department of Transport Technology at Loughborough University of Technology, under the direction of RARDE, Chertsey. The dissertation is in the main a report of the independent work of the author: the work of others has been referenced where appropriate.

The author would like to express sincere thanks to his supervisor, Dr. D. Mclean, for his continued guidance and counsel throughout the period of this research.

ABSTRACT

Mathematical models were presented for both the traverse and elevation gun drive systems of a modern main battle tank. The models were based upon the generation of torque, through the gun drive gearboxes, arising from collision engagement of the mating gears, and included a full description of the non-linear effects of both backlash and friction.

Digital simulation studies, based upon the mathematical models, showed that, under open-loop conditions, the initial backlash condition was predominant in controlling the form of torque generation, and the associated angular displacement error, at each mesh.

The representation of the gun dynamics as a lumped stiffness and inertia excluded barrel frequencies higher than the fundamental, which resulted in low frequency gun vibrations as a result of its relatively low natural frequency (5 Hz).

The results from the digital simulation of the closed-loop traverse gun drive system showed that backlash was not significant to pointing accuracy, providing that there was no non-linear friction in the system. The inclusion of the non-linear friction components resulted in a steady-state pointing error of the system. The pointing accuracy of the system decreased with increased Coulomb friction.

CONTENTS

LIST OF FIGURES

NOTATION

All symbols are defined in the text immediately following their use.

CHAPTER 1 INTRODUCTION

The drive system for the gun turret of a modern main battle tank (M.B.T.) usually comprises two independent mechanical systems: azimuth and elevation. The azimuth, often referred to as the traverse system is associated with the rotation of the turret and its main weapon system, and the elevation system is used to establish the vertical angle of the weapon system relative to the turret.

The turret is supported on the hull of the tank by a bearing assembly which permits the turret to rotate relative to the hull. The torque required to drive the turret to a desired azimuth position is provided by an electric drive motor and an associated reduction gearbox. This gearbox is usually located in the turret itself, and it rotates as the turret rotates. The drive to the turret is from a pinion gear meshing with a large ring gear mounted on the hull. Rotation of the pinion establishes relative turret-to-hull azimuth position. The weapon system is usually attached to the turret by a pin-type connection which allows weapon elevation relative to the turret and provides vertical, lateral, and longitudinal support.

The elevation system usually comprises an electric drive motor and reduction gearbox whose output is delivered via a pinion gear which mates with the gun rack gear, thereby providing elevation of the weapon relative to the

hull.

Each of these systems has independent, closed-loop, electronic controls which receive feedback signals from the stabilized gun sight, as well as possibly from rate gyroscopes and accelerometers which may be mounted in the turret and hull. These electronic control systems usually require high system gains and correspondingly complex compensation techniques to meet the extremely stringent bandwidth requirements, while still maintaining adequate stability margins. The optimum design of the controller for the closed-loop drive system for the gun turret requires a detailed knowledge of the open-loop load characteristics because of the possibility of the phenomenom of resonance, as a result of the nature of the mechanical load characteristics, and also because of the existence of non-linear characteristics of the performance of the dynamic system.

The objectives of the research work reported in this dissertation were to produce an accurate mathematical model of both the traverse and the elevation gearboxes for the gun drive system of a modern main battle tank and also to carry out extensive digital simulation studies which would permit validation of the developed models whilst allowing further studies to be made of particular aspects of gearbox design and performance. However, so strongly did the electric drive and mechanical load influence the dynamic characteristics of

the gearbox that it was necessary to include in the research work a detailed study of their effects.

The dynamic environment in which the gearboxes were presumed to operate is shown schematically in Figure 1.1. The general layout of each gearbox is shown in Figure 1.2 for the azimuth system and in Figure 1.3 for the elevation system.

A gear train is often considered to be an ideal component represented by a simple transfer function ,N , which is the gear ratio. Although this assumption is sometimes adequate for certain applications, whenever the gear train is the major component of a servomechanism, such as that in an M.B.T. gun drive system , then a more detailed approach is required with all losses in the gears being taken into account. These factors invalidate the representation of a gearbox as a simple speed and torque converter.

A detailed approach requires accurate modelling of all the gearbox elements in terms of their inertial properties ie. the accelerations, velocities, and displacements, and also must take into account the finite distribution of inertia through the gearbox and the losses due to friction and backlash.

Such an approach has several advantages, and not only for the design of control systems for existing gearboxes. Any generalised model permits the investigation of the

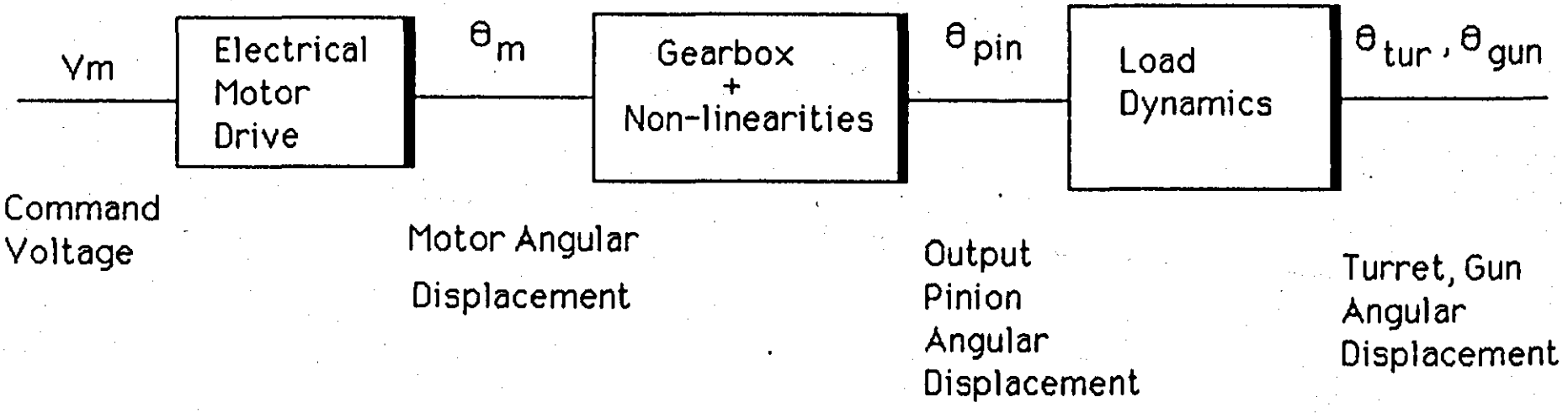

Figure 1.1 : Dynamic Environment of Gearboxes

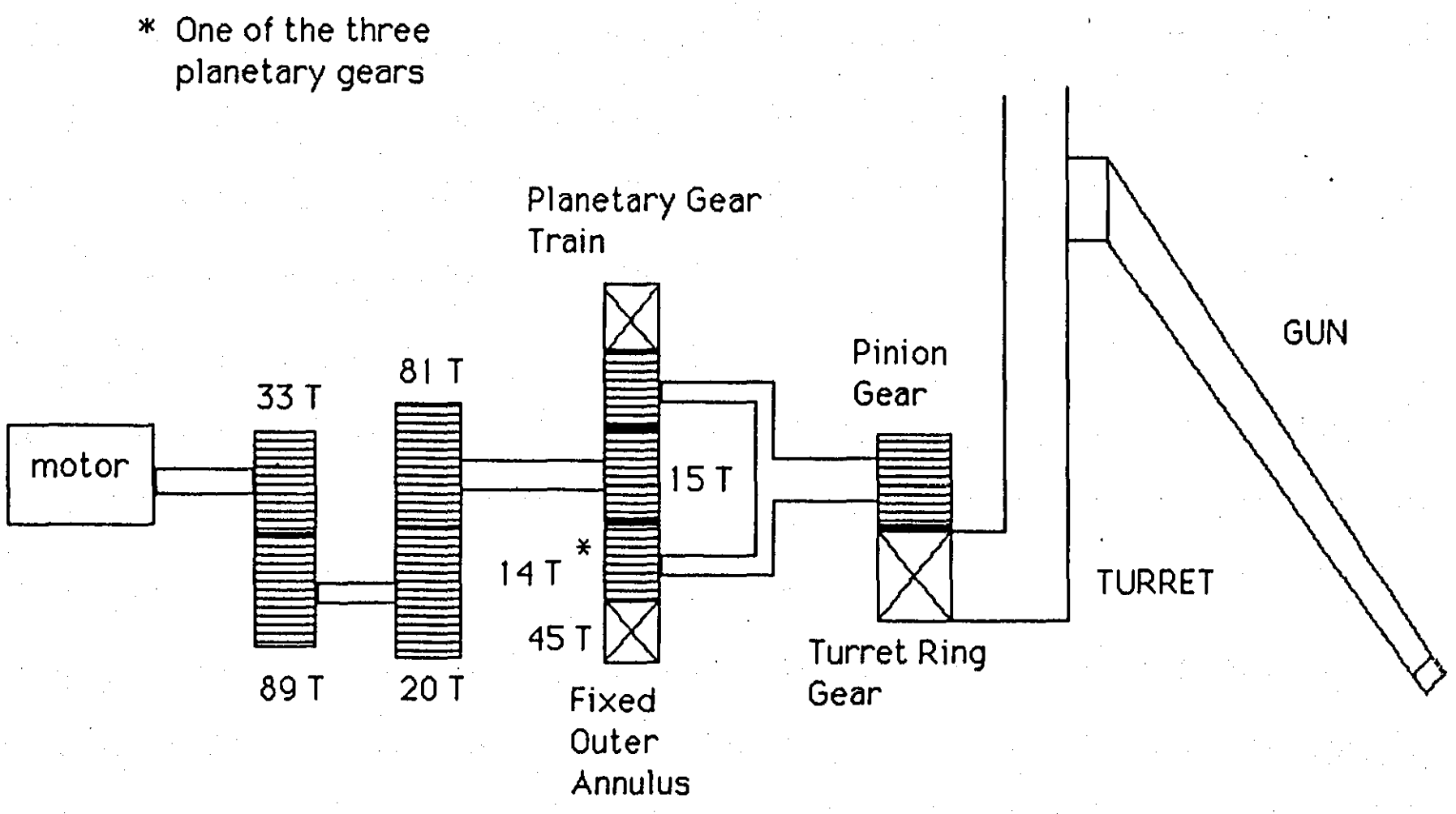

Figure 1.2 : Schematic of Traverse Gun Drive System

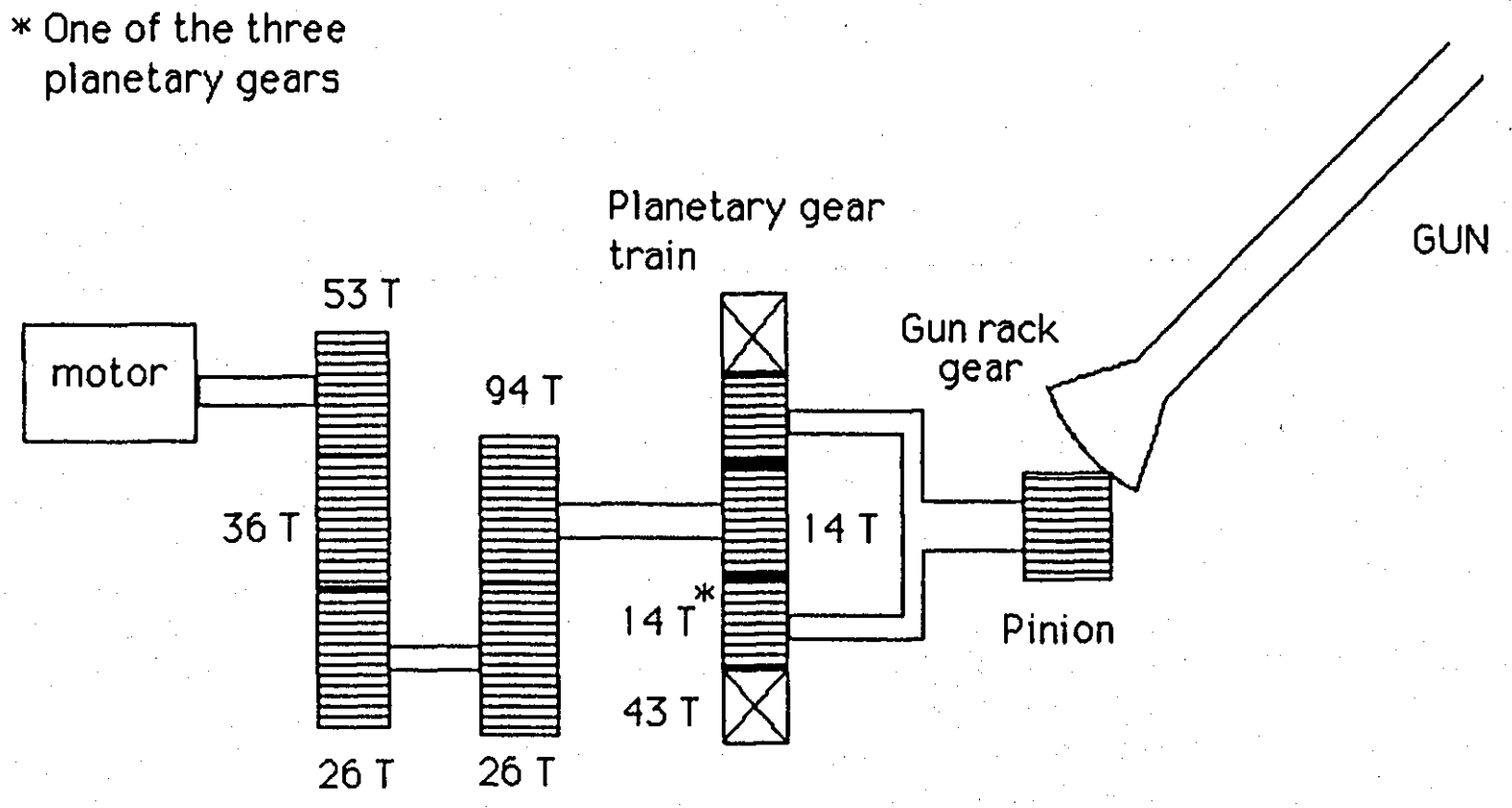

Figure : 1.3 Schematic of elevation gun drive system

performance at any point in the gearbox thereby allowing modifications to be made to suit specific required dynamic performance.

The models presented in this work are based upon the generation of torque at each gear mesh through the collision engagement of the gears. The collision engagement at each mesh is itself a function of both the backlash condition prevailing at each mesh and the associated initial condition. The torque arising from the collision engagement at a gear mesh, through the associated mesh stiffness, results in a displacement of the collision-engaged member. This displacement then forms the input to the next gear mesh.

Backlash, or free play, occurs when two mechanical elements are not rigidly coupled, but are connected through an inactive zone of displacement within which no direct mechanical coupling exists. Care has been taken to accurately model the non-linear effects of backlash at each mesh, as the effect is not only one of lost motion between mating gears, thereby causing instability in some instances, and subsequently deterioration in pointing accuracy of the system, but it also acts as a switching mechanism for torque generation.

The term 'friction' has a number of meanings, but, at its simplest, it may be regarded as a linear (or viscous) term which is a continuous linear function of the velocity.

Such friction is, of course, the easiest to represent in any simulation program and it results in a net loss of torque in the system. However, in many instances, the type of friction occurring is usually a combination of both linear and non-linear phenomena. Two very common discontinuous types of friction, which occur when mechanical surfaces are in direct contact (eg. they are not seperated by a viscous film of lubricant) are Coulomb friction and stiction. When Coulomb friction exists, stiction will exist as well.

The continuous linear friction term is usually added to the constant Coulomb component which results in a combined linear term with its origin on the friction/speed characteristic curve offset by the value of the Coulomb fricton. Care has been taken to model accurately the appropriate friction characteristic at each gear mesh.

In a position control servomechanism, the presence of friction may be desirable for some conditions and undesirable for others. The non-linear components produce a steady-state, or static, error, and are therefore undesirable from the viewpoint of accuracy. However, under certain conditions, linear friction can provide appreciable damping. It can be shown (ref. 1) that all positional servomechanisms with backlash would display continuous oscillations about null, except for the existence of linear friction in the system.

In any event it must be emphasised that friction, in

general, is a very variable effect. Different mechanical elements from the same production batch may exhibit markedly different characteristics, and the same element itself may exhibit markedly different characteristics throughout its life , dependent upon such factors as past wear, its state of lubrication, and its operating temperature, for example. Hence any simulation of a friction effect is neccessarily approximate, based upon 'typical' values.

The stiffnesses of the gears and shafts and the associated inertias were calculated from geometric properties of the gearbox elements. The effects upon the gearbox dynamics of such finite stiffnesses and inertias can be significant. Owing to the nature of the models it is important to distinguish between absolute and referred values. Although the inertias of the individual gears and shafts may be small, their effective inertias are increased by the referral of the inertias of all the other gears and shafts loadside, and, also by the referred inertia of the load itself. Similarly, frictional effects and stiffnesses are also referred parameters. The models have been arranged to recalculate referred values where an absolute value is altered, thus making re-design possible at simulation run-time. The methods of referral of the various parameters are outlined more fully in the appropriate sections of this dissertation.

Although backlash has been carefully modelled, the effects of referred parameters when a gear becomes unmeshed have not been included in the models because of the gross non-linearities which resulted and their effect on the stability of the integration method. Thus, referred values are constant for a given simulation run. A detailed discussion of this point is presented in Appendix 1.

The models have been arranged so that the system dynamics can be set up under the complete control of the user to reflect any required initial state and includes options to remove any, or all, of the non-linearities thereby allowing their effects upon system performance to be studied.

The gearboxes are used to drive representative load dynamics, namely turret and gun for the traverse system, and gun alone for the elevation system, with the inclusion of the appropriate out-of-balance forces. The description of the load properties must be considered to be the least satisfactory component of these models for it is based only upon informed estimates and does not represent particular turrets or particular guns, since such classified information was not available to the author. In particular, the representation of the gun as a lumped inertia and stiffness results in the exclusion of barrel frequencies higher than the fundamental, although the modes associated with these higher frequencies may be significant in terms of achieved pointing accuracy.

No effects of external inputs from vehicle motions were studied although these too may be significant for system performance.

Chapters 2 and 3 of this dissertation are devoted to the necessary geometric relationships required by the models for the calculation of component inertias and stiffnesses. A detailed presentation of friction, together with the appropriate mathematical representation of the non-linear friction characteristics throughout the gun drive systems, is given in Chapter 4. The torque/speed characteristic of a simple drive motor is detailed in Chapter 5, as the output from such a model forms the forcing input to each gearbox model. Although the same motor model has been used for both systems, the dynamic characteristics of the motor will be different in each case due to the differing distribution of inertia and friction effects and the difference in gear ratios for each system. Backlash, and the associated mathematical representation of torque generation following collision engagement of the gears, is presented in Chapter 6. The modelling of a planetary gear train is detailed in Chapter 7, with the transformations necessary for its representation as a single effective mesh.

The digital simulation, presented in chapter 8, is based on ACSL, Advanced Continuous Simulation Language. This digital simulation language is interactive and allows variables, simulation conditions, outputs, graphical plots

etc. to be changed at any time during a run. It provides for the selection of any of four integration algorithms, which are fixed-step, first-order and second-order Runge Kutta, and a variable step Euler routine and a 'stiff' variable step algorithm developed by W. Gear (ref.2). Control of the integration parameters can be handled from within the simulation program or reset at run time. Thus, for example, step length or communication interval can be adjusted at run time to suit the particular dynamics of the system under consideration. In the work presented here the most satisfactory results were obtained using the 'stiff' algorithm (developed by Gear) which is outlined more fully in Appendix 1. Some results are presented to illustrate the nature of problems encountered when attempting to use the fixed-step Runge Kutta, second-order algorithm. These problems arose due to the 'stiff' nature of the modelling equations. 'Stiff' differential equations frequently arise from physical problems in which there exist greatly differing local time constants. This condition implies that the solution will contain 'fast' and 'slow' components in decay. The short time-constant components then control the stability of the integration method even though they may have decayed to insignificant levels, so that the truncation or rounding error is determined by the components with the longer time-constants. If flexibility effects of the gun dynamics or the effects of gear meshing on referred

parameters, for example, were to be included, then the choice of Gear's method is strongly recommended.

The dissertation is completed with results showing the responses of both azimuth and elevation systems to step inputs of motor torque for a range of initial conditions. Although the objectives of the work presented here were concerned with the modelling of the open-loop gun drive systems, it became apparent in the course of the research work that, apart from small torque inputs, the effects of non-linear friction on performance only became appreciable under closed-loop conditions. Therefore, simple control laws were developed to examine system performance under closed-loop conditions. It is not intended that these control laws should be considered as 'optimum' for the systems, but were developed merely as a means for illustrating the effects and inter-relationship of the non-linearities on system performance.

CHAPTER 2 GEAR AND SHAFT INERTIAS

The determination of system inertia is of major importance for design and analysis as it directly affects the damping, stability, and response of the system. Although the inertia of the individual gears and shafts may be small, their effective value, when summed and reflected, can be significant.

A great majority of servo rotating components are by nature symmetrical about the axis of rotation and lend themselves to easy calculation. In fact the inertia of most of these can be calculated by subdividing each component into hollow right circular cylinders. The various cylinder inertias are then summed to provide the total inertia for the component. The general equation for calculating the inertia of a hollow right circular cylinder in terms of diameters is:

$$I = \frac{M}{8}(D^2 + d^2) \qquad \text{.....(1)}$$

where D is the outside diameter (m),

d is the inside diameter (m),

and M is the mass of cylinder (Kg).

The mass of the cylinder is defined by the equation:

$$M = \frac{\pi \rho h}{4g}(D^2 - d^2) \qquad \text{.....(2)}$$

where ρ is the density of the material (Kg/m^3) ,

h is the height of cylinder (m) ,

and g is the acceleration of gravity (m/s^2).

The various cylinder inertias are then summed to provide the total inertia for the component.

The inertias of the shafts may also be determined in a similar manner, however, since in this case d is zero Eq.(1) reduces to:

$$I = \frac{MD^2}{8} \qquad \text{.....(3)}$$

The distribution of inertias through the traverse and elevation gun drive systems are shown in Figure 2.1 and Figure 2.2 respectively. The variables used in these figures refer to the digital simulation presented in Chapter 8. Since it is the torque developed at each mesh that will accelerate the inertia, the inertia is assumed to act on the output member of each gear mesh. Thus, all the n inertias on a common shaft are added to form the inertia of the output member, which is given by:

$$I = \sum_{c=0}^{n} I_c \qquad \text{.....(4)}$$

where I_c is a component inertia on the same shaft as the output member.

In addition, the output member has all output member inertias loadside referred onto it through the appropriate gear ratio. The total effective inertia on the output member of the i^{th} gear mesh is then given by:

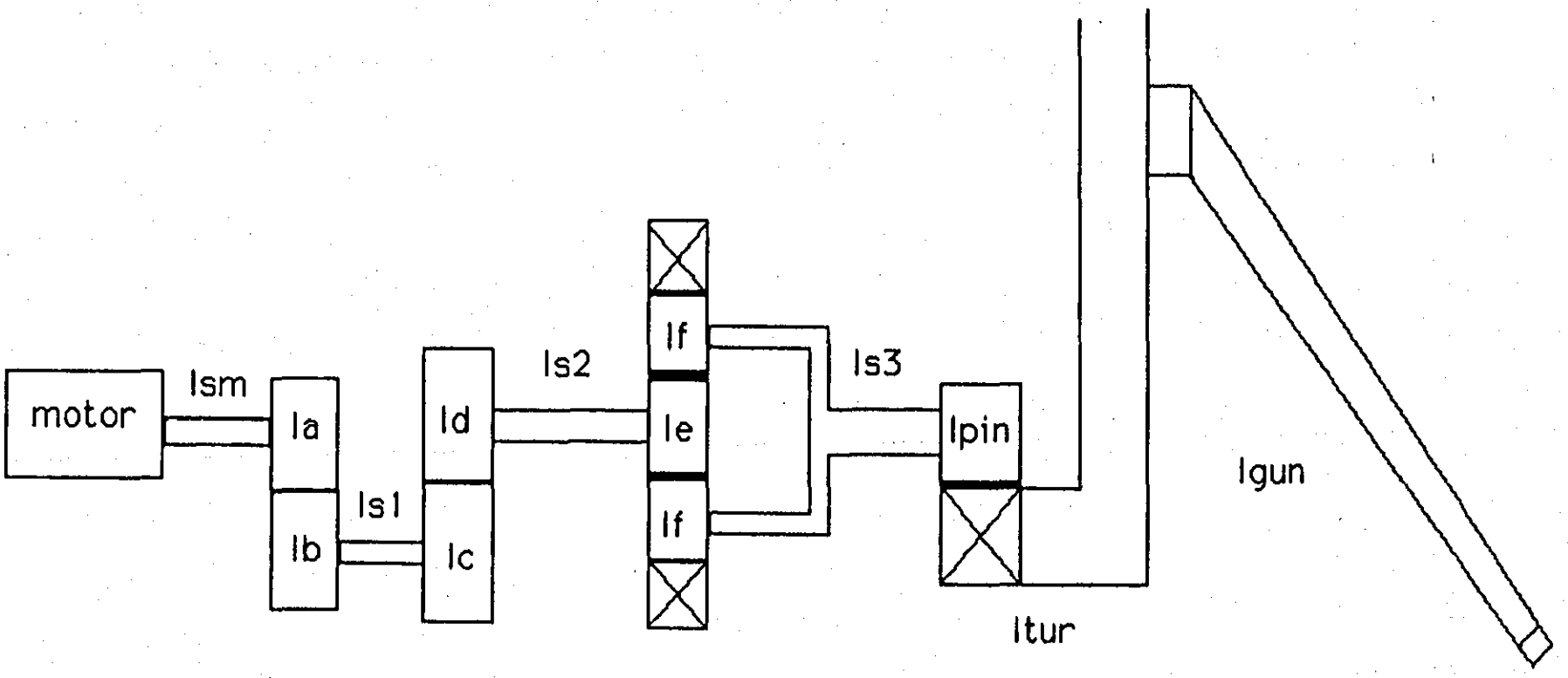

Figure 2.1 : Distribution of inertia through traverse system

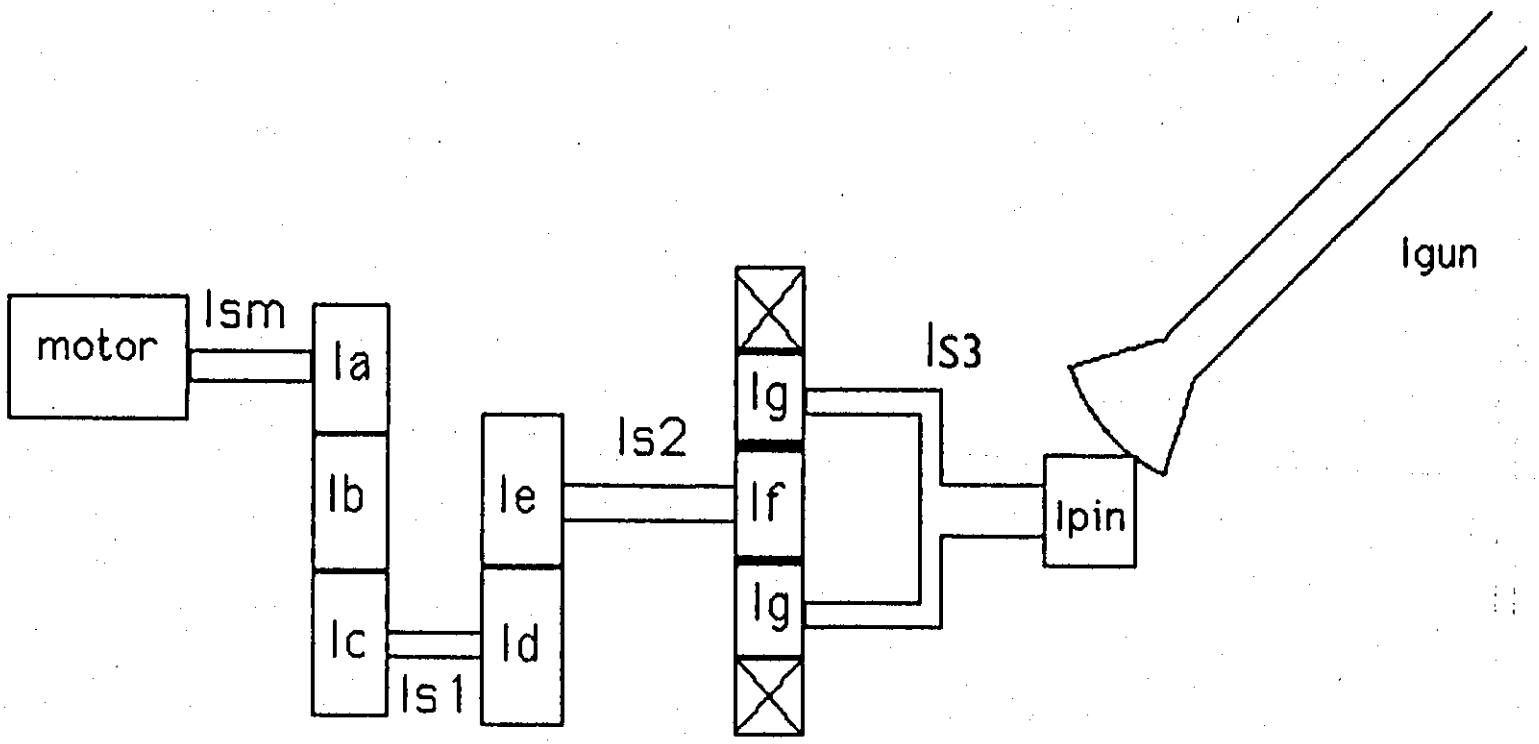

Figure 2.2 : Distribution of inertia through elevation system

$$I_i = \Sigma I_{ci} + \Sigma I_{cj} . N_j^2 \quad \text{.....(5)}$$

where I_{cj} is a component inertia on a common shaft with the output member j loadside of i ,

and N_j is the gear ratio from the output member i to the output member j.

Usually a component is mounted so that its axis of rotation is through the centre of gravity. If this is the case then the above equations yield the correct inertia directly. If this is not the case, as when referring inertias back through the gear train, the inertia about the desired axis of rotation can be determined by using the parallel axis theorem. The inertia of the component about the desired parallel axis may then be calculated as:

$$I = I_{cg} + \tfrac{1}{2} Md^2 \quad \text{.....(6)}$$

where I is the inertia about the desired axis

I_{cg} is the inertia through the centre of gravity parallel to the axis desired ,

and d is the distance between the two parallel axes.

The absolute inertias in the gear train are calculated from eq.(1) and eq.(3) for gears and shafts respectively. The referred inertias loadside are then added to give the total effective inertia on the output member of the gear mesh. If the parallel distance between shafts is significant, then the parallel axis theorem must be used

prior to reffering an inertia through the appropriate gear ratio.

The values of absolute and the corresponding referred inertias used for the traverse system were:

Element	Absolute Inertia (Kgm^2)	Referred Inertia (Kgm^2)
Motor shaft	0.005	0.0797
First gear	0.000197	
Second gear	0.00488	0.5417
Shaft 1	0.00001	
Third gear	0.00006	
Fourth gear	0.0077	8.8037
Shaft 2	0.000345	
Fifth gear	0.000199	
Sixth gear	0.000148	152.699
Shaft 3	0.00596	
Pinion gear	0.01074	
Turret	43000	51051.89
Gun	8051.89	8051.89

TABLE 2.1

Note that the fifth and sixth gears are the equivalent gears representing the planetary gear system. The

representation of the planetary gear system as a single equivalent mesh is shown in Chapter 7.

The values of absolute and the corresponding referred inertias used for the elevation system were:

Element	Absolute Inertia (Kgm^2)	Referred Inertia (Kgm^2)
Motor shaft	0.005	0.25166
First gear	0.0012	
Second gear	0.0002	0.11316
Third gear	0.0004	0.05889
Shaft 1	0.000312	
Fourth gear	0.00024	
Fifth gear	0.00085	0.76881
Shaft 2	0.00025	
Sixth gear	0.00067	
Seventh gear	0.00055	12.2229
Shaft 3	0.0026	
Pinion gear	0.00023	
Gun	5913.52	5913.52

TABLE 2.2

The planetary gears are represented in the elevation system by the equivalent mesh between gear 6 and gear 7.

It is only important to calculate the effective inertia on each collision-engaged member as it is the effective inertia of this member that the torque developed at each mesh will accelerate.

The increase in effective inertia at each mesh is due mainly to the referred load inertia, although ignoring the gear and shaft inertias themselves, particularly at the motor end of the gearbox, may result in significant errors. For example, the referred load inertia accounts for 92.5% of the total effective inertia on the motor shaft in the traverse system and 96.3% of the total effective inertia on the motor shaft in the elevation system. The ratio of referred load inertia to the total effective inertia is likely to increase loadwards through the system, dependent on the gear ratios.

However insignificant the gear and shaft inertias may appear to be, their inclusion does allow a realistic design appraisal at simulation run-time.

CHAPTER 3 DETERMINATION OF GEAR AND SHAFT STIFFNESSES

The torque at each mesh is generated through the stiffness associated with a pair of meshing gears. An analytical description of stiffness provides insight into the factors that should be considered to ensure that maximum stiffness is obtained. For a pair of meshing spur gears the deflection, δ, of the gear teeth, assuming one tooth contact at the tooth centre, is given by:

$$\delta = \frac{P(E_a Z_a + E_b Z_b)}{F E_a Z_a E_b Z_b} \quad .....(7)$$

Where Z_a and Z_b are the elasticity deformation factors for the mating gear teeth ,

E_a and E_b are the the material moduli of elasticity for the mating gears ,

and P and F are the applied tangential load and the gear face width respectively.

The elasticity deformation factors for each gear are given by:

$$Z = \frac{Y}{(0{\cdot}242 + 7{\cdot}25Y)} \quad .....(8)$$

where Y is the Lewis form factor, a function of the circular pitch, number of teeth, pressure angle, and tooth profile.

The Lewis form factor for a conventional 20 degree pressure angle, full depth gear is shown in Table 3.1.

No. of teeth	Form factor	No. of teeth	Form factor
10	0.064	26	0.110
11	0.072	28	0.112
12	0.078	30	0.114
13	0.083	34	0.118
14	0.088	38	0.122
15	0.092	43	0.126
16	0.094	50	0.130
17	0.096	60	0.134
18	0.098	75	0.138
19	0.100	100	0.142
20	0.102	150	0.146
24	0.107	300	0.150

TABLE 3.1 LEWIS FORM FACTOR

The stiffness of the gear mesh, represented by a torsional spring of stiffness, K, may be obtained from eq.(7). Thus,

$$K = \frac{T}{\theta} = \frac{4D_2^2 F E_a Z_a E_b Z_b}{E_a Z_a + E_b Z_b} \qquad .....(9)$$

When the gears are made of identical material eq.(9) reduces to:

$$K = \frac{4D_2^2 F E Z_a Z_b}{Z_a + Z_b} \qquad .....(10)$$

where D_2 is the pitch diameter of the collision engaged gear.

The gear mesh stiffness computed by the preceding equation is based on one tooth contact. Some texts multiply this result by the tooth contact ratio to arrive at a more 'accurate' stiffness value. However, Chubb (Ref.1) suggests that even the unfactored stiffnesses are often higher than those experienced for actual hardware.

The stiffnesses of the various shafts in the gearbox assemblies were calculated according to the following equation:

$$K_s = G_s D^4 \frac{\pi}{32L} \qquad .....(11)$$

where D is the shaft diameter ,

L is the shaft length ,

and G_s is the shear modulus of elasticity of the shaft material.

The stiffness at any point in the gear train is the sum of the absolute stiffness, as calculated above, and the referred stiffnesses, loadside, such that the effective stiffness at any point, i,is given by:

$$K_i = K + \Sigma K_j . N_{ij}^2 \qquad \text{.....(12)}$$

where K is the absolute stiffness at the point i ,

K_j is a stiffness at a point j, loadside of i ,

and N_{ij} is the gear ratio from the point i to the point j.

The angular displacement error due to the finite stiffness of the shaft may be obtained by dividing the torque applied to the shaft by the effective shaft stiffness. If the angular displacement of the output member of the i^{th} gear mesh is given by θ_i , then, the input angle to the succeeding $(i+1)^{th}$ mesh is given by:

$$\theta_{i+1} = \theta_i - \frac{T_i}{K_s} \qquad \text{.....(13)}$$

The effect of shaft stiffness is an extra term, $\frac{T_i}{K_s}$, controlling the angular input into the subsequent gear mesh.

The distribution of stiffness through the traverse system is shown in Figure 3.1, and in Figure 3.2 for the elevation system. The variables shown in these figures refer to the digital simulation presented in Chapter 8.

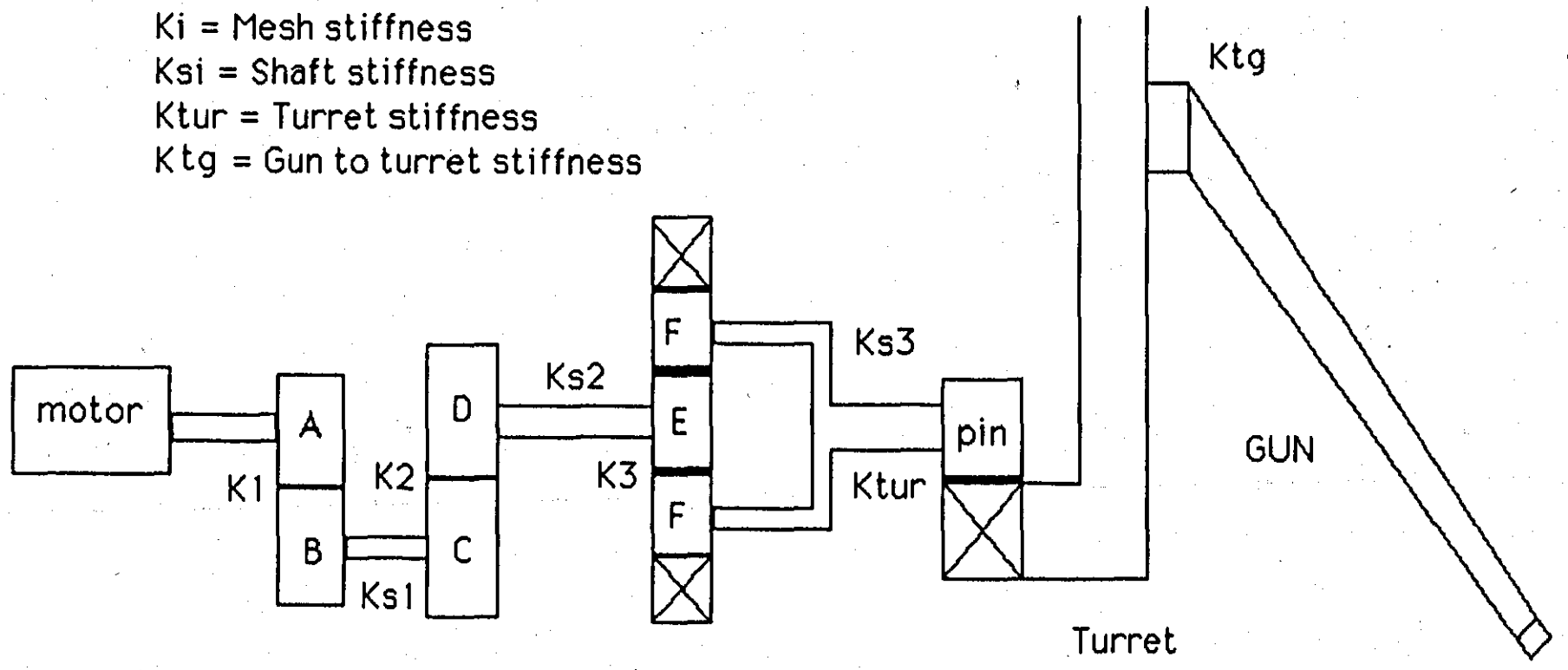

Figure 3.1 : Distribution of stiffness through traverse system

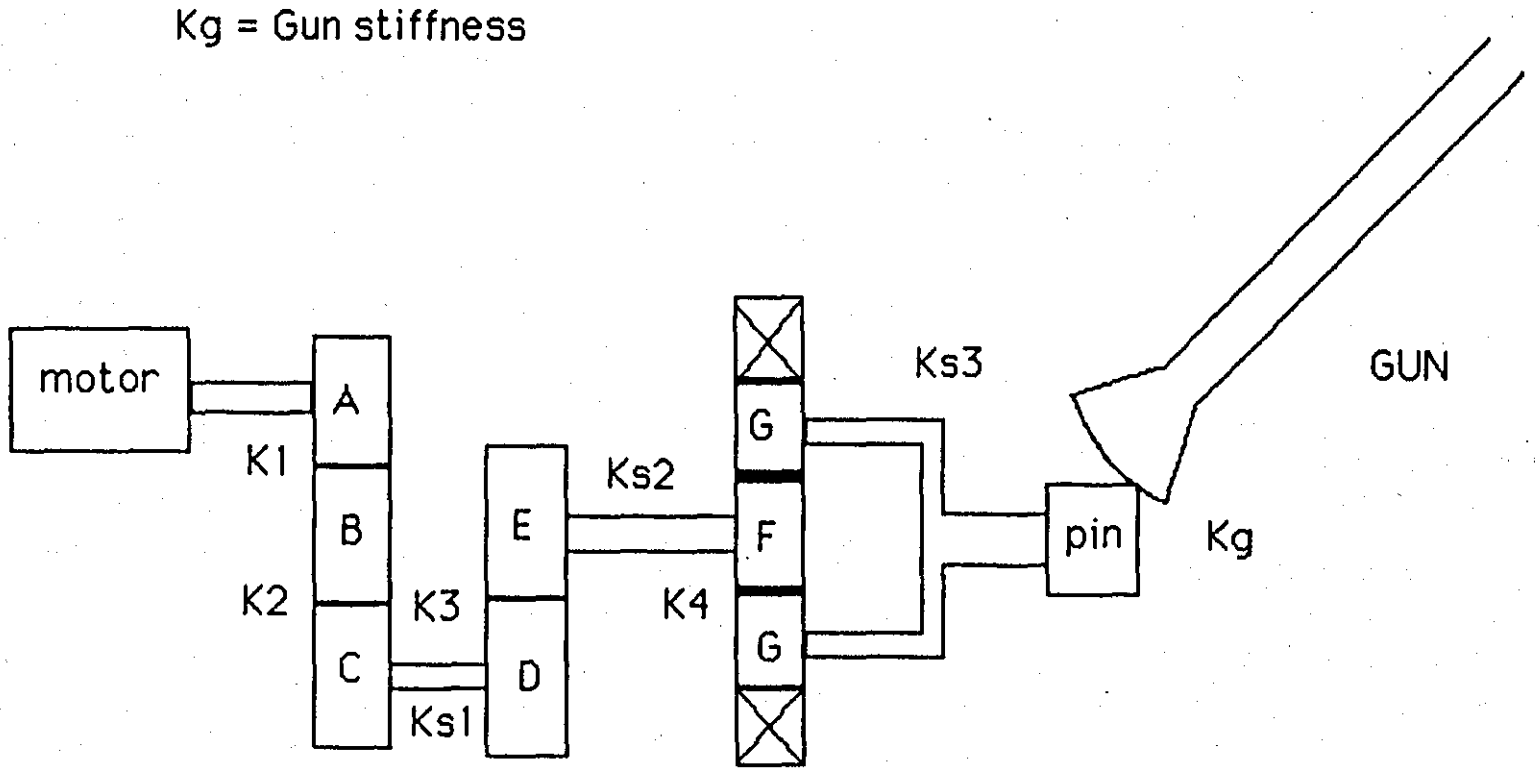

Figure 3.2 : Distribution of stiffness through elevation system

The absolute and referred values of stiffness for the traverse and elevation systems are detailed below:

Element	Absolute Stiffness (Nm/rad)	Referred Stiffness (Nm/rad)
(1) Traverse;		
Motor shaft	∞	∞
1st mesh	$1.697*10^{7}$	$1.631*10^{8}$
Shaft 1	$1.135*10^{8}$	$1.460*10^{8}$
2nd mesh	$1.972*10^{7}$	$5.348*10^{8}$
Shaft 2	$1.116*10^{8}$	$5.151*10^{8}$
3rd mesh	$1.014*10^{8}$	$7.005*10^{9}$
Shaft 3	$6.994*10^{9}$	$6.994*10^{9}$
4th mesh	$2.890*10^{8}$	$2.982*10^{9}$
5th mesh	$9.220*10^{6}$	$9.220*10^{6}$
(2) Elevation;		
Motor shaft	∞	∞
1st mesh	$3.119*10^{6}$	$9.282*10^{6}$
2nd mesh	$1.601*10^{6}$	$3.212*10^{6}$
Shaft 1	$6.352*10^{5}$	$1.612*10^{6}$
3rd mesh	$2.104*10^{6}$	$2.112*10^{7}$
Shaft 2	$7.215*10^{6}$	$8.234*10^{6}$
4th mesh	$1.302*10^{6}$	$1.318*10^{6}$
Shaft 3	$2.553*10^{5}$	$1.545*10^{6}$
5th mesh	$7.480*10^{6}$	$7.480*10^{6}$

The motor shaft was assumed to have been infinitely stiff, both in the traverse system and in the elevation system.

The distribution of stiffness, unlike that of inertia, is not dominated by any one element, and it is therefore important that all the finite stiffnesses in the system should be taken into account. In general, the load end of the gearbox will have higher stiffness values than the motor end, due to the effective increase in torque through the system. However, this effect may not be relised as stiffness is a function of the individual component geometry, which is itself a function of the overall system requirements for torque and speed conversion. Thus, the local stiffness values obtained will not only be a function of the loading of the individual component, but will also be a function of gearbox geometry.

However, even when the gear and shaft stiffnesses are based upon the appropriate static load analysis of the individual members, the dynamic effects that such finite stiffnesses have on system performance are ignored. The inclusion of the finite inertias and stiffnesses in the mathematical models, and subsequently in the digital simulation, therefore allows these effects to be studied, and allows for the re-design of any gearbox element to be made to suit the required dynamic performance.

CHAPTER 4 FRICTION EFFECTS

The friction levels associated with typical gear trains and load components vary considerably with component life and usage for 'identical' production line units. This variation is a function of temperature and possibly a function of angular position. If the mathematical models required for the gearboxes were to be used for such 'life' studies, then appropriate methods of statistical analysis and simulation would be required. It is adequate for this research simply to use typical values to investigate the effects on system performance.

Friction can be divided into the following distinct components:

(1) Stiction;

(2) Coulomb friction;

(3) Viscous friction;

Stiction and Coulomb friction are two very common forms occurring discontinuously whenever mechanical surfaces are in direct contact, eg. when they are not separated by a viscous film, eg. lubricant. Viscous friction is essentially linear and occurs in mechanical elements by virtue of the relative angular motion. Windage effects in the motor and bearing friction are frequently taken as being viscous friction terms.

When the velocity is zero, only stiction applies. The

application of any torque to the member involved will result in the development of a stiction torque of magnitude exactly equal, but of opposing direction, so that the angular velocity remains at zero. When the applied torque reaches a particular value, the stiction limit, then the opposing stiction torque disappears suddenly. This corresponds to 'breakaway', and an immediate acceleration of the member results. Once motion does occur, following breakaway, the Coulomb, or sliding-friction, effect will apply, together with any viscous components.

Kochenburger (Ref.3) recommended that the function shown in Figure 4.1 be used to represent the stiction effect. This representation is adequate for some simulation problems. However, its major disadvantage is that it permits the existance of a small, but finite, velocity when stiction is in being. A typical friction characteristic for a gear train servomechanism is shown in Figure 4.2. From this figure a continuous relationship between friction and velocity can be established for all non-zero velocities. However, such a characteristic is usually obtained under motor acceleration. A different characteristic usually obtains when the motor is decelerating. Therefore, the disadvantage with this characteristic, as with Kochenburger's model, is that upon deceleration the stiction effect is again encountered. Such an occurrence contradicts the definition of stiction in that the stiction effect does

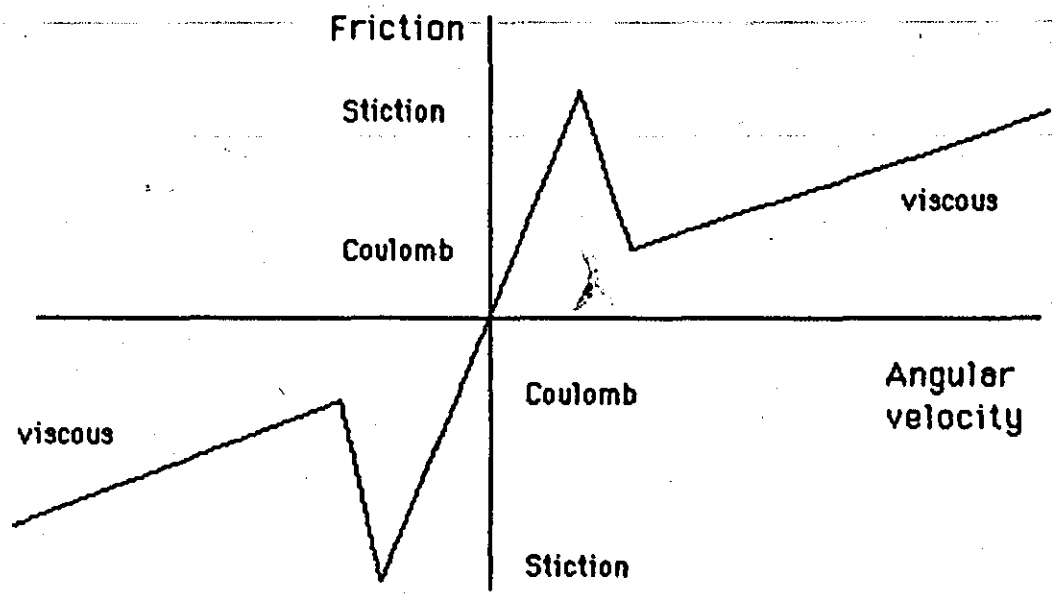

Figure 4.1 : Kochenburger's suggested friction characteristic

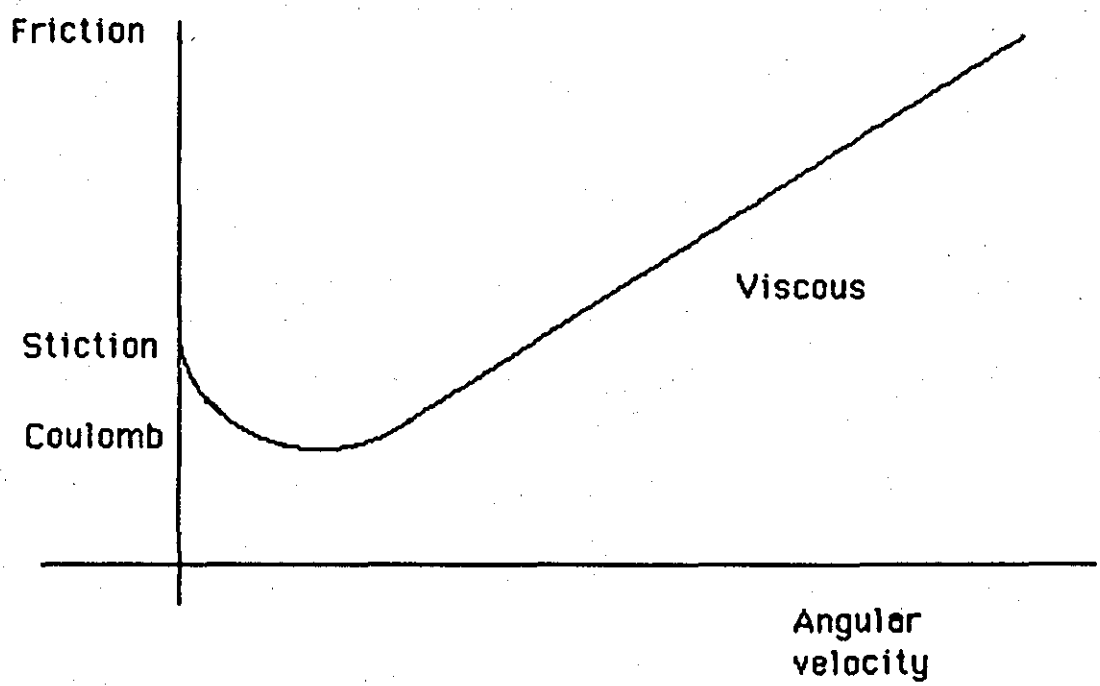

Figure 4.2 : Typical gear train friction characteristic obtained under motor acceleration.

not again become effective until the velocity reaches zero.

The friction model developed for the motor is shown in Figure 4.3. This characteristic is split into four distinct regions relating to the velocities at the stiction boundaries, $-w_s$, $+w_s$. Each of the regions is unique in its combination of acceleration and velocity as may be inferred from Figure 4.3. Thus the governing mathematical equations can be readily established. The underlying assumption is that upon deceleration Coulomb friction is encountered at velocities within the stiction boundary, and stiction does not become effective until zero velocity is reached. Note how this model obeys the definition of stiction.

The function shown in Figure 4.3 was achieved by assigning several logic conditions to friction, depending upon the relative signs of motor speed and acceleration and also upon the value of motor speed, ie.

for $-w_s < w_m < +w_s$;

$$F_m = F_s \,.Sgn(w_m) - K.w_m \qquad \text{when } \alpha_m.w_m > 0 \quad ....(14)$$

$$F_m = F_c \,.Sgn(w_m) \qquad \text{when } \alpha_m.w_m < 0 \quad ....(15)$$

where Sgn(i) is defined as:

$$Sgn(i) = \begin{cases} +1 & \text{for } i > 0 \\ 0 & \text{for } i = 0 \\ -1 & \text{for } i < 0 \end{cases} \qquad .....(16)$$

α_m is the motor angular acceleration

and w_m is the motor angular velocity

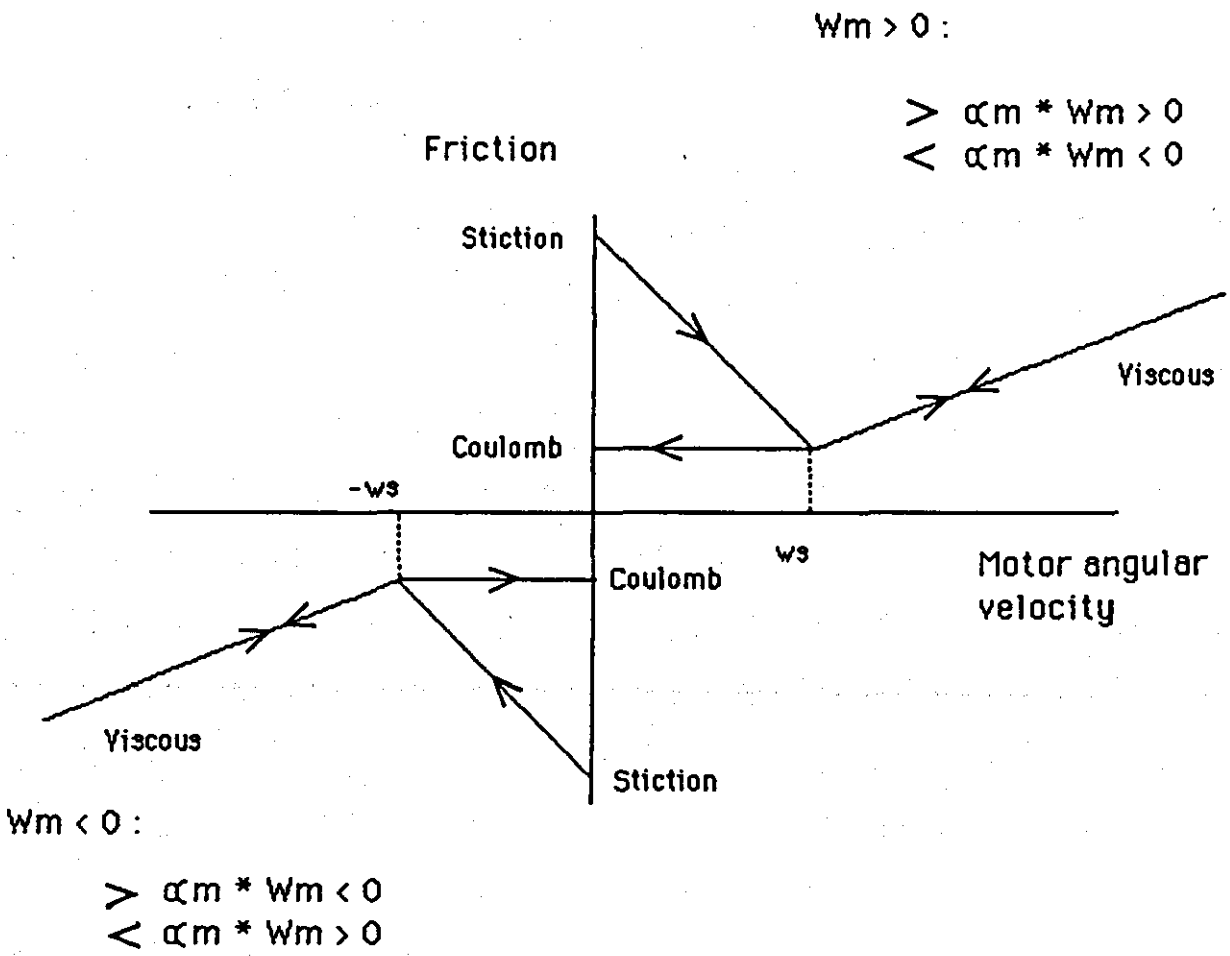

Figure 4.3 : Developed motor friction characteristic

K is given by:

$$K = \frac{(F_s - F_c)}{w_s} \qquad \text{.....(17)}$$

for $-w_s \geqslant w_m \geqslant +w_s$;

$$F_m = [F_v . (w_m - w_s) + F_c] . Sgn(w_m) \qquad \text{....(18)}$$

for $w_m = 0$;

$F_m = F_s . Sgn(\alpha_m)$ when $T_m > F_m$ ....(19)

$F_m = T_m$ when $T_m \leqslant F_m$ ....(20)

where F_m is the total friction at the motor shaft

F_s is the referred stiction at the motor shaft

F_c is the referred Coulomb friction at the motor shaft

F_v is the referred viscous friction at the motor shaft

To avoid an implicit structure arising in the simulation, the accelerating torque, $T_m - F_m$, was used to assign conditions upon acceleration for it has identical sign. T_m represents the torque delivered by the drive motor.

Viscous friction is a velocity-dependent term and is therefore referred as the gear ratio squared, such that the total linear viscous friction on the motor shaft is given by:

$$F_v = F_{m_v} + \Sigma F_{jv} . N_j^2 \qquad \text{.....(21)}$$

where F_{m_v} is the linear friction coefficient of the motor shaft,

F_{jv} is the linear friction coefficient of a point j loadside ,

and N_j is the gear ratio from the motor shaft to the point j.

Both stiction and Coulomb friction are torques and are therefore referred as the gear ratio:

$$F_s = F_{m_s} + \Sigma F_{js} . N_j \quad \text{.....(22)}$$

$$F_c = F_{m_c} + \Sigma F_{jc} . N_j \quad \text{.....(23)}$$

where F_{m_s} , F_{m_c} are the stiction and Coulomb friction components of the motor shaft ,

F_{js} , F_{jc} are the stiction and Coulomb friction components of a point j loadside,

and N_j is the gear ratio from the motor shaft to the point j.

Owing to the manner in which torque was generated at each gear mesh, it was found to be impossible to achieve the same friction characteristic as that being used at the motor. The friction function used throughout the gearbox, and at the load, is shown in Figure 4.4. The logic is identical to that used at the motor, with the motor accelerating torque being used to define correctly the sign of stiction.

The characteristic, for the i^{th} gear mesh is defined as:

$$F_i = F_{i_s} . Sgn(\alpha_m) \quad \text{when } w_i = 0 \quad \text{.....(24)}$$

$$F_i = F_{i_v} . w_i + F_{i_c} \quad \text{when } w_i \neq 0 \quad \text{.....(25)}$$

where F_i is the total friction acting on the output member

F_{i_s} is the referred stiction at the output member

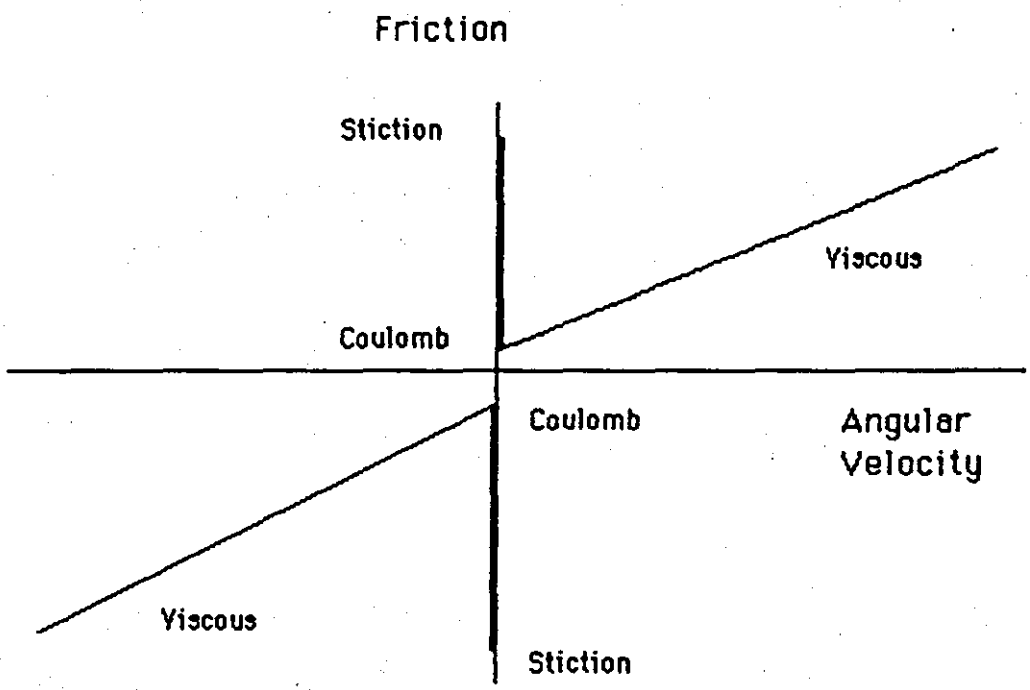

Figure 4.4 : Developed friction characteristic for gear meshes and load.

F_{i_c} is the referred Coulomb friction at the output member ,

F_{i_v} is the referred linear friction at the output member ,

and w_i is the velocity of the output member.

The referred friction at the output member is given by:

$$F_{i_s} = F_s + \Sigma F_{j_s} \cdot N_{ij} \quad \text{.....(26)}$$

$$F_{i_c} = F_c + \Sigma F_{j_c} \cdot N_{ij} \quad \text{.....(27)}$$

$$F_{i_v} = F_v + \Sigma F_{j_v} \cdot N_{ij}^2 \quad \text{.....(28)}$$

where F_s , F_c , F_v are now the absolute friction components at the mesh

and N_{ij} is the gear ratio from the output member to the point j.

Figures 4.5 and 4.6 show the distribution of friction through the traverse and elevation systems respectively. The variables shown in these figures refer to the digital simulation presented in Chapter 8. Thus, at the i^{th} mesh, the absolute values of stiction, Coulomb friction, and viscous friction coefficient are denoted by F_{s_i} , F_{c_i} , and F_{v_i} respectively.

The absolute values of friction torque for stiction and Coulomb friction, together with the corresponding value of the viscous friction coefficient, used in this study are as follows for the traverse system:

Fs = Stiction component
Fc = Coulomb component
Fv = Viscous friction coefficient

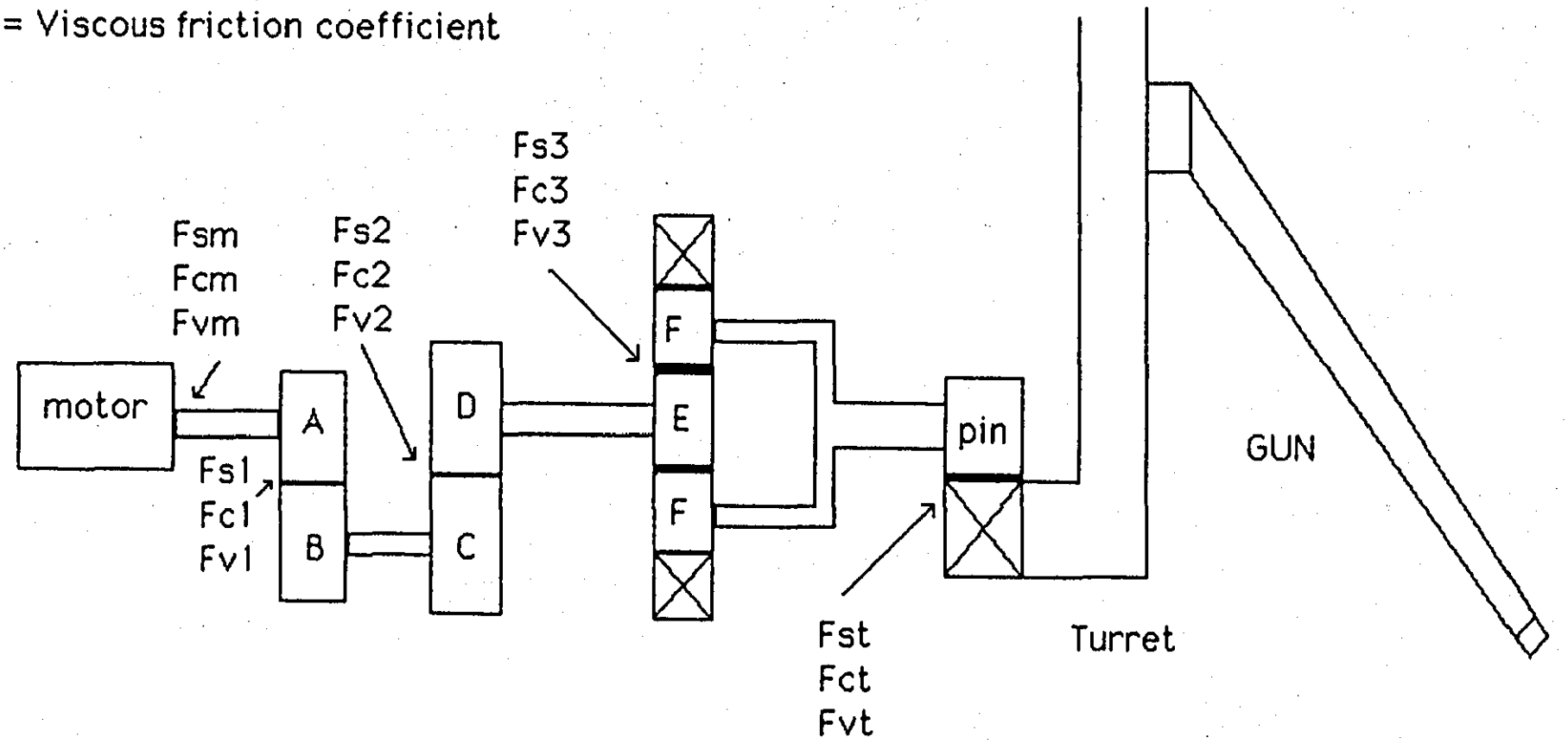

Figure 4.5 : Distribution of friction through traverse system

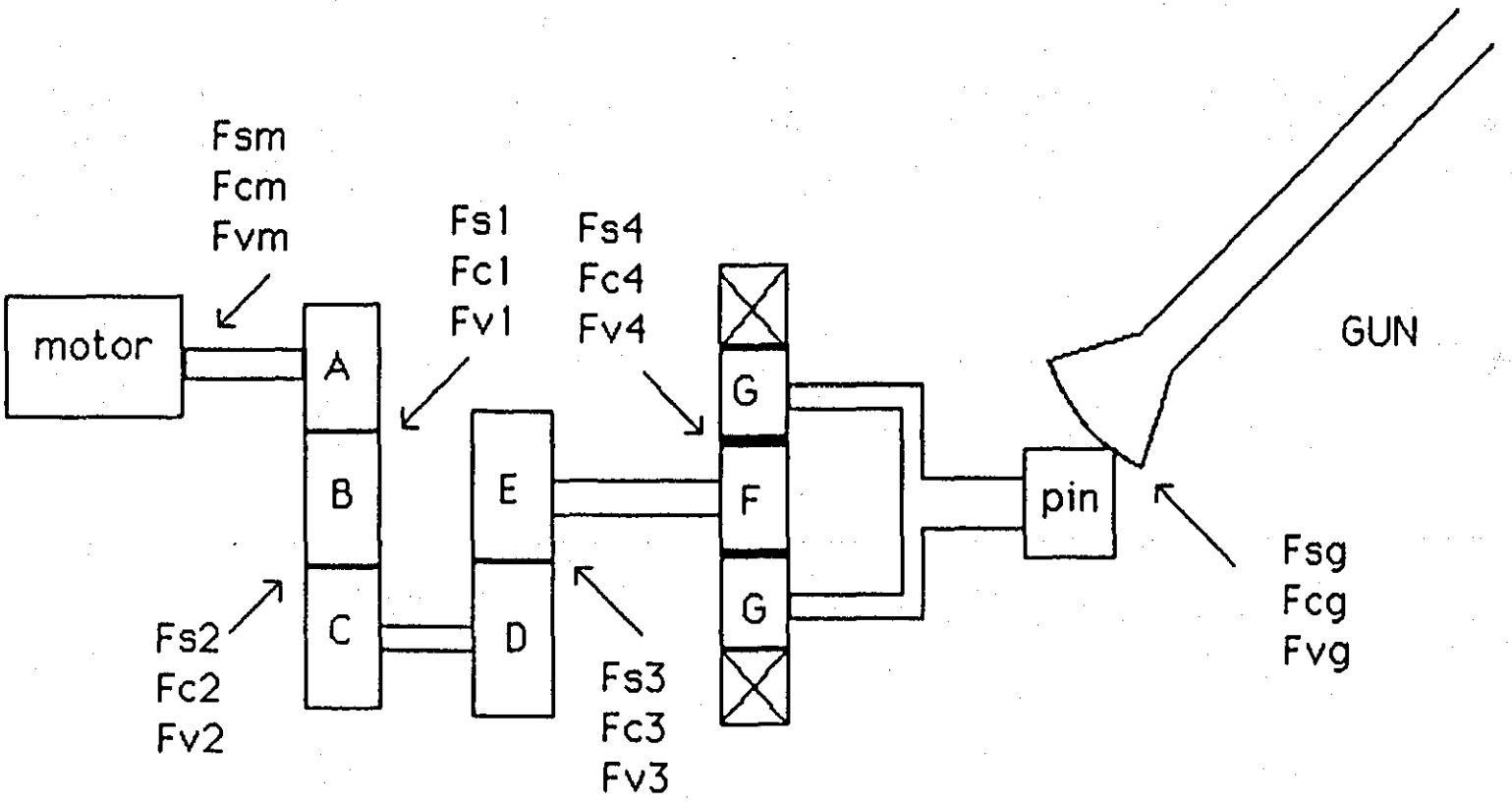

Figure 4.6 : Distribution of friction through elevation system

1. Motor shaft;

Stiction = 0.46 (Nm) (29)

Coulomb = 0.26 (Nm) (30)

Viscous = 0.046 (Nm-s) (31)

2. First mesh;

Stiction = 0.419 (Nm) (32)

Coulomb = 0.245 (Nm) (33)

Viscous = 0.573 (Nm-s) (34)

3. Second mesh;

Stiction = 0.419 (Nm) (35)

Coulomb = 0.245 (Nm) (36)

Viscous = 0.573 (Nm-s) (37)

4. Third mesh;

Stiction = 0.532 (Nm) (38)

Coulomb = 0.311 (Nm) (39)

Viscous = 0.614 (Nm-s) (40)

5.Fourth mesh;

Stiction = 1520 (Nm) (41)

Coulomb = 1410 (Nm) (42)

Viscous = 1300 (Nm-s) (43)

6. Fifth mesh;

Stiction = 0.00 (Nm) (44)

Coulomb = 0.00 (Nm) (45)

Viscous = 0.00 (Nm-s) (46)

Note that the fourth mesh is between the gearbox

output pinion and the turret ring and consequently the friction values are those of the load. The fifth mesh is the gun/turret interface which has been modelled as a conventional mesh as the turret engages the gun through the deadspace between them. In this case the gear ratio is unity. It has been assumed that there is no friction at the gun/turret interface as they are directly coupled once engaged through the deadspace.

The referred values for the traverse system are calculated from above as follows:

1. Motor shaft;

Stiction = 2.492 (Nm) (47)

Coulomb = 2.074 (Nm) (48)

Viscous = 0.132 (Nm-s) (49)

2. first mesh;

Stiction = 5.481 (Nm) (50)

Coulomb = 4.893 (Nm) (51)

Viscous = 0.623 (Nm-s) (52)

3.Second mesh;

Stiction = 20.50 (Nm) (53)

Coulomb = 18.83 (Nm) (54)

Viscous = 0.832 (Nm-s) (55)

4. Third mesh;

Stiction = 83.66 (Nm) (56)

Coulomb = 77.42 (Nm) (57)

Viscous = 4.502 (Nm-s) (58)

5.Fourth mesh;

Stiction = 1520 (Nm) (59)

Coulomb = 1410 (Nm) (60)

Viscous = 1300 (Nm-s) (61)

6. Fifth mesh;

Stiction = 0.00 (Nm) (62)

Coulomb = 0.00 (Nm) (63)

Viscous = 0.00 (Nm-s) (64)

The absolute values of friction used in the elevation system are:

1. Motor shaft;

Stiction = 0.424 (Nm) (65)

Coulomb = 0.254 (Nm) (66)

Viscous = 0.065 (Nm-s) (67)

2. first mesh;

Stiction = 0.115 (Nm) (68)

Coulomb = 0.089 (Nm) (69)

Viscous = 0.0023 (Nm-s) (70)

3.Second mesh;

Stiction = 0.115 (Nm) (71)

Coulomb = 0.089 (Nm) (72)

Viscous = 0.0023 (Nm-s) (73)

4. Third mesh;

Stiction = 0.115 (Nm) (74)

Coulomb = 0.089 (Nm) (75)

Viscous = 0.0023 (Nm-s) (76)

5.Fourth mesh;

Stiction = 0.144 (Nm) (77)

Coulomb = 0.111 (Nm) (78)

Viscous = 0.0025 (Nm-s) (79)

6. Fifth mesh;

Stiction = 125.76 (Nm) (80)

Coulomb = 102.64 (Nm) (81)

Viscous = 99.02 (Nm-s) (82)

The referred values for the elevation system are then calculated from the above as follows:

1. Motor shaft;

Stiction = 1.719 (Nm) (83)

Coulomb = 1.249 (Nm) (84)

Viscous = 0.0802 (Nm-s) (85)

2. first mesh;

Stiction = 0.8791 (Nm) (86)

Coulomb = 0.702 (Nm) (87)

Viscous = 0.009 (Nm-s) (88)

3.Second mesh;

Stiction = 0.552 (Nm) (89)

Coulomb = 0.4429 (Nm) (90)

Viscous = 0.0035 (Nm-s) (91)

4. Third mesh;

Stiction = 1.580 (Nm) (92)

Coulomb = 1.283 (Nm) (93)

Viscous = 0.0153 (Nm-s) (94)

5.Fourth mesh;

Stiction = 5.860 (Nm) (95)

Coulomb = 4.776 (Nm) (96)

Viscous = 0.2071 (Nm-s) (97)

6. Fifth mesh;

Stiction = 125.76 (Nm) (98)

Coulomb = 102.64 (Nm) (99)

Viscous = 99.02 (Nm-s) (100)

It has been assumed that the absolute values of friction at each mesh were equal, as the only known friction characteristics for the system were:

(1) motor friction;

(2) load friction;

(3) load friction referred onto motor shaft (from (2));

(4) motor + load friction + gearbox friction, referred to the motor shaft;

From these, the total effective gearbox friction referred onto the motor shaft can be calculated. This effective friction is assumed to result from an equal distribution of friction through the gearbox, and thus the absolute values of friction at each mesh may be calculated.

Table 4.1 shows the breakdown of the total effective motor friction into its constituent components, ie motor friction, effective load friction, and effective gearbox friction, for both the traverse and elevation systems.

		% of total effective friction on motor shaft		
		load	motor	gearbox
(1) Traverse:				
	Stiction	73.3	18.5	8.2
	Coulomb	81.7	12.5	5.8
	Viscous	1.4	34.9	63.7
(2) Elevation:				
	Stiction	46.9	24.7	28.4
	Coulomb	52.6	20.3	27.1
	Viscous	5.1	81.0	13.9

TABLE 4.1 BREAKDOWN OF EFFECTIVE MOTOR FRICTION

From Table 4.1 it can be seen that the inclusion of gearbox friction is significant. In addition, the contribution of the load to viscous damping is small in both systems. The load friction is the major contribution to the non-linear friction components, these components being most significant in terms of achieved pointing accuracy.

The inclusion of the full non-linear friction effects in the mathematical models, allows their effects on system performance to be studied under a wide range of dynamic conditions. If pointing accuracy of the system is of major importance, then it is essential that the models contain a full description of the non-linear friction effects at each point in the gearbox.

CHAPTER 5 MODEL OF ELECTRICAL DRIVE MOTORS

The inputs to the mathematical models of the gearboxes are taken to be the torques provided by the respective drive motors. Consequently it was necessary first to establish a suitable mathematical model for the electric motors which were used in this application.

Only the mechanical properties of these motors are of concern in this work. Thus, the electrical characteristics were not specifically included, ie. the time constants associated with the magnetic fields of the motor have been neglected. Therefore, the electrical drive motors have been assumed to produce torque instantaneously. Each motor, nevertheless, has its own mechanical dynamics which have been modelled. The input from the motors to the digital simulation has usually been taken as a step function, although any deterministic function could have been used. This ideal motor is assumed to have no internal torque losses and the assumption is made that the speed vs. torque characteristic is wholly linear for any given set of applied voltages. For a fixed reference voltage, the motor develops a stall torque which is proportional to the voltage applied. Once the motor begins to run, with any value of applied voltage, the torque available for acceleration decreases due to bearing friction and any system friction referred onto the motor shaft. As the torque developed is taken as being

proportional to the applied voltage it is only neccessary to state the required torque as an input to the modelling equations. The block diagram representation of the motor is shown in Figure 5.1. It should be noted that the transfer function transforming velocity into friction torque is representative only, as it takes no account of referred friction torque loadside of the motor. The non-linear friction components were shown in Chapter 4 to be functions of motor angular acceleration, motor speed, and direction of rotation.

Newton's second law states that:

$$T = I.\alpha_m \quad \text{.....(101)}$$

where T represents all torque inputs (Nm),

I is the inertia on the motor shaft ($Kg.m^2$),

and α_m is the motor angular acceleration (rad/s^2)

The inertia, I, is composed of the motor inertia plus all referred inertias loadside, ie.

$$I = I_m + \Sigma I_j . N_j^2 \quad \text{.....(102)}$$

where I_m is the motor inertia ($Kg.m^2$),

I_j is an inertia at a point j loadside ($Kg.m^2$),

and N_j is the gear ratio from the motor shaft to the point, j

I_{m_r} : referred inertia onto motor shaft

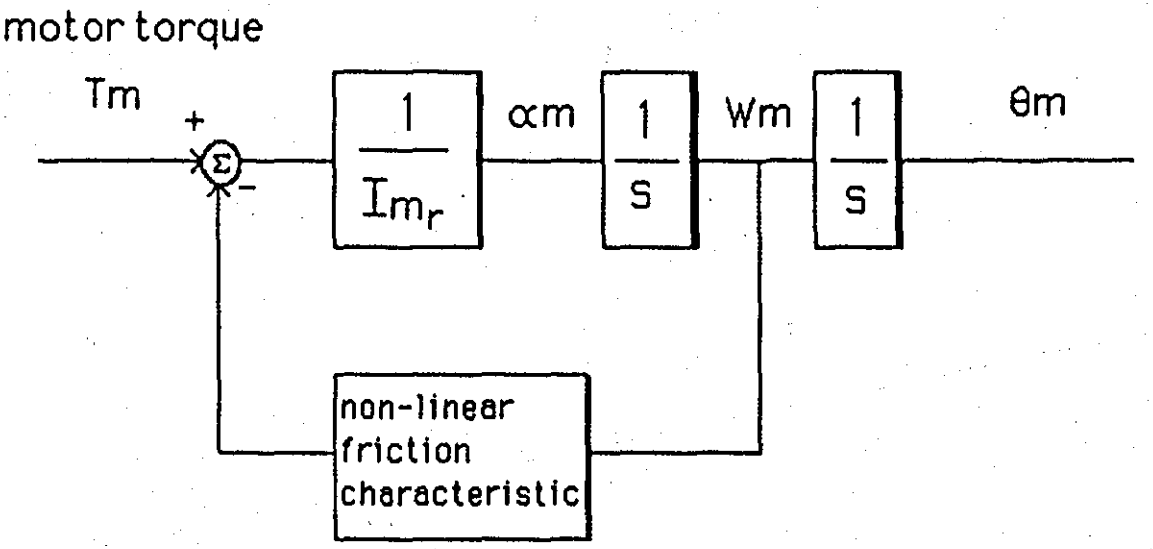

Figure 5.1 : Block diagram of electric drive motor

The input torque to the system is given by:

$$T = T_m - F \quad \text{.....(103)}$$

where T is the motor stall torque (Nm) ,

and F is the friction on the motor shaft. (Nm-s).

The friction term, F, dependant on motor speed, may be expressed as the following components:

$$F = F_{m_s} + \Sigma F_{j_s} . N_j + F_{m_c} + \Sigma F_{jc} . N_j + F_{m_v} + \Sigma F_{jv} . N_j^2 \quad \text{.....(104)}$$

where F_{m_s}, F_{m_c} , and F_{m_v} are the stiction, Coulomb, and viscous friction components of the motor shaft,

F_{j_s} , F_{jc} , and F_{jv} are the stiction, Coulomb, and viscous friction components of a point j loadside ,

and N_j is the gear ratio from the motor shaft to the point, j

In this study it has been adopted as a convention that the gear ratio is given as follows:

$$N = \frac{N_{t_i}}{N_{t_{i+1}}} \quad \text{.....(105)}$$

where N_{t_i} is the number of teeth on the ith gear.

ie. for a reduction ratio, N is less than unity.

From equation (101) and equation (103) the angular acceleration of the motor can be established as:

$$\alpha_m = \frac{(T_m - F)}{I} \quad \text{.....(106)}$$

The velocity and displacement of the motor arising

as a result of this angular acceleration are therefore:

$$w_m = \int_o^t \alpha_m \, dt \qquad \text{.....(107)}$$

$$\theta_m = \int_o^t w_m \, dt \qquad \text{.....(108)}$$

where w_m has the units rad/s ,

and θ_m has the units of radians.

The value of torque, or corresponding voltage input, may be positive or negative, ie the motor displacement may be clockwise or counter-clockwise.

From Eq.(102) the inertia at the motor shaft is the sum of the referred system inertias through the gear meshes, which is true for any point in the gearbox, where the inertia is increased by the reflected system inertias loadside, as described in Chapter 2.

It can be seen from the above set of describing equations that, apart from the non-linear friction components, the motor model is an essentially linear one. The motor torque has been assumed to be a linear function of voltage and no account has been included in the model of either motor torque saturation or of any non-linear speed-torque curve. However, most servomotors are designed to have a linear torque characteristic throughout their rated operating range. Therefore, as a first approximation, motor torque saturation is usually omitted from the analysis. In the work here it has been assumed for generality that the slope of the speed-torque curve is unity.

If the speed range over which the friction characteristics are non-linear is small compared to the overall speed range of the motor, then for all, except small, torque inputs the motor will be operating chiefly in its linear region. The mechanical time-constant of the motor can then be determined from an analysis of the differential equations. The motor transfer function can be obtained by transforming the above equations using the Laplace operator, and assuming zero initial conditions, ie.

$$\text{Friction torque} = F_{m_v}\, s\, \theta_m(s) \qquad \text{.....(109)}$$

$$\text{Accelerating torque} = I.s^2\theta_m(s) \qquad \text{.....(110)}$$

Therefore:

$$I.s^2\theta_m(s) = T_m - F_{m_v}.s\,\theta_m(s) \qquad \text{.....(111)}$$

Hence the motor transfer function is given as:

$$\frac{\Theta_m}{T_m}(s) = \frac{1}{Is^2 + F_{m_v}s} \qquad \text{.....(112)}$$

The mechanical time constant, t_m, is given by:

$$t_m = \frac{I}{F_{m_v}} \quad \text{sec.} \qquad \text{.....(113)}$$

ie. t_m is the ratio of the referred inertia to the referred viscous friction.

The time constant is defined as the time required by the motor to reach 63.2 % of its final speed for a step torque input. As soon as the motor develops any value of angular velocity, friction torque begins to develop, which subtracts from the developed motor torque, thereby

decreasing the torque available for acceleration until, eventually, the friction torque equals the developed torque. At this point the net torque available to accelerate the inertia is zero and consequently the motor speed remains constant. The motor reaches 63.2% of this steady speed in t_m seconds.

In reality, any motor torque developed must be used to accelerate the complete system inertia. Equation (113) demonstrates the use of referred parameters to guarantee that the motor 'sees' the full effective system inertia in the modelling equations. The mechanical time constant of the motor is increased by the effect of the inertias loadside. Similarly, the torque generated at each mesh must accelerate the effective system inertia loadside of the mesh.

By substituting the appropriate values of effective motor inertia and viscous friction coefficient into eq.(113) the motor time constant can be calculated:

$$(t_m)\text{traverse} = 0.606 \text{ secs.} \qquad (114)$$

$$(t_m)\text{elevation} = 3.142 \text{ secs.} \qquad (115)$$

The effective increase in motor time constant due to the effects of the load on the motor shaft can be calculated by substituting the absolute values of motor inertia and viscous friction coefficient into eq.(113). Thus the unloaded motor time constant is given by:

$$(t_m)\text{traverse} = 0.109 \text{ secs.} \qquad (116)$$

$$(t_m)\text{elevation} = 0.077 \text{ secs.} \qquad (117)$$

Thus the effect of loading the motor is to increase the time taken to reach steady speed by a factor of 5.5 for the traverse system, and by a factor of 40 for the elevation system.

The effect is more marked in the elevation system for a number of reasons. First the overall gear ratio is smaller than that in the traverse gearbox, thus increasing the effective loading on the motor shaft. This effect is magnified by the fact that the first gear ratio in the elevation system is not a reduction ratio, thus referred inertias are increased across this ratio. This greater loading of the motor shaft is not balanced by a similar increase in friction due to the relatively low values of viscous friction throughout the elevation system.

The linear analysis of the motor presented above is valid only for large torque inputs where, at high steady speeds, the viscous friction component is large compared to the constant Coulomb friction . However, its study does help in achieving an understanding of the modelling techniques and clearly shows the effect that the system's inertia has upon the dynamic characteristics of the motor.

The output of the motor is taken to be its angular displacement, θ_m . This displacement is then taken as being the input to the gearbox with the torsional stiffness of the motor being assumed to be infinite.

CHAPTER 6 BACKLASH

Backlash, or free play, occurs when two mechanical elements are not coupled rigidly, but rather through an inactive zone of displacement within which no direct mechanical coupling exists. Excessive backlash can cause difficulties in controlling mechanical systems. However, most procedures used to reduce the amount of backlash can, when carried too far, result in excessive friction instead. In design, some form of 'trade-off' is often necessary.

For a theoretical set of perfectly mating gears, the tooth gap is equal to the tooth thickness on the line of contact and the backlash would be zero provided the centre distance, C_s, was fixed at:

$$C_s = \frac{(no_1 + no_2)}{2P} \qquad \text{.....(118)}$$

where

C_s is the standard centre distance ,

no_1, no_2 are the number of teeth for gears 1 and 2 respectively,

and P is the diametral pitch associated with the gear pair.

Such a gear pair, however, cannot exist because of inevitable discrepancies in its manufacture. Moreover, the chance of 'binding', even for a set of 'perfect' gears, is always possible due to thermal expansion of the gears. For

these reasons some backlash is always 'built' into conventional spur gears by cutting the teeth thinner than the thickness required by theory , which is equal to half the circular pitch. Also, it is customary to increase the centre distance by an amount equal to that resulting from differential thermal expansion. Because of this increase there will be additional backlash at lower temperatures.

Consider the backlash introduced by the non-ideal tooth thickness. This is equal to the difference d_{T_t} between the actual and the ideal tooth thickness:

$$d_{T_t} = \frac{\pi}{2P} - T_1 + \frac{\pi}{2P} - T_2$$

$$= \frac{\pi}{P} - T_1 - T_2 \quad \ldots\ldots\ldots(119)$$

where T_1 and T_2 are the tooth thicknesses associated with gears 1 and 2 respectively.

The backlash d_{T_c} introduced by a non-ideal centre distance is determined by the involute relationship illustrated in Figure 6.1.

The following analytical relationship can be established for d_{T_c} as a function of d_c:

$$d_{T_c} = (2\tan\phi)d_c + \frac{2P}{(no_1 + no_2)\tan\phi}(d_c)^2$$

$$+ \frac{(1+3\tan^2\phi)(2P)^2 (d_c)^3}{(3\tan^3\phi)(no_1+no_2)^2} + \ldots\ldots\ldots \quad \ldots\ldots(120)$$

where ϕ is the standard pressure angle and d_c is the difference between the operating and standard centre

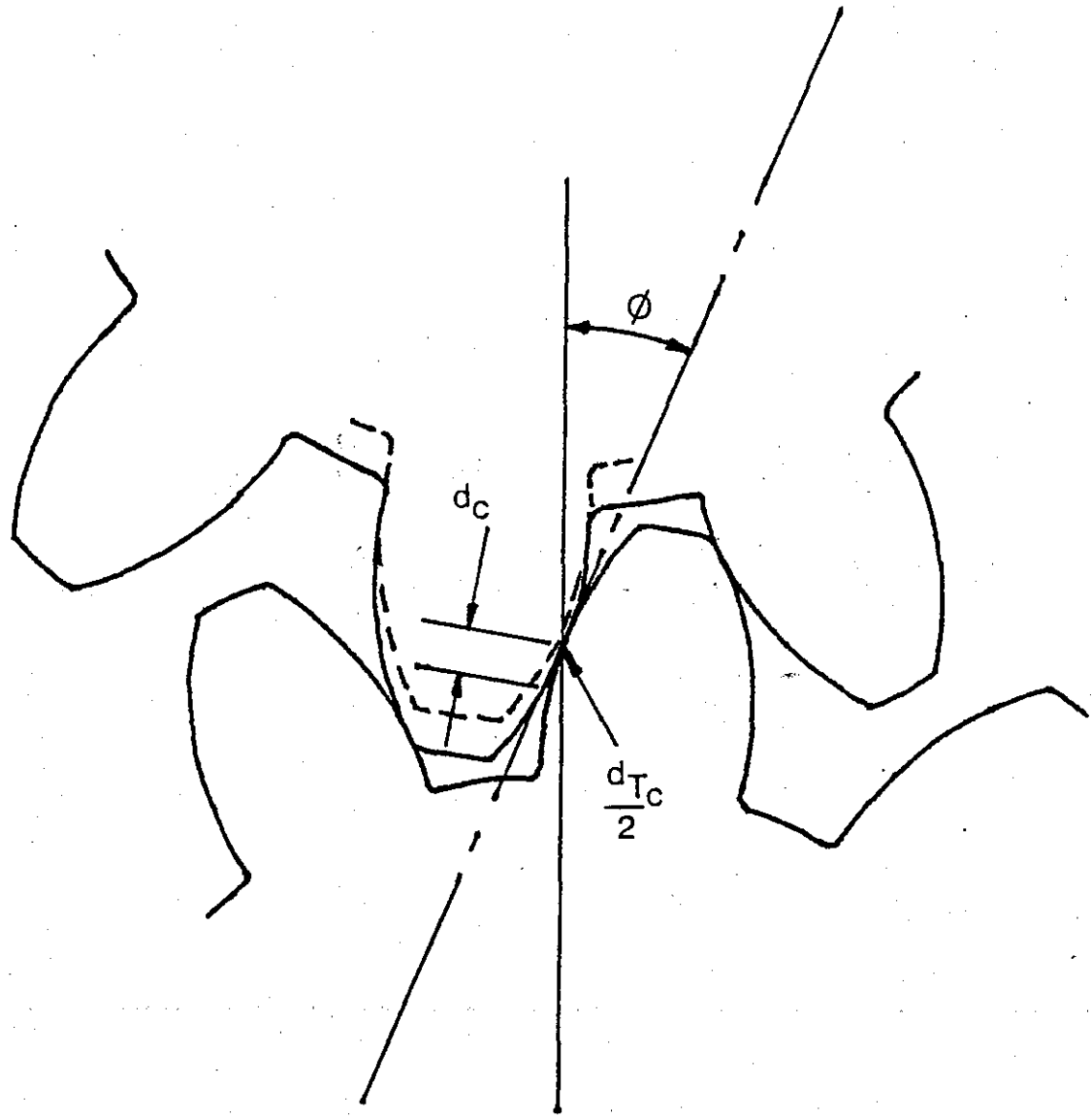

FIGURE 6.1: RELATIONSHIP BETWEEN BACKLASH AND CENTRE DISTANCE

distance.

Equation (120) represents an infinite series accounting for the effect of the involute curve. Calculations may be carried out to any desired accuracy by including a sufficient number of terms. For a typical precision gear train, d_c is sufficiently small so that the higher order terms in this series may be neglected. If this is considered to be the case, the backlash, d_{T_c}, resulting from centre distance variations, may be calculated as:

$$d_{T_c} = 2\tan\phi(C - C_s) \qquad .....(121)$$

where C is the actual centre distance.

Radial play in the bearings also contributes to a variation in centre distance. Running gears tend to force each other apart to the extent allowed by the bearing play. This tendency increases the operating centre distance and can be included in the calculations by appropriately increasing d_c.

One additional factor, the gear pitch diameter runout, or eccentricity, must be considered when calculating backlash. In a perfect gear, the pitch circle would be concentric about the axis of rotation. In reality a curve drawn through all points of constant tooth thickness would be both eccentric and jagged. The latter results from tooth-to-tooth spacing and involute variations. The total variation of the curve is defined as the total composite error (TCE). Figure 6.2 shows a typical gear error chart

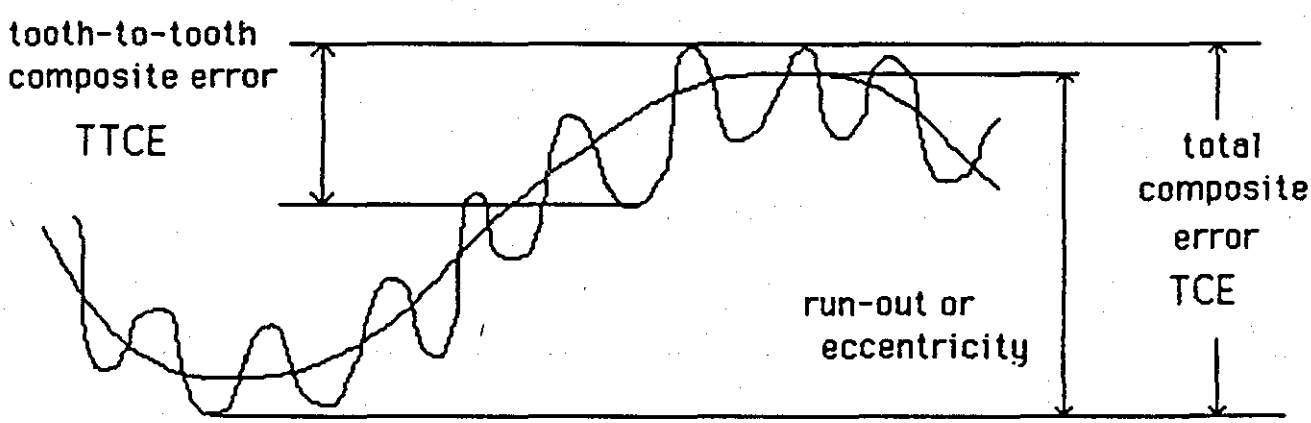

Figure 6.2 : Typical gear error chart obtained by variable centre text fixtures

obtained by variable centre distance test fixtures. The run out, or eccentricity, is given by the difference between the TCE and the tooth-to-tooth composite error (TTCE). Since the eccentricity is representative of a centre distance variation, it contributes to the total backlash in the same manner as the true centre distance. Using the same approximation as before:

$$T_{tce} = 2\tan\phi[TCE1-TTCE1+TCE2-TTCE2] \quad ..(122)$$

For any fixed collection of errors, Eq. (122) represents a 'worst case' situation since it assumes that both gears are meshed at their low point of eccentricity. If a hunting tooth exists, however, this point will always occur.

The total backlash existing between two mating gears is then given by:

$$B = d_{T_t} + d_{T_c} + T_{tce} \quad .....(123)$$

Having established the backlash at each gear mesh throughout the gear train, either by analytical methods, or by direct measurement, there are considerable difficulties in predicting the effects on the system dynamics by purely analytical techniques. Consequently, simulation procedures are frequently necessary to study these effects.

The dynamic simulation of backlash is illustrated diagrammatically in Figure 6.3. Θ_1 and Θ_2 are the angular

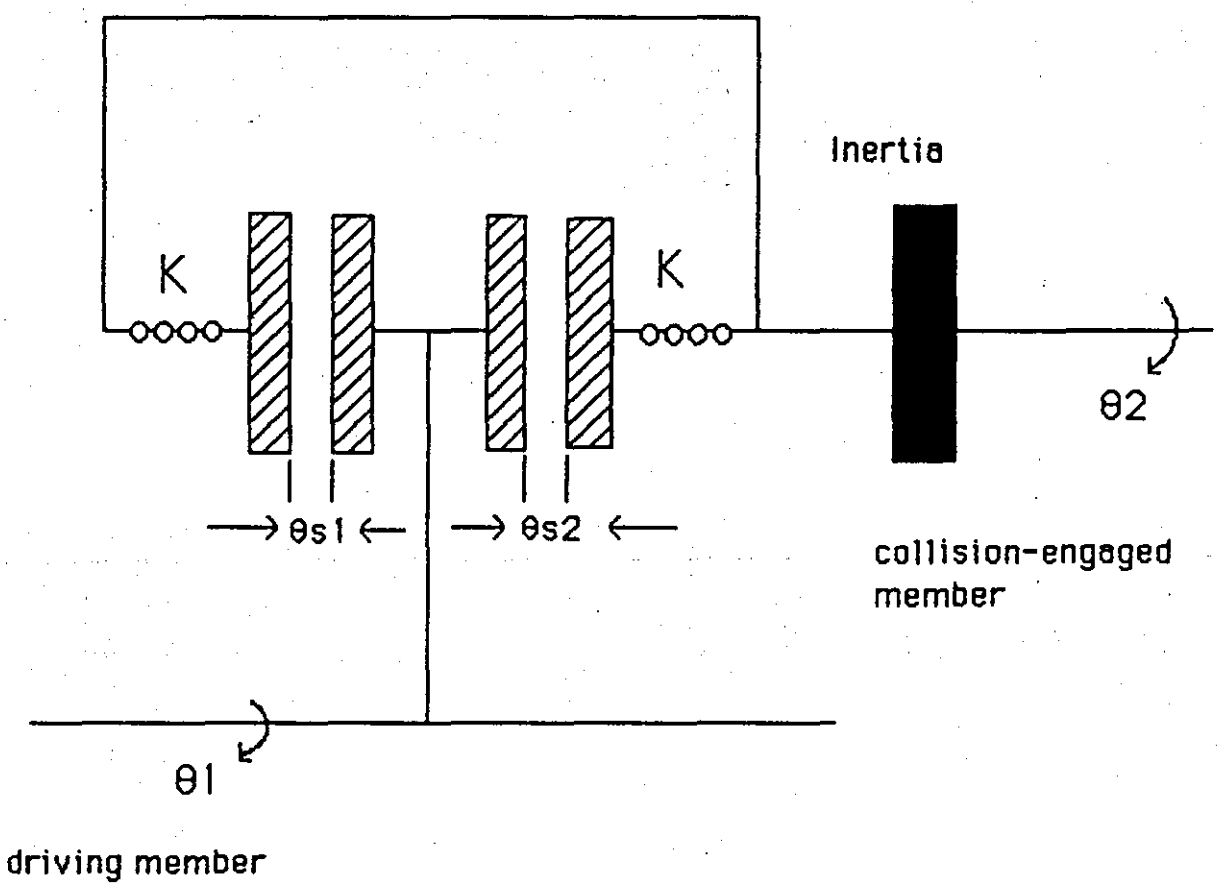

Figure 6.3 : Dynamic simulation of backlash

displacements of the driving and collision engaged members. Actually it is only their difference, $(\theta_2-\theta_1)$, which is significant here. This difference governs the engagement gap spacings, θs_1 and θs_2, which are given by:

$$\theta s_1 = B_1-(\theta_2 - N_1.\theta_1) \qquad \ldots\ldots(124)$$

$$\theta s_2 = B_2+(\theta_2 - N_1.\theta_1) \qquad \ldots\ldots(125)$$

B_1 and B_2 are the neutral settings of the gaps, ie. the initial conditions on θs_1 and θs_2. Consequently, the total backlash, B, is given by;

$$B = B_1 + B_2 \qquad \ldots\ldots\ldots\ldots\ldots(126)$$

Hence for the i^{th} gear mesh

$$B_i = B_{1_i} + B_{2_i} \qquad \ldots\ldots\ldots\ldots\ldots(127)$$

By letting;

$$B_{1_i} = d_i . B_i \qquad \ldots\ldots\ldots\ldots\ldots(128)$$

then adjustment of d_i in the range 0 to 1 corresponds to a change in the initial condition of the gear mesh as shown in Figure 6.4.

In this study all gear meshes have their backlash set to 0.00762 cm , which is then referred onto the output member as;

$$B_i = \frac{0.00762}{r_i} \qquad \ldots\ldots\ldots\ldots\ldots(129)$$

where B_i is the referred backlash (rads) onto the output member of the i^{th} mesh, of radius r_i (cm.)

From equation (129) it can be seen that angular losses in the gearbox may be reduced by increasing the radius of

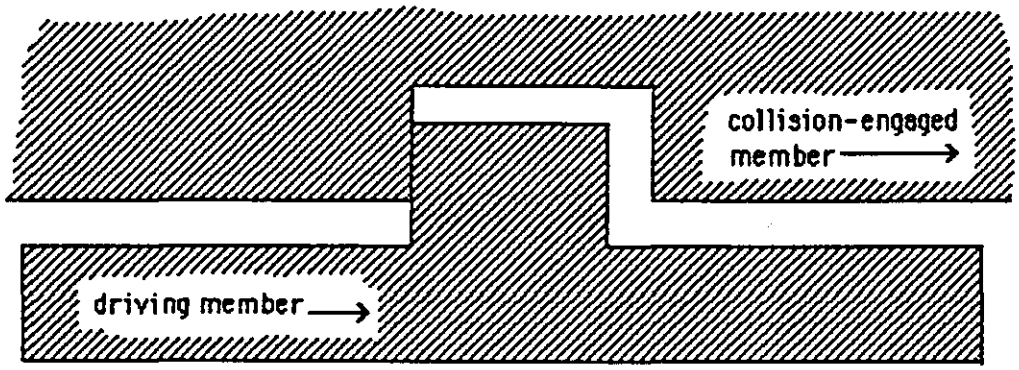

(a) di = 0 : Gears fully unmeshed in direction of rotation as an initial condition.

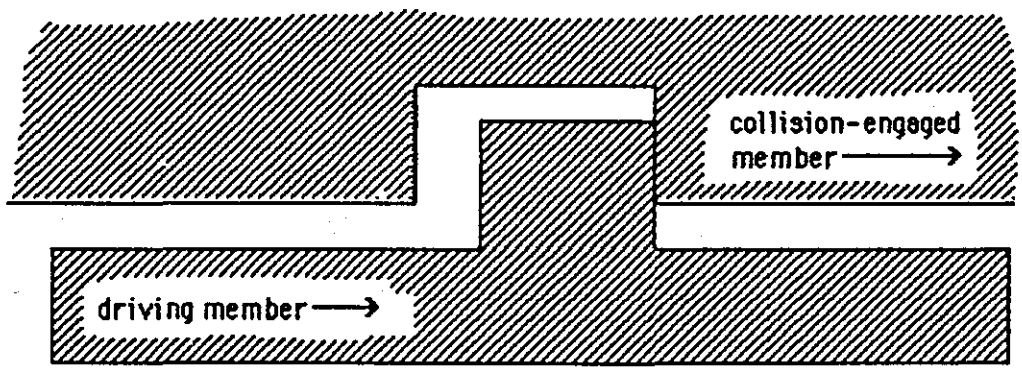

(b) di = 1 : Gears fully meshed in direction of rotation as an initial condition.

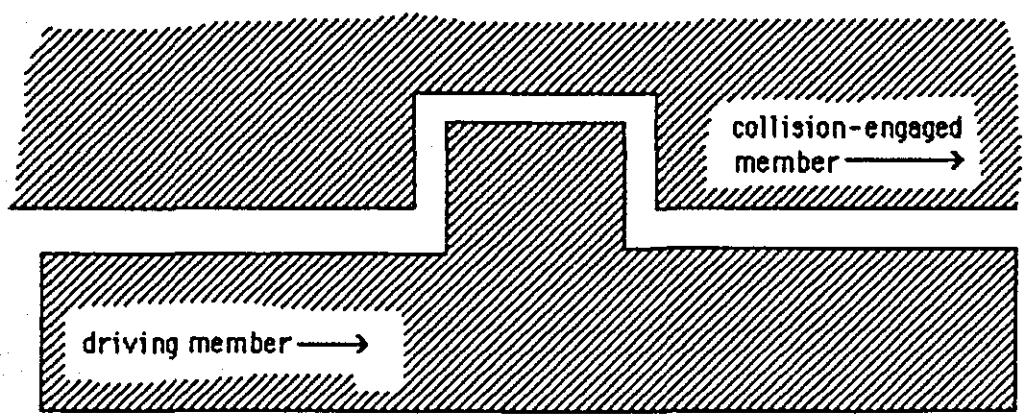

(c) di = 0.5 : ie mid-way between (a) and (b)

Figure 6.4 : Change of initial condition on gear mesh

the driven gear. Consequently the angular loss due to backlash at the load end, which is the most significant in the system , will be small for the traverse system, owing to the relatively large diameter of the turret ring. The referred angular losses in the traverse system resulting from a 0.00762 cm. tolerance on all meshes, are given by:

1. First mesh;

$$B = 0.000953 \text{ (rads)} \quad .....(130)$$

2.Second mesh;

$$B = 0.000904 \text{ (rads)} \quad .....(131)$$

3. Third mesh;

$$B = 0.007284 \text{ (rads)} \quad .....(132)$$

4.Fourth mesh;

$$B = 0.000502 \text{ (rads)} \quad .....(133)$$

5.Fifth mesh ;

$$B = 0.0001 \text{ (rads)} \quad .....(134)$$

The referred angular losses in the elevation system resulting from a 0.00762 cm tolerance on all meshes are:

1. First mesh;

$$B = 0.00229 \text{ (rads)} \quad (135)$$

2.Second mesh;

$$B = 0.003175 \text{ (rads)} \quad (136)$$

3. Third mesh;

$$B = 0.000884 \text{ (rads)} \quad (137)$$

4.Fourth mesh;

$$B = 0.011106 \text{ (rads)} \quad (138)$$

5. Fifth mesh;

$$B = 0.001232 \text{ (rads)} \qquad (139)$$

The torque which arises at the engagement of the i^{th} gear mesh is given by:

$$\begin{aligned} T_i &= -K_i . \theta s_2 && \text{if } \theta s_2 \leqslant 0 \\ T_i &= 0 && \text{if } \theta s_1 , \theta s_2 > 0 \\ T_i &= K_i . \theta s_1 && \text{if } \theta s_1 \leqslant 0 \end{aligned} \qquad .....(140)$$

where K_i is the mesh stiffness.

As a result of this engagement torque the acceleration of the collision engaged member can be shown to be:

$$\alpha_i = \frac{(T_i - F_i)}{I_i} \qquad .....(141)$$

where F_i is the referred friction onto the output member

I_i is the referred inertia onto the output member

Consequently, the velocity of the collision engaged member is given by:

$$w_i = \int_o^t \alpha_i \, dt \qquad .....(142)$$

and its displacement by:

$$\theta_i = \int_o^t w_i \, dt \qquad .....(143)$$

If shaft stiffnesses are ignored then the output displacement, θ_{2_i} , from the i^{th} mesh is the input

displacement into the $(i+1)^{th}$ mesh, ie:

$$\theta_{2_i} = \theta_{1_{i+1}} \qquad \text{.....(144)}$$

Obviously, each engaging surface posseses resilience, surface or contact friction, and some inertia. To analyse exactly the transmission of forces and velocities following gear collision would involve the study of distributed parameter differential equations. However, to a first approximation, such effects are negligible, and it is adequate to show the effects of engagement by representing the collision engaged member as a combination of a spring constant, K, and some viscous friction.

The nature of the torque generated is essentially oscillatory, as the the two engaging members come into and out-of-mesh. This effect is particularly marked if there is insufficient contact friction, leading to poor damping of the collision-engaged member. Since values of surface friction are only imperfectly known, it is likely that any consideration of collision-engaged response will produce highly oscillatory, undamped motion.

The block diagram arrangement for a representative gear mesh is shown in Figure 6.5.

The linearisation of a set of non-linear differential equations is a useful technique, whereby the equations may then be analysed without recourse to digital computing methods. In addition, results obtained from the linearised

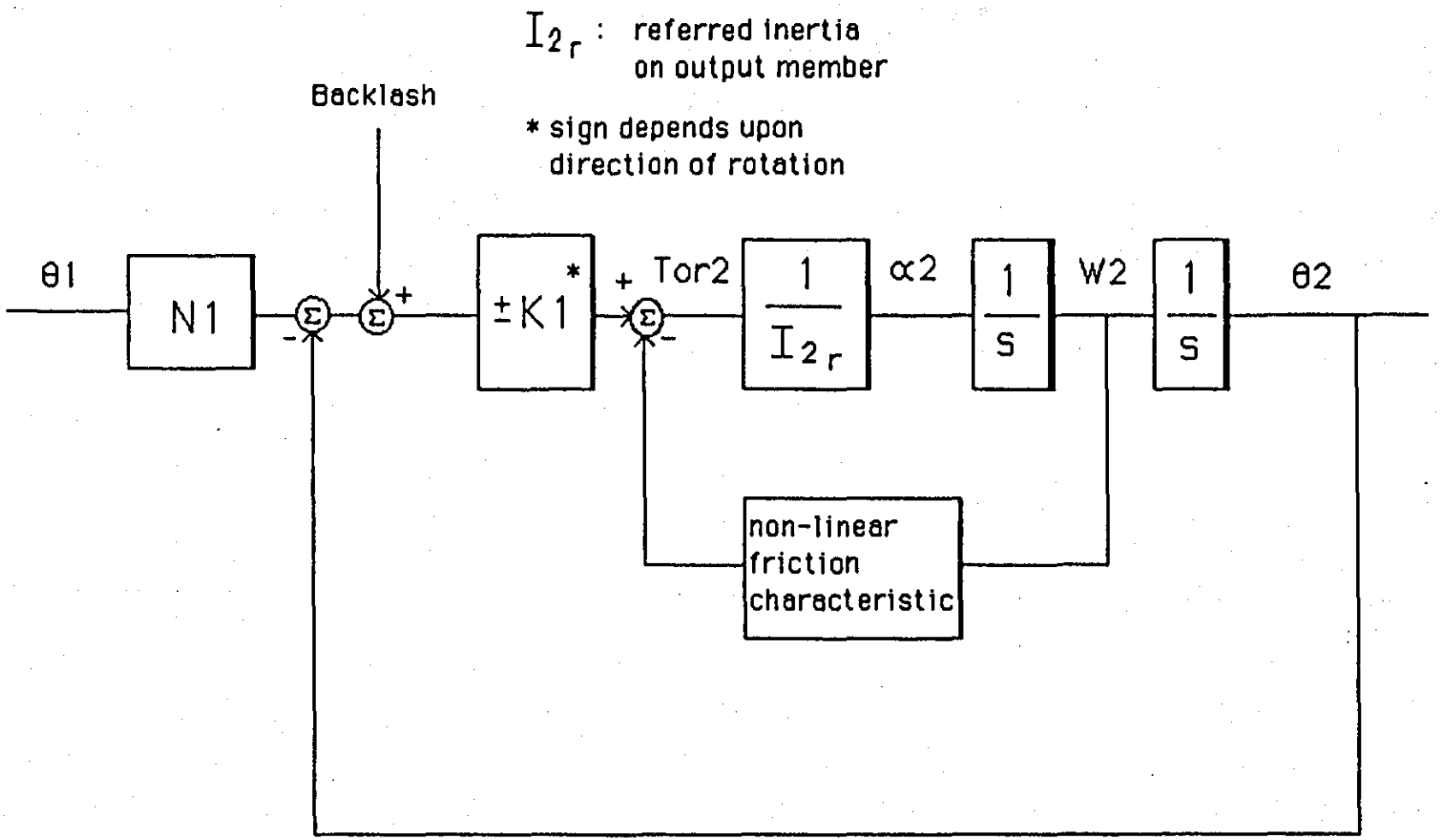

Figure 6.5: Block diagram of representative gear mesh

equations may be compared with those from the full non-linear model thus highlighting any effects of the non-linearities on dynamic performance. However, it must be emphasised that conclusions reached from a study of the linearised equations may not be applied to the full system model. Analysis of a set of linear differential equations usually requires that the equations first be transformed using the Laplace operator, s.

The equations modelling the torque generation at each mesh can be linearised by removing the dependence of torque on the backlash condition. Without this dependence on backlash, eq.(124) and eq.(125) reduce to:

$$\theta s_1 = -(\theta_2 - N_1.\theta_1) \quad .....(145)$$

$$\theta s_2 = (\theta_2 - N_1.\theta_1) \quad .....(146)$$

Dependent upon the backlash condition, eq.(140) gives the torque arising from collision-engagement of the gears, ie.

$$T_i = -K_i.\theta s_2 \quad .....(147)$$

and

$$T_i = K_i.\theta s_1 \quad .....(148)$$

Without backlash, eq.(147) and eq.(148) are identical and the torque generated at the mesh is given by:

$$T_i = -K_i(\theta_2 - N_1.\theta_1) \quad .....(149)$$

The angular acceleration of the output member arising from this torque is given by:

$$\alpha_i = (T_i - F_i)/I_i \quad .....(150)$$

where F_i and I_i are the referred viscous friction and

inertia at the output member.

The corresponding angular velocity and displacement are, therefore:

$$w_i(s) = \frac{\alpha_i}{s} \qquad \text{.....(151)}$$

$$\theta_i(s) = \frac{w_i}{s} \qquad \text{.....(152)}$$

where s is the Laplace operator.

The viscous friction acting on the output member is a function of the angular velocity and can be written as:

$$F_i = F_{v_i} . w_i \qquad \text{.....(153)}$$

where F_{v_i} is the effective viscous friction component for the output member.

By rearranging the above equations and by suitable substitution, the transfer function relating output angular displacement to input angular displacement can be shown to be given by:

$$\frac{\Theta_{2i}}{\Theta_{1i}}(s) = \frac{N_i K_i}{I_i s^2 + F_{v_i} s + K_i} \qquad \text{.....(154)}$$

or:

$$\frac{\Theta_{2i}}{\Theta_{1i}}(s) = \frac{N_i \frac{K_i}{I_i}}{s^2 + \frac{F_{v_i}}{I_i} s + \frac{K_i}{I_i}} \qquad \text{..... (155)}$$

which may be represented in the standard form for a

second order linear system, ie.

$$G(s) = \frac{\beta W_n^2}{s^2 + 2\zeta W_n s + W_n^2} \qquad \ldots(156)$$

where W_n is the undamped natural frequency, ζ is the damping ratio, and β is a scaling factor.

By comparing eq.(155) with eq.(156) then the undamped natural frequency of the gear mesh, W_{n_i} (rad/s), is given by:

$$W_{n_i} = \sqrt{\frac{K_i}{I_i}} \qquad \ldots.(157)$$

and the damping ratio is given by:

$$\zeta_i = \frac{\frac{1}{2} F_{vi}}{\sqrt{\frac{I_i}{K_i}}} \qquad \ldots.(158)$$

The frequency and damping associated with the gear meshes in the gun drive system, using the values of stiffness and inertia previously detailed, are therefore:

(1) Traverse:

	Frequency		Damping
	(Hz)	(rad/s)	
First mesh	2761	17348	$3.316*10^{-5}$
Second mesh	1240	7791	$6.062*10^{-6}$
Third mesh	1077	6767	$2.176*10^{-6}$
Fourth mesh	12	75	$1.666*10^{-4}$
Fifth mesh	5	31	0.000

(2) Elevation:

	Frequency		Damping
	(Hz)	(rad/s)	
First mesh	1441	9054	$4.390*10^{-6}$
Second mesh	1175	7382	$4.003*10^{-6}$
Third mesh	834	5240	$1.893*10^{-6}$
Fourth mesh	52	327	$2.580*10^{-5}$
Fifth mesh	5	31	$2.354*10^{-4}$

It can be seen that the frequency decreases through both systems as the effective inertia increases. The low gun frequency (5 Hz) is due to its representation as a lumped inertia. This neglects higher barrel frequencies even though the modes associated with these may be significant.

The damping at each mesh, in both systems, is extremely low, due to the omission of the damping associated with the mating gear teeth during collision-engagement. As stated earlier, this lack of knowledge of contact friction between mating teeth is likely to produce torque generation that is oscillatory in nature.

Although the values of backlash presented in this chapter appear to be very small, it is important to note that the required pointing accuracy of the gun drive system for a modern M.B.T. is likely to be of the order of 0.001 radians.

CHAPTER 7 THE PLANETARY GEAR SYSTEM

Planetary gear trains are frequently used in M.B.T. gun drive systems where a relatively large gear ratio is required within a small area, due to design limitations on space inside the turret and hull, which prohibits the use of a series of conventional meshes. Such planetary gears are usually stiffer than conventional meshes and usually have less backlash associated with them for a given tolerance. For these reasons they are usually positioned at the load end of a gearbox, where the torque levels are higher, and where excessive backlash is more critical for pointing accuracy. The structure of the planetary gear train, used in both the traverse and elevation gearboxes is shown schematically in Figure 7.1.

The input into the planetary train is via a sunwheel gear which meshes with each of the three planet gears. Since the outer annulus is fixed, the planet gears are constrained to rotate around the sunwheel in addition to rotating about their own individual axes. It is this rotation of the three planet gears about the sunwheel, as a fixed unit, which provides the output from the train, on a shaft co-axial with the sunwheel.

In addition to the electrical inputs, both traverse and elevation systems will ususally have a mechanical input option, via a gunner's handle, which can be used in the

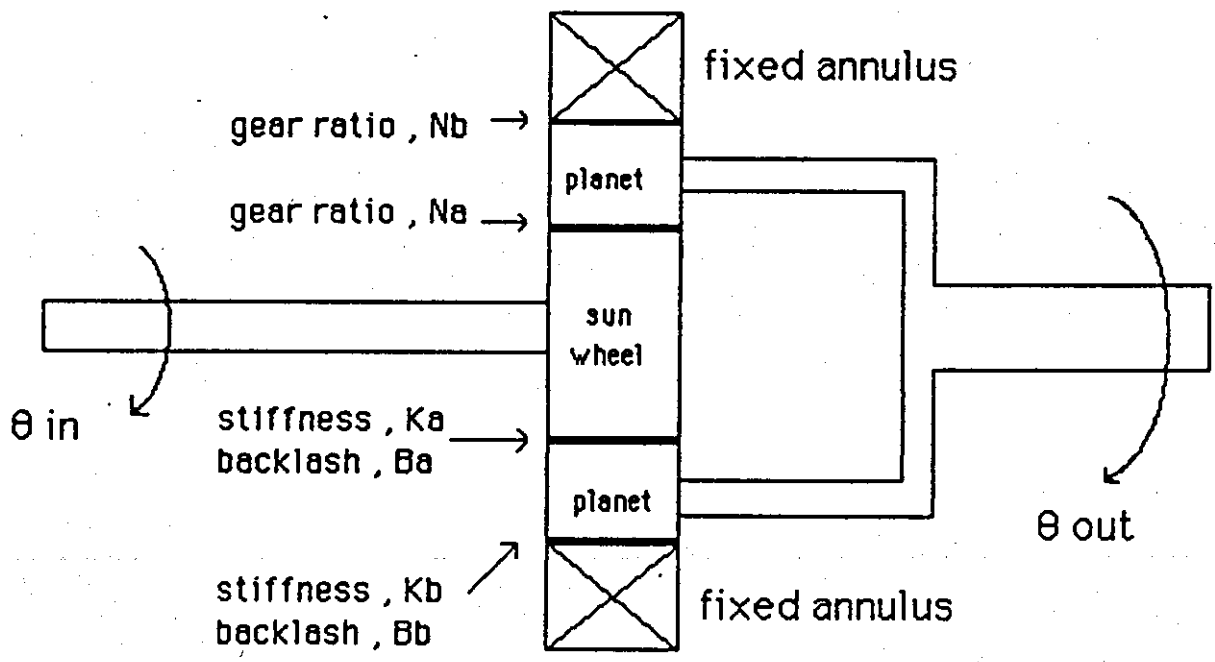

Figure 7.1 : Planetary gear train

event of an electrical power failure. Therefore, as a safety precaution, it is usual to make the gun drive system non-reversible by fitting a clutch to the outer annulus of the planetary system. A large reverse torque input, such as that arising from the gun colliding with a stationary object, frees the outer annulus, thereby preventing associated gun accelerations from being transmitted back through the gearbox to the gunner's handle.

This option has not been incorporated into the modelling equations.

Since the outer annulus is fixed, in normal operation, and the drive is taken off from the rotation of the planet gears around the sunwheel, the planetary train may be modelled as a single mesh with the same effective stiffness, backlash and friction as the planetary train. It is necessary to decompose the overall gear ratio, N_p, of the planetary train into it's two constituent components, N_a and N_b, made up of the engagements of the sunwheel with the planet gears, and the planet gears with the outer annulus, in order that the correct effective parameters for the single mesh can be calculated. The overall gear ratio of the planetary train is given by :

$$N_p = N_a N_b = 1 + \frac{NoP.Noa}{Nos.NoP} \simeq \frac{Noa}{Nos} + 1 \quad \ldots\ldots\ldots (159)$$

where Nop, Nos, Noa are the number of teeth on the planet gear (one of the three planet gears),the sunwheel, and the outer annulus respectively.

The gear ratio between the sunwheel and the planet gears is given by:

$$N_a = \frac{NoP}{Nos} \qquad .....(160)$$

Consequently:

$$N_b = \frac{Noa}{NoP} + \frac{Nos}{NoP} \qquad .....(161)$$

Thus, the single mesh which effectively replaces the planetary gear train must have the the following absolute parameters:

(a) Stiffness:

$$K = \frac{3}{\frac{1}{K_a} + \frac{N_b^2}{K_b}} \qquad .....(162)$$

The numerator accounts for the number of planet gears.

(b) Backlash:

$$B = B_a + N_b . B_b \qquad .....(163)$$

(c) Stiction:

$$F_S = F_{S_a} + N_b . F_{S_b} \qquad .....(164)$$

(d) Coulomb friction:

$$F_c = F_{c_a} + N_b . F_{c_b} \qquad .....(165)$$

(e) Viscous friction coefficient:

$$F_v = F_{v_a} + N_b^2 . F_{v_b} \qquad .....(166)$$

CHAPTER 8 THE DIGITAL SIMULATION

The digital simulations used for the traverse and elevation systems are identical in structure, differing only in the number of gear meshes and the values used. Therefore, to avoid repetition and confusion over the variable names, only a detailed account of the traverse system is presented here.

8.1 Inertia

The representation of the distribution of inertia through the traverse system was presented in Figure 2.1. Since the torque developed at each gear mesh accelerates the effective inertia of the output member, it is necessary to calculate the effective inertia of the output member at each mesh by substitution of the appropriate values into eq.(5). This procedure can be somewhat simplified by first applying eq.(4) to calculate the absolute inertia existing on each shaft, consisting of the inertia of the shaft itself, in addition to the inertias of any gears on the shaft, ie:

$$I_i = I_{S_i} + \Sigma I_j \qquad \text{.....(167)}$$

where I_i is the absolute inertia on the shaft,

I_{S_i} is the inertia of the shaft itself,

I_j is a gear inertia on the shaft.

Thus, from Figure 2.1, the absolute inertias on each

shaft in the traverse system are given by:

$$I_m = I_{S_m} + I_a \qquad \text{.....(168)}$$

where the motor shaft inertia, I_{S_m}, may include inertia terms for the motor itself.

$$I_1 = I_{S_1} + I_b + I_c \qquad \text{.....(169)}$$

$$I_2 = I_{S_2} + I_d + I_e \qquad \text{.....(170)}$$

$$I_3 = I_{S_3} + 3I_f + I_{Pin} \qquad \text{.....(171)}$$

The effective inertia of the turret is given by:

$$I_t = I_{tur} + I_{gun} + \tfrac{1}{2}M_g d^2 \qquad (172)$$

where I_{tur} is the turret inertia

I_{gun} is the gun inertia

M_g is the gun mass

and d is the distance from the centre of gravity of the gun to the centre of rotation of the turret.

Therefore, the effective inertia acting on each output member, assuming that the parallel distance between shafts is negligible, is given by:

$$I_{m_r} = I_m + N_1^2.I_1 + N_1^2.N_2^2.I_2 + N_1^2.N_2^2.N_3^2.I_3 + N_1^2.N_2^2.N_3^2.N_4^2.I_t \qquad \text{.....(173)}$$

$$I_{1_r} = I_1 + N_2^2.I_2 + N_2^2.N_3^2.I_3 + N_2^2.N_3^2.N_4^2.I_t \qquad \text{....(174)}$$

$$I_{2_r} = I_2 + N_3^2.I_3 + N_3^2.N_4^2.I_t \qquad \text{....(175)}$$

$$I_{3_r} = I_3 + N_4^2 I_t \qquad \ldots.(176)$$

There are no other inertia terms associated loadside with the gun and hence it is represented by its absolute value.

8.2 Stiffness

The representation of the distribution of stiffness through the traverse system was shown in Figure 3.1. By substitution of the appropriate values into eq.(12), the effective stiffness at any point in the system, when the shafts are asumed to be infinitely stiff, may be calculated:

$$K_{1_r} = K_1 + N_2^2 . K_2 + N_2^2 . N_3^2 . K_3 + N_2^2 . N_3^2 . N_4^2 . (K_t + K_{tg}) \qquad \ldots\ldots\ldots(177)$$

where K_t is the turret stiffness, and K_{tg} is the stiffness of the gun relative to the turret.

$$K_{2_r} = K_2 + N_3^2 . K_3 + N_3^2 . N_4^2 . (K_t + K_{tg}) \qquad \ldots\ldots\ldots(178)$$

$$K_{3_r} = K_3 + N_4^2 (K_t + K_{tg}) \qquad \ldots\ldots\ldots(179)$$

8.3 Friction

The distribution of friction through the traverse system was represented in Figure 4.5. From this figure the following referred values may be calculated:

(a) Motor shaft

$$F_{Sm_r} = F_{Sm} + N_1 F_{S_1} + N_1 N_2 F_{S_2} + N_1 N_2 N_3 F_{S_3} + N_1 N_2 N_3 N_4 F_{S_t} \quad \ldots\ldots\ldots(180)$$

$$F_{Cm_r} = F_{Cm} + N_1 F_{C_1} + N_1 N_2 F_{C_2} + N_1 N_2 N_3 F_{C_3} + N_1 N_2 N_3 N_4 F_{C_t} \quad \ldots\ldots\ldots(181)$$

$$F_{Vm_r} = F_{Vm} + N_1^2 . F_{V_1} + N_1^2 . N_2^2 . F_{V_2} + N_1^2 . N_2^2 . N_3^2 . F_{V_3} + N_1^2 . N_2^2 . N_3^2 . N_4^2 . F_{V_t} \quad \ldots\ldots\ldots(182)$$

(b) First mesh;

$$F_{S_{1_r}} = F_{S_1} + N_2 F_{S_2} + N_2 N_3 F_{S_3} + N_2 N_3 N_4 F_{S_t} \quad \ldots\ldots(183)$$

$$F_{C_{1_r}} = F_{C_1} + N_2 F_{C_2} + N_2 N_3 F_{C_3} + N_2 N_3 N_4 F_{C_t} \quad \ldots\ldots(184)$$

$$F_{V_{1_r}} = F_{V_1} + N_2^2 . F_{V_2} + N_2^2 . N_3^2 . F_{V_3} + N_2^2 . N_3^2 . N_4^2 . F_{V_t} \quad (185)$$

(c) Second mesh;

$$F_{S_{2_r}} = F_{S_2} + N_3 F_{S_3} + N_3 N_4 F_{S_t} \quad \ldots\ldots(186)$$

$$F_{C_{2_r}} = F_{C_2} + N_3 F_{C_3} + N_3 N_4 F_{C_t} \quad \ldots\ldots(187)$$

$$F_{V_{2_r}} = F_{V_2} + N_3^2 . F_{V_3} + N_3^2 . N_4^2 . F_{V_t} \quad \ldots\ldots(188)$$

(d) Third mesh;

$$F_{S_{3_r}} = F_{S_3} + N_4 F_{S_t} \qquad \text{.....(189)}$$

$$F_{C_{3_r}} = F_{C_3} + N_4 F_{C_t} \qquad \text{.....(190)}$$

$$F_{V_{3_r}} = F_{V_3} + N_4^2 F_{V_t} \qquad \text{.....(191)}$$

The absolute values of load friction are used at the pinion gear/ turret mesh. In the digital simulation, the non-linear friction terms are multiplied by a real constant, FOFF, which is nominally set to unity. Setting FOFF to zero will cause the non-linear friction components to be removed, and will cause the effect of the stiction boundary in the motor friction characteristic to be removed, thereby linearising the friction characteristic throughout the system.

8.4 Torque generation

The engagement gap spacings at each gear mesh are given from eqs.(124) & (125), therefore:

(a) First mesh;

$$\theta s_1 = B_1 - (\theta_1 - N_1 . \theta_m) \qquad \text{.....(192)}$$

$$\theta s_2 = B_2 + (\theta_1 - N_1 . \theta_m) \qquad \text{.....(193)}$$

(b) Second mesh;

$$\theta s_3 = B_3 - (\theta_2 - N_2 . \theta_1) \qquad \text{.....(194)}$$

$$\theta s_4 = B_4 + (\theta_2 - N_2 . \theta_1) \qquad \text{.....(195)}$$

(c) Third mesh;

$$\theta s_5 = B_5 - (\theta_3 - N_3.\theta_2) \quad \text{.....(196)}$$

$$\theta s_6 = B_6 + (\theta_3 - N_3.\theta_2) \quad \text{.....(197)}$$

(d) Fourth mesh;

$$\theta s_7 = B_7 - (\theta_t - N_4.\theta_3) \quad \text{.....(198)}$$

$$\theta s_8 = B_8 + (\theta_t - N_4.\theta_3) \quad \text{.....(199)}$$

(e) Fifth mesh;

$$\theta s_9 = B_9 - (\theta_g - \theta_t) \quad \text{.....(200)}$$

$$\theta s_{10} = B_{10} + (\theta_g - \theta_t) \quad \text{.....(201)}$$

In the digital simulation, the initial conditions on the engagement gap spacings at each mesh, B_1, B_2 ,....B_{10} , are multiplied by a real constant, BOFF, which is nominally set to unity. By setting BOFF to zero removes the backlash at each mesh. Thus, by appropriate selection of either FOFF or BOFF, non-linear friction and backlash effects may be eliminated from the study independently, or complete linearisation may be achieved by setting both to zero.

The motor torque, T_m, is a declared constant in the digital simulation. The torque generated at each subsequent mesh, dependent upon the backlash condition, is given by:

(a)First mesh;

$$\begin{aligned} Tor_1 &= -K_{1_r}.\theta s_2 && \text{when } \theta s_2 \leqslant 0 \\ Tor_1 &= 0 && \text{when } \theta s_1, \theta s_2 > 0 \\ Tor_1 &= +K_{1_r}.\theta s_1 && \text{when } \theta s_1 \leqslant 0 \end{aligned} \quad \text{....(202)}$$

(b) Second mesh;

$$\begin{aligned} Tor_2 &= -K_{2_r}.\theta s_4 && \text{when } \theta s_4 \leqslant 0 \\ Tor_2 &= 0 && \text{when } \theta s_3, \theta s_4 > 0 \\ Tor_2 &= +K_{2_r}.\theta s_3 && \text{when } \theta s_3 \leqslant 0 \end{aligned} \qquad \ldots.(203)$$

(c) Third mesh;

$$\begin{aligned} Tor_3 &= -K_{3_r}.\theta s_6 && \text{when } \theta s_6 \leqslant 0 \\ Tor_3 &= 0 && \text{when } \theta s_5, \theta s_6 > 0 \\ Tor_3 &= +K_{3_r}.\theta s_5 && \text{when } \theta s_5 \leqslant 0 \end{aligned} \qquad \ldots.(204)$$

(d) Fourth mesh;

$$\begin{aligned} T_{tur} &= -K_{t_r}.\theta s_8 && \text{when } \theta s_8 \leqslant 0 \\ T_{tur} &= 0 && \text{when } \theta s_7, \theta s_8 > 0 \\ T_{tur} &= +K_{t_r}.\theta s_7 && \text{when } \theta s_7 \leqslant 0 \end{aligned} \qquad \ldots.(205)$$

(e) Fifth mesh;

$$\begin{aligned} Tor_{gun} &= -K_g.\theta s_{10} && \text{when } \theta s_{10} \leqslant 0 \\ Tor_{gun} &= 0 && \text{when } \theta s_9, \theta s_{10} > 0 \\ Tor_{gun} &= +K_g.\theta s_9 && \text{when } \theta s_9 \leqslant 0 \end{aligned} \qquad \ldots.(206)$$

The subsequent accelerations, velocities, and displacements are given by:

$$\alpha_m = (T_m - F_m)/I_{m_r} \qquad \ldots.(207)$$

$$w_m = \int_o^t \alpha_m dt \qquad \ldots.(208)$$

$$\theta_m = \int_o^t w_m \, dt \qquad \ldots.(209)$$

where F_m, dependent upon the conditions outlined in Chapter 4, is a function of the referred stiction, Coulomb, and viscous friction components. The motor angular displacement, θ_m, is then used as the input into the first gear mesh which results in the generation of the torque, Tor_1, in eq.(202).

The acceleration, velocity, and displacement of the output member arising from this torque are given by:

$$\alpha_1 = (Tor_1 - F_1)/I_{1_r} \quad .....(210)$$

$$w_1 = \int_o^t \alpha_1 \, dt \quad .....(211)$$

$$\theta_1 = \int_o^t w_1 \, dt \quad .....(212)$$

The output displacement, θ_1, is then the input into the second mesh, if shaft stiffness is assumed to be infinite, reulting in the generation of the torque, Tor_2, in eq.(203). The acceleration, velocity, and displacement of the output member arising from this torque are given by:

$$\alpha_2 = (Tor_2 - F_2)/I_{2_r} \quad .....(213)$$

$$w_2 = \int_o^t \alpha_2 \, dt \quad .....(214)$$

$$\theta_2 = \int_o^t w_2 \, dt \quad .....(215)$$

Similarly for the third mesh:

$$\alpha_3 = (Tor_3 - F_3)/I_{3_r} \quad .....(216)$$

$$w_3 = \int_o^t \alpha_3 \, dt \quad .....(217)$$

$$\theta_3 = \int_o^t w_3 \, dt \quad .....(218)$$

θ_3 is then the angular displacement of the pinion gear, ie the output displacement from the gearbox. The torque generated at the turret is then given by eq.(205), and the resulting acceleration, velocity and angular displacement are given by:

$$\alpha_{tur} = (T_{tur} - F_{tur})/I_t \quad .....(219)$$

$$w_{tur} = \int_o^t \alpha_{tur} \, dt \quad .....(210)$$

$$\theta_{tur} = \int_o^t w_{tur} \, dt \quad .....(211)$$

The acceleration, velocity, and angular displacement

of the gun, arising from the gun torque developed in eq.(206), are given by:

$$\alpha_{gun} = (Tor_{gun})/I_{gun} \qquad .....(212)$$

$$w_{gun} = \int_0^t \alpha_{gun}\, dt \qquad .....(213)$$

$$\theta_{gun} = \int_0^t w_{gun}\, dt \qquad .....(214)$$

In the elevation system there exists an out-of-balance torque at the gun rack. This out-of-balance torque is assumed only to exist when the system is in motion. The resulting angular acceleration of the gun in the elevation system is therefore:

$$\alpha_g' = (Tor_g + T_b - F_g)/ I_g' \qquad .....(215)$$

where Tor_g is the torque input to the gun from the elevation gearbox, T_b is the out-of-balance torque, and F_g is the gun friction.

The functional relationship used to model this out-of-balance torque is given by the graph shown in Figure 8.1, from which eq.(216) is obtained, ie.

$$T_b = 1500.\theta_g' + 200 \qquad .....(216)$$

T_b is in Nm and θ_g' in radians. It is emphasised here that the functional relationship chosen for the out-of-balance torque of the gun is merely representative: it does not represent a true function, such being unknown to the author. The relationship used assumed that the range of deflection angle for the gun was from -7.5° to $+20^{\circ}$.

Note that there is no gun friction in eq.(212) and that the friction values F_1, F_2, F_3, etc., are functions of

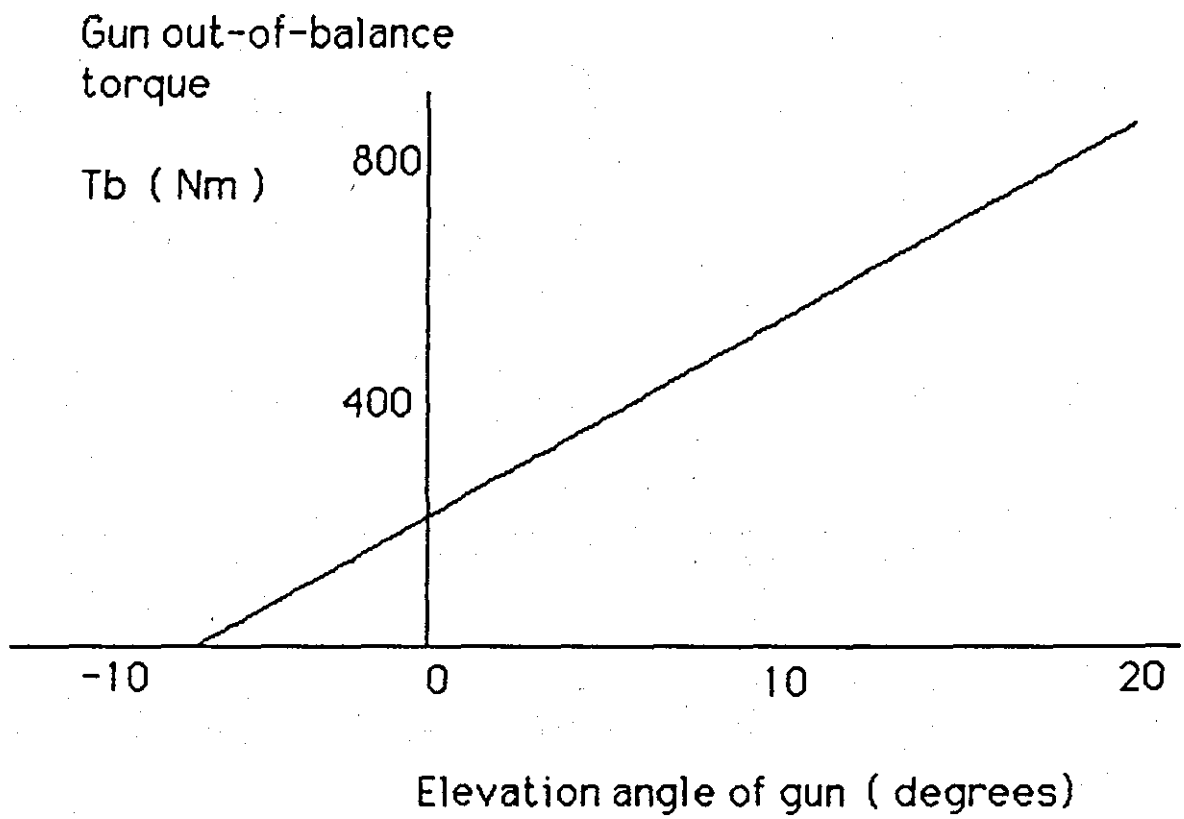

Figure 8.1 : Out-of-balance torque due to elevation of gun

the friction characteristics in eq.(183) to eq.(191), dependent on the conditions outlined in Chapter 4.

The above relationships define the basic traverse gun drive system in the digital simulation. However, in open-loop analysis, these provide no indication of system performance, and therefore the variable $Perr_i$ is defined:

$$Perr_i = (\theta_m.N_i)-\theta_i \qquad .....(217)$$

where the product $\theta_m.N_i$ gives the ideal angular displacement at a point in the gearbox.

Thus $Perr_i$ gives the error between the achieved and ideal displacement at any point in the gearbox, ie.

$$Perr_1 = (\theta_m.N_1)-\theta_1 \qquad .....(218)$$

$$Perr_2 = (\theta_m.N_1.N_2)-\theta_2 \qquad .....(219)$$

$$Perr_3 = (\theta_m.N_1.N_2.N_3)-\theta_3 \qquad .....(220)$$

$$Perr_t = (\theta_m.N_1.N_2.N_3.N_4)-\theta_{tur} \qquad .....(221)$$

$$Perr_g = (\theta_m.N_1.N_2.N_3.N_4)-\theta_{gun} \qquad .....(222)$$

The effects of turret eccentricity can also be studied by the inclusion of the appropriate function which varies the gear ratio, N_4, with angular position. As an example of this the case is considered where the turret ring is assumed to be elliptical. Consequently, the effective radius of the turret, R_t, varies with angular position, as represented by:

$$R_t = \sqrt{(A.\sin\theta_t)^2+(B.\cos\theta_t)^2} \qquad .....(223)$$

where A and B are the major and minor axes of the ellipse.

The gear ratio, N_4, is then given by:

$$N_4 = \frac{Rp}{R_t} \qquad .....(224)$$

where R_p is the radius of the pinion gear.

8.5 Simulation of closed-loop gun positioning system

A simple control law was developed for the positioning of the gun in its traverse drive mode. Under closed-loop conditions the motor torque is controlled via a 3-term controller as shown in Figure 8.2. This controller had the following gains:

$$G_1 = 9.0 \qquad .....(225)$$

$$G_2 = 0.001 \qquad .....(226)$$

$$G_3 = -7.0 \qquad .....(227)$$

The input to the closed-loop simulation is the required azimuth position of the turret, ie. θ_{td} . The angular error, θ_e, arising from a step demand in turret position is therefore:

$$\theta_e = \theta_{td} - \theta_{tur}' \qquad .....(228)$$

where θ_{td} , and θ_{tur}' are in degrees.

Consequently:

$$T_m = G_1 . \theta_e + G_2 . \int_o^t \theta_e \, dt + G_3 . W_t' \qquad ...(229)$$

where w_t' is turret angular velocity, deg./s.

8.6 The simulation programs

The listing of the ACSL programs which simulate the gun drive systems are given in Appendix 2 , for the traverse drive system, and in Appendix 3 , for the elevation drive system. The integration method used was Gear's stiff method

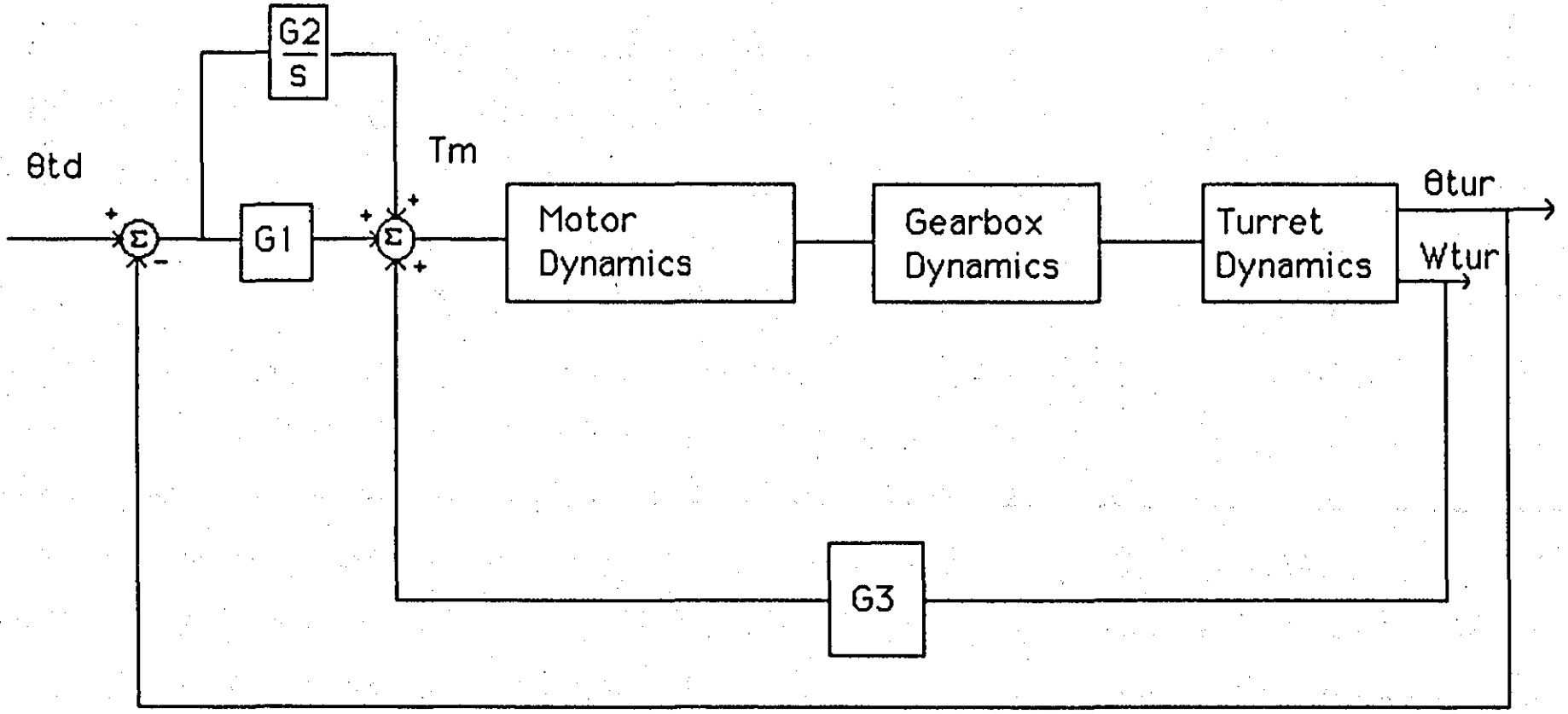

Figure 8.2 : Closed-loop traverse system

which is outlined in Appendix 1. The integration parameters used throughout the study were:

CINT - communication interval, set at 0.001s

NSTP - defines the initial calculation interval, c, in terms of the communication interval, such that:

$$c = CINT/NSTP$$

NSTP has been set at 10

MERROR - relative error bound for individual, defined state variables. All relative error bounds were set at 0.1.

XERROR - absolute error bound for individual state variables. All absolute error bounds were set at 0.1.

CHAPTER 9 RESULTS OF THE DIGITAL SIMULATION

In this chapter results of the digital simulations are presented for the traverse and elevation gun drive models of a modern M.B.T. Although any of the gearbox characteristics can be studied, the results have been limited for reasons of space and clarity. The following characteristics are therefore presented and discussed to illustrate the performance of the gun drive systems under open-loop conditions.

(1) torque generation at each mesh;

(2) velocity under conditions of collision-engagement;

(3) the pointing error associated with each mesh;

The main purpose of the research work was to investigate the effects of non-linear friction and backlash on the dynamic performance of the drive systems. However, results are also presented illustrating the effects of finite gear and shaft stiffnesses, and the effects of the load dynamics. The predominant feature for open-loop conditons is the dependence of torque generation upon the backlash condition at each mesh, and in particular the effect of the initial backlash condition on pointing error. The effects of non-linear friction, particularly the Coulomb component, are not significant until the models are operated under closed-loop conditions.

With reference to Chapter 6 the range of conditions on backlash for all meshes is as follows:

(a) di=0% ie. as an initial condition all gears are fully unmeshed in the direction of rotation.

(b) di=100% ie. as an initial condition all gears are fully meshed in the direction of rotation.

(c) di=50% ie mid-way between conditions (a) and (b).

The above conditions also apply to the pinion-turret mesh and the gun/turret interface.

9.1 Traverse gun drive system under open-loop conditions

Figure 9.1 shows the torque, collision-engaged velocity, and pointing error of the system resulting from a step input motor torque of 46 Nm, with di set to 0%. The effects of shaft stiffness have been ignored, ie. the shafts have been assumed to be infinitely stiff. The peak torque levels at each mesh are greater than would be expected from consideration of the gear ratios alone, as is illustrated in Table 9.1.

	Gear ratio	Ideal torque (Nm)	Peak torque (Nm)
First mesh	2.697	124	442
Second mesh	4.050	502	1,615
Third mesh	4.170	2,095	16,154
Pinion/turret	18.290	37,710	169,231
Turret/gun	1.000	37,710	20,769

TABLE 9.1

These higher peak torque levels are due to the impulse torques generated on collision engagement of the gears.

The effect of backlash on torque generation is clearly seen, particularly at the first mesh, resulting in the form of torque generation as shown, with zero levels of torque indicating that the gear pair have become unmeshed. The presence of backlash allows the gears to come into and out-of-mesh with a frequency dependent upon the effective stiffness and inertia at the mesh. This effect is particularly noticeable when the first gear pair become unmeshed for a substantial period of the simulation run. This period of non-engagement is followed by another period of collision-engaged torque activity, which is itself reflected in the torque generated at the second mesh. These high frequency components are filtered out by the subsequent lower frequency meshes. The oscillatory nature of the torque is due to low contact friction between the engaging surfaces, which results in poor damping. The peak torques throughout the rest of the system occur during the initial collision-engagement of the gears, and, with greater damping than for the first mesh, the torque amplitudes decay quickly. With higher effective inertias on the output members, the frequency of meshing is decreased through the gearbox, as predicted from the linear analysis.

Although not shown in Figure 9.1, the velocity of the motor at the end of the simulation run was 332 rad/s. A comparison between the subsequent collision-engaged velocities, obtained from Figure 9.1, and the ideal velocities resulting from a consideration of the gear ratios, is shown in Table 9.2. The mesh efficiency is defined as the ratio of the collision-engaged velocity to the ideal velocity.

	Gear ratio	Velocity (rad/s) Ideal	/ Collision-engaged	Mesh efficiency
w1	2.697	123.10	121.5	98.7%
w2	4.05	30.39	30.0	98.7%
w3	4.17	7.29	6.9	94.7%
wtur	18.29	0.40	0.39	97.5%
wgun	1.00	0.40	0.39	100.0%

TABLE 9.2

It can be seen that the collision-engaged velocities are close to the ideal values, taking into account losses in the gearbox, and therefore the mean torque at each mesh must also be close to ideal. This indicates that the gearbox model is functioning correctly as a speed and torque converter.

The stepped turret velocity is a result of the

collision-engagement of the pinion gear with the turret ring, with constant turret velocity during periods of non-engagement. This effect is transmitted through to the gun, resulting in a low frequency vibration as a consequence of representing the gun as a lumped inertia.

Figure 9.2 and 9.3 show the effect of the initial conditions on backlash on torque generation , with di set to 50% and 100% respectively. The effect of the stepped turret velocity disappears when the gears are initially meshed, as the pinion gear and the turret are no longer collision-engaged. As would be expected from such open-loop operation, the initial backlash condition predominates in controlling the pointing error at each mesh. The form of the pointing error follows closely that of the associated torque, ie higher frequencies are observed at the early meshes. This is due to the torque itself being a function of the relative gear angles. A comparison between the pointing error of the turret arising from the change in the initial backlash condition is shown in Table 9.3.

di	Turret Pointing Error (millirad)
0%	0.90
50%	0.46
100%	0.0077

TABLE 9.3

From Table 9.3 it can be seen that the pointing accuracy of the turret increases as the initial backlash decreases in the direction of rotation.

Figures 9.4, 9.5, and 9.6 are for the same conditions as the previous figures, but with the inclusion now of finite shaft stiffnesses. The shafts themselves are then able to twist, and in doing so produce an extra angular loss during periods of high torque activity. This results in the increased dynamic pointing errors being shown. The dynamic twisting of the shafts also influences the torque generation at each mesh for they absorb and release energy, thus controlling the angular input into each mesh. The effects of finite shaft stiffnesses couple strongly with the gun dynamics assumed. A more detailed gun model, with the inclusion of higher barrel frequencies, would result in improved responses.

Figure 9.7 shows the torque generation, velocity, and pointing error of the linearised system to a motor torque step input of 46 Nm. In this case, therefore, the backlash is zero at each mesh, and the friction is wholly viscous. In addition, the shaft stiffnesses are assumed infinitely stiff. The form of torque generation in the linearised model is similar to that arising from the non-linear model when the gears are initially meshed, and the resulting pointing error of the turret is identical. Although the simulation was terminated at 3 seconds, it is evident from both Figure

9.3 and Figure 9.7, that the pointing error of the turret is tending to zero in both cases.

Figure 9.8 shows results for the linearised model, but with the inclusion of finite shaft stiffnesses. The inclusion of finite shaft stiffnesses results in increased torque activity at the third mesh, and and increased damping of the turret torque. In addition, the pointing error activity in the the rest of the system is reduced.

The above sets of results show how the dynamic performance of the system, whether linear or non-linear, is affected by the inclusion of finite shaft stiffnesses. This leads to the conclusion that the shafts are not stiff enough, particularly for torque levels produced from collision-engagement of the gears. In the remainder of the results presented for the traverse drive, under open-loop conditions, it has been assumed that the shafts are infinitely stiff, and it has been taken that the gears are fully unmeshed as an initial condition, ie di=0%, as this represents the 'worst case' for the system.

Figure 9.9 shows the effect of increased turret stiffness on performance. The stiffness of the turret has been increased to $4.0*10^{9}$ Nm/rad. Comparing Figure 9.9 with Figure 9.1, it can be seen that the frequency of the turret is increased, as would be predicted from a linear analysis. This increase in frequency results in the pinion gear and turret ring becoming unmeshed less frequently than

previously, and therefore a smoother generation of velocity is obtained. Although the pointing error of the turret settles to the same value as previously, the decreased time to settle would be beneficial under closed-loop conditions.

Figures 9.10 shows the effect of turret ring eccentricity on performance. The diameter of the conventional, circular, turret ring is 2.0 m. In this case, the turret ring is assumed to have been elliptical, with major and minor axes set to 2.10 m and 2.0 m, respectively. The effect on performance is only clearly seen in the turret velocity. Comparing Figure 9.10 with Figure 9.1, the turret reaches speed more quickly, although this 'steady' speed will undergo fluctuations as the gear ratio is changed by the effective change in turret radius with angular position. This final velocity of the turret is now reduced to 0.34 rad/s as compared with the 0.39 rad/s previously. Fluctuations in turret velocity due to eccentricity of the turret ring may cause problems in closed-loop position control, if turret velocity were to be used in the feedback path.

Figure 9.11 shows the problems encountered when attempting to use the fixed-step, second-order, Runge Kutta algorithm. The response is 'noisy' due to the inability of the integration method to deal with the 'stiff' modelling equations.

9.2 Elevation gun drive system under open-loop conditions

As the elevation system is similar to the traverse system, and the same considerations apply to the effects of the non-linearities and finite shaft stiffnesses on system performance, results are presented merely to show the effects of tne out-of-balance torque. The simulation runs were terminated at gun angles corresponding to the gun limit stops, ie -7.5°, $+20^{\circ}$.

Figure 9.12 shows the torque generation, collision-engaged, velocity, and pointing error of the system to a step motor torque input of 15 Nm, ie. gun elevating. Figure 9.13 shows the torque generation, collision-engaged velocity, and pointing error of the system to a step motor torque of -15 Nm, ie gun depressing. In both cases the effects of finite shaft stiffnesses have been included, and the initial condition on backlash for both is identical, with di set to 50%. Clearly the effects of shaft stiffnesses are not as pronounced as in the traverse system, due to the lower torque levels through the system. It must be remembered that the first two meshes have gear ratios greater than unity, and therefore the torque is reduced through them. The effect of the out-of-balance torque is clearly seen. The effect is to increase the effective torque during gun elevation, and to decrease it during gun depression. The offset of the effective gun torque is clearly seen, decreasing with time for gun depression, and

increasing with time for gun elevation. The low frequency of the gun is again due to its representation as a lumped inertia. This low frequency results in a pulsing of the gun torque resulting in the stepped gun velocity obtained.

9.3 Traverse gun drive system under closed-loop conditions

Figure 9.14 shows the response of the turret to step input demands of turret angle, for a range of initial conditions, using the control law discussed in Chapter 8. The control law was developed for the linearised system, and subsequently used to study the effects of the non-linearities on performance. In the closed-loop study, the developed motor torque has not been limited, although the motor is known to have a maximum torque rating of 46 Nm. The advantage of this is that the performance of the closed-loop system is then dictated by the performance of the gearbox itself. The demanded turret azimuth position was 20° in all cases.

Figure 9.14(a) shows the response of the turret when the system is linearised. It can be seen that there is no steady-state pointing error of the system.

Figure 9.14(b) shows the response of the turret with the inclusion of the nominal backlash values, but still with linear friction. It can be seen that the response of the turret is identical, with no steady-state pointing error.

Figure 9.14(c) shows the response of the turret with

increased system backlash. The backlash at each mesh is ten times greater than the nominal values. The response of the system is again identical. This indicates that, providing there is no non-linear friction present, the motor can develop enough torque to overcome the errors due to backlash in the system. The damping of the system may be affected by further increasing the backlash, and excessive backlash may result in limit cycling, dependent upon the level of viscous friction in the system, although this effect has not been studied. Backlash-friction curve theory (ref.1) outlines empirical relations for calculating the amount of backlash that a servomechanism can withstand without a null oscillation.

Figure 9.14(d) shows the response of the turret with the inclusion of the non-linear friction characteristics, in addition to backlash. The pointing error at the end of the simulation run was -0.47^{o}.

Figure 9.14(e) shows the response of the turret with increased system Coulomb friction. The Coulomb friction at each mesh, and at the motor, is five times that of the nominal values. The pointing error at the end of the simulation run was -1.25^{o}.

Providing that the backlash at each mesh is not excessive, the digital simulation predicts that it is the non-linear friction in the system, particularly the Coulomb component, that is the limiting factor for the performance

of the system under closed-loop conditions.

9.4 Summary of digital simulation conditions

	System	initial condition on gears (di)	shaft stiffness
Case A:	Traverse	0%	removed
Case B:	Traverse	50%	removed
Case C:	Traverse	100%	removed
Case D:	Traverse	0%	finite
Case E:	Traverse	50%	finite
Case F:	Traverse	100%	finite
Case G:	Traverse	removed	removed
Case H:	Traverse	removed	finite
Case I:	Traverse	as Case A: increased turret stiffness	
Case J:	Traverse	as Case A: elliptical turret ring	
Case K:	Traverse	as Case A: Runge Kutta integration	
Case L:	Elevation	50% (elevating)	finite
Case M:	Elevation	50% (depressing)	finite
Case N:	Traverse: closed-loop, linear system		
Case O:	Traverse: closed-loop, plus nominal backlash		
Case P:	Traverse: closed-loop, plus increased backlash		
Case Q:	Traverse: closed-loop, full non-linear system		
Case R:	Traverse: closed-loop, increased Coulomb friction		

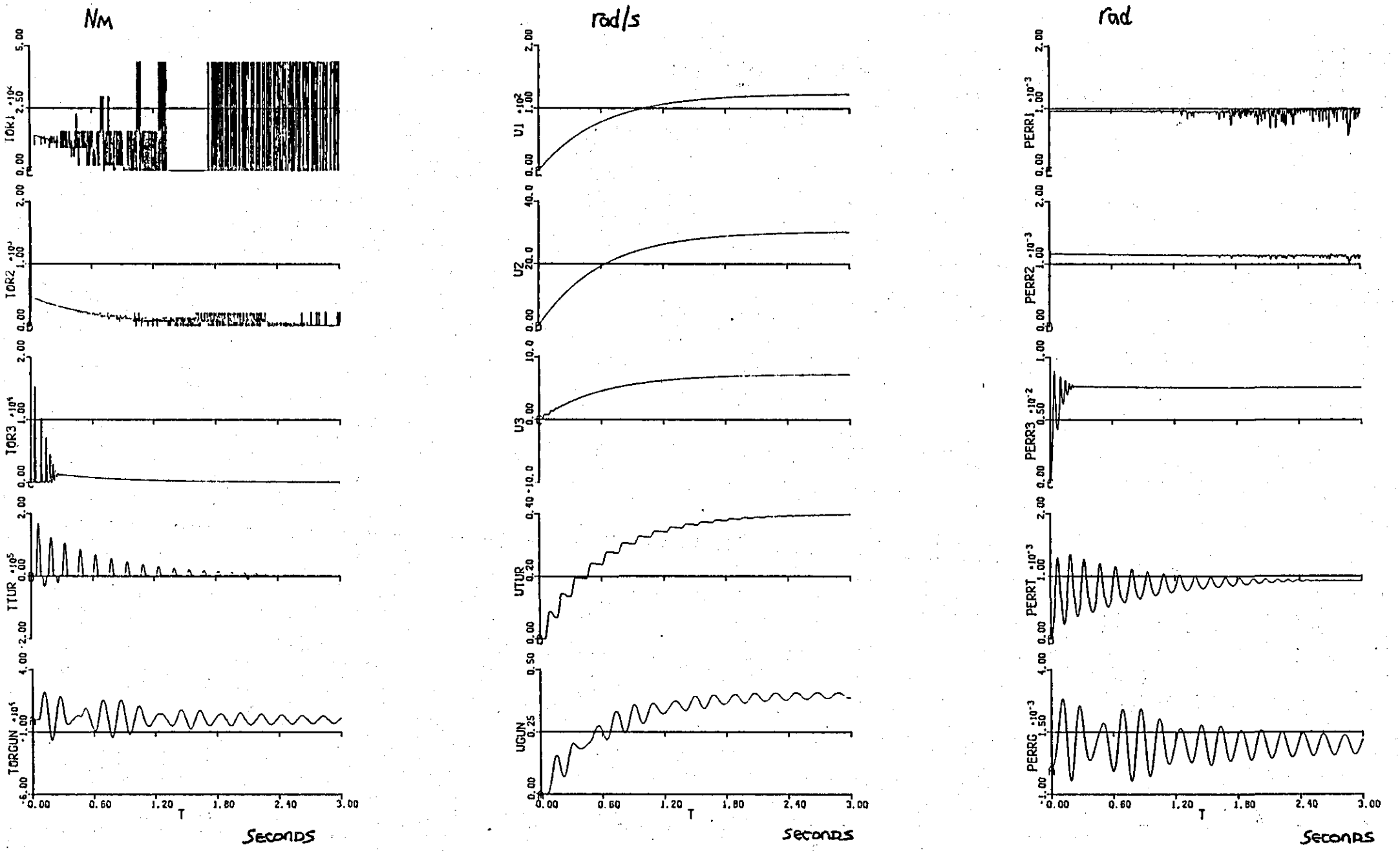
Nm
rad/s
rad
TOR1 ·10⁴
TOR2 ·10⁴
TOR3 ·10⁴
TTUR ·10⁵
TORGUN ·10⁵
U1 ·10²
U2
U3
UTUR
UGUN
PERR1 ·10⁻³
PERR2 ·10⁻³
PERR3 ·10⁻²
PERRT ·10⁻³
PERRG ·10⁻³
T
Seconds

Fig. 9·1: CASE A

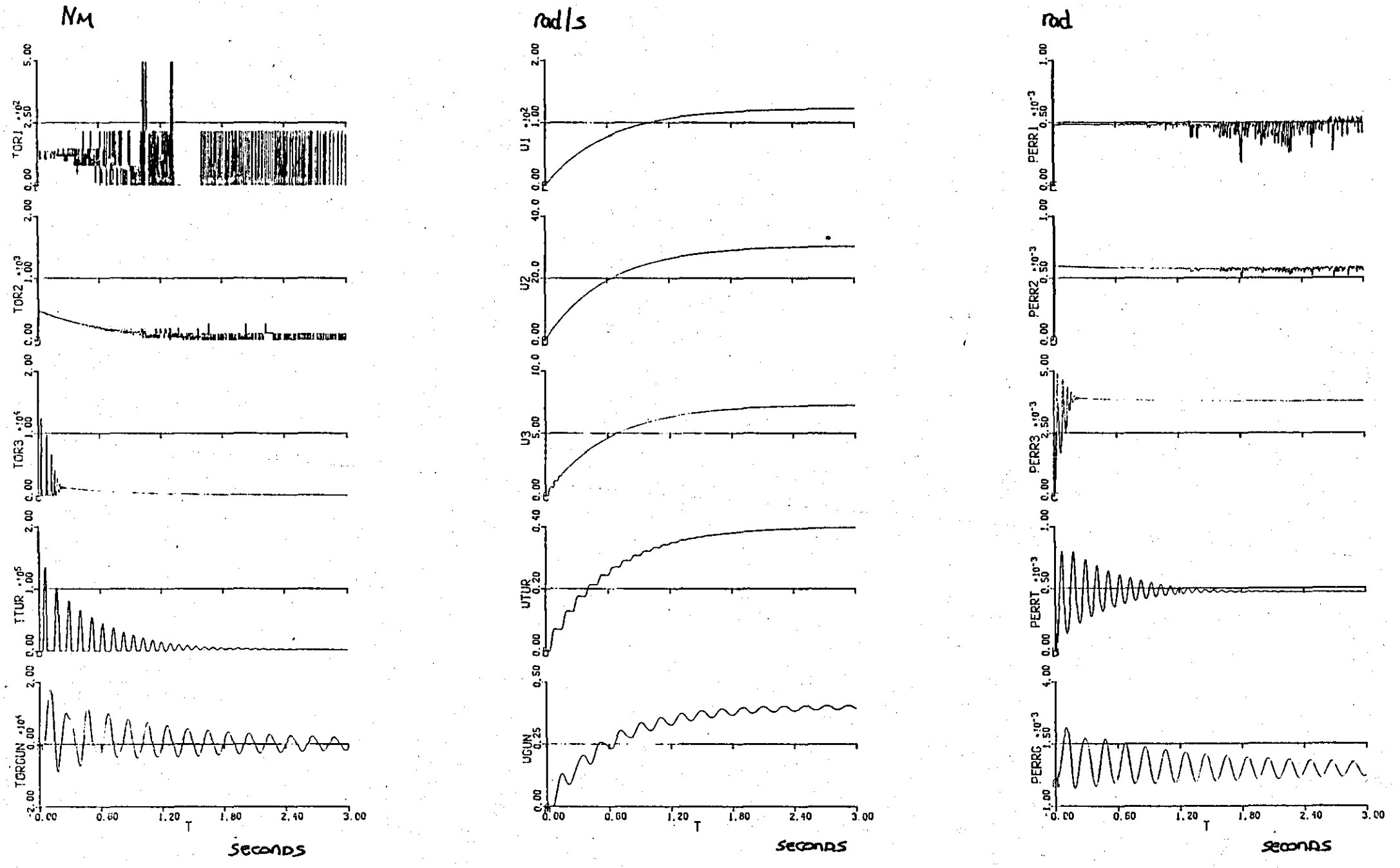
Nm
rad/s
rad
TOR1 ·10²
TOR2 ·10³
TOR3 ·10⁴
TTUR ·10⁵
TORGUN ·10⁴
U1 ·10²
U2
U3
UTUR
UGUN
PERR1 ·10⁻³
PERR2 ·10⁻³
PERR3 ·10⁻³
PERRT ·10⁻³
PERRG ·10⁻³
T
seconds

Fig. 9·2: CASE B

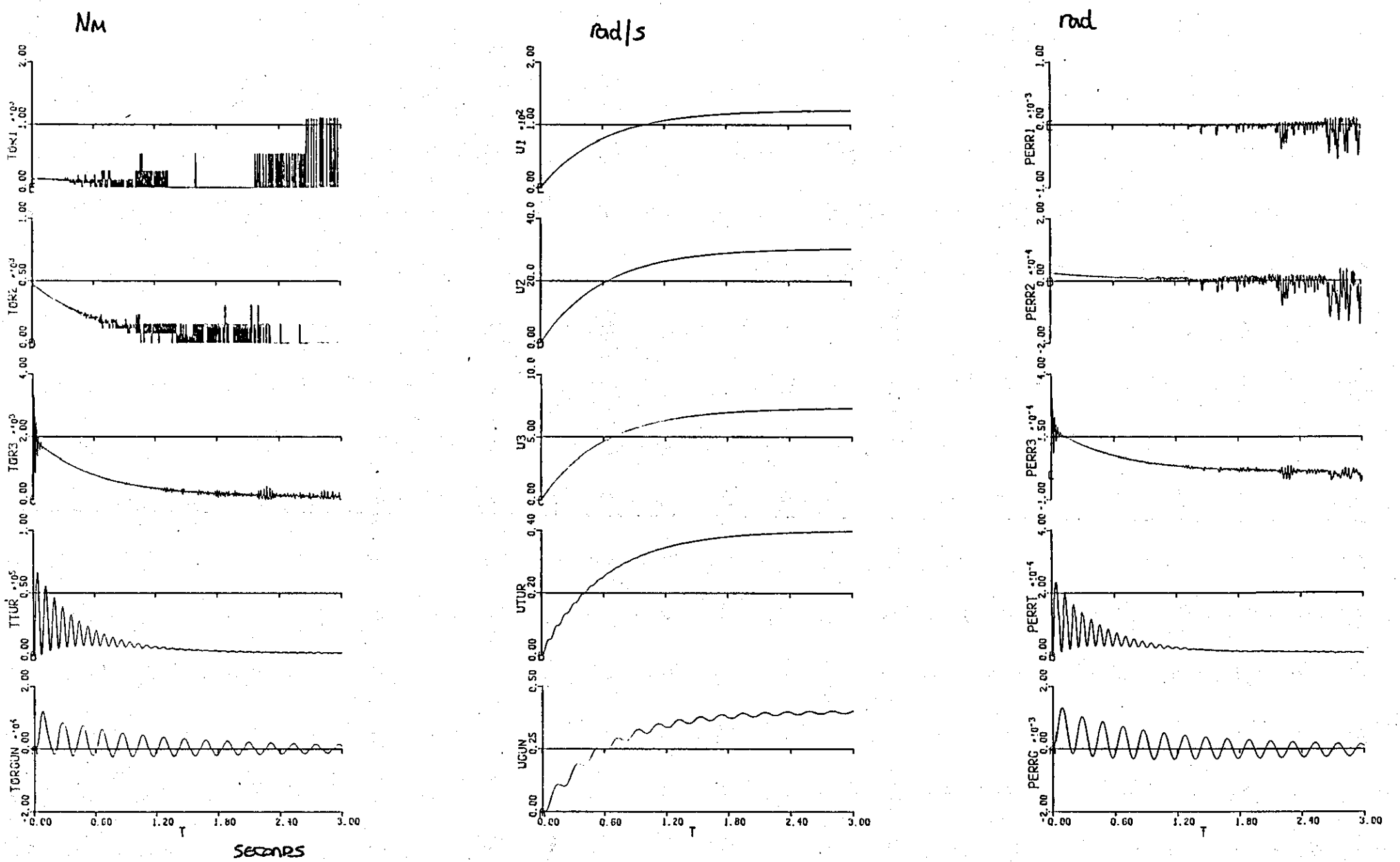
Nm
rad/s
rad
TGR1 ·10³
TGR2 ·10³
TGR3 ·10³
TTUR ·10⁵
TØRGUN ·10⁴
U1 ·10²
U2
U3
UTUR
UGUN
PERR1 ·10⁻³
PERR2 ·10⁻⁴
PERR3 ·10⁻⁴
PERRT ·10⁻⁴
PERRG ·10⁻³
T
Seconds

Fig. 9·3: CASE C

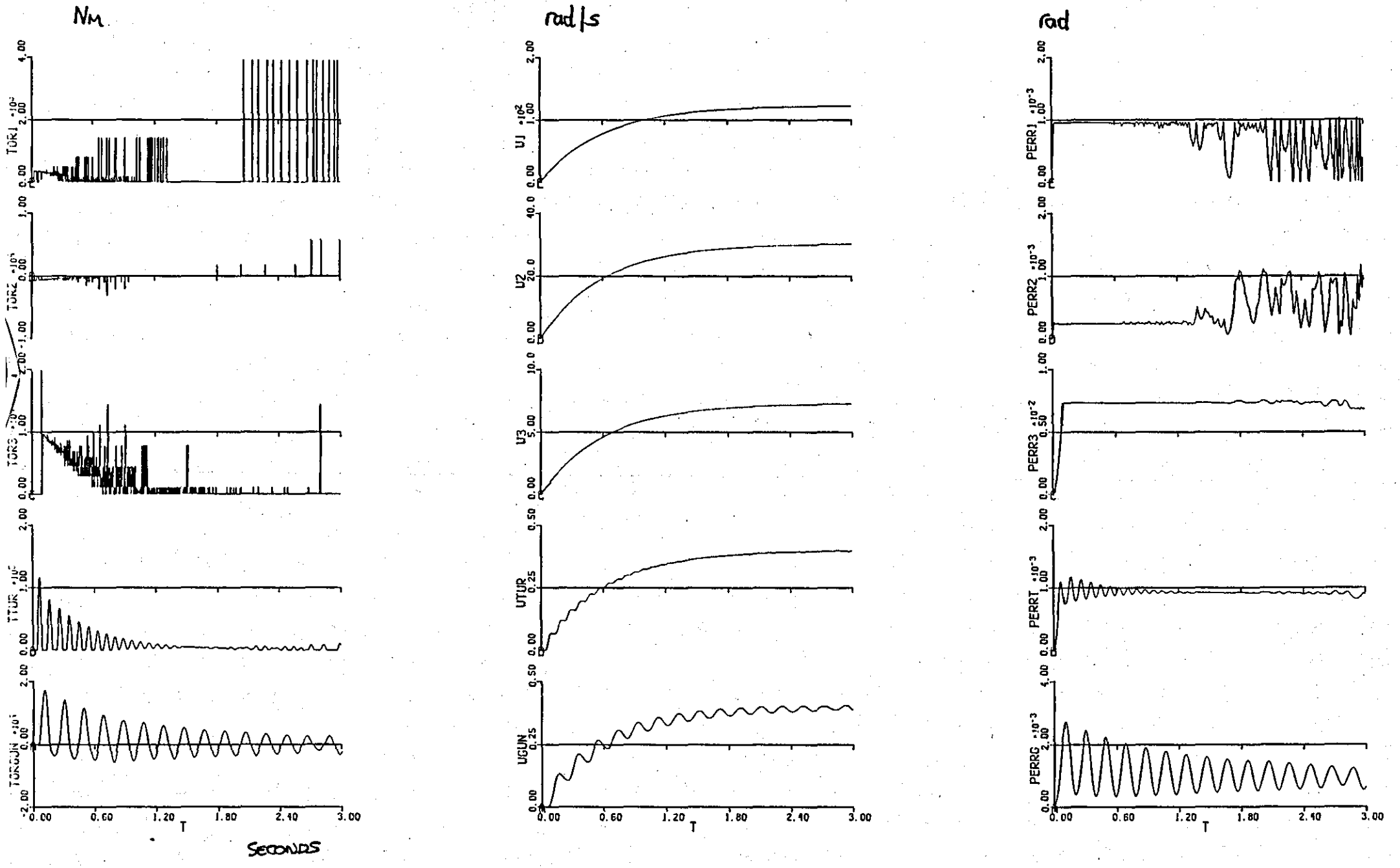
Nm
rad/s
rad
TORJ
TORG
TTUR
TORGUN
UJ
U2
U3
UTUR
UGUN
PERRJ
PERR2
PERR3
PERRT
PERRG
T
Seconds

Fig. 9·4: CASE D

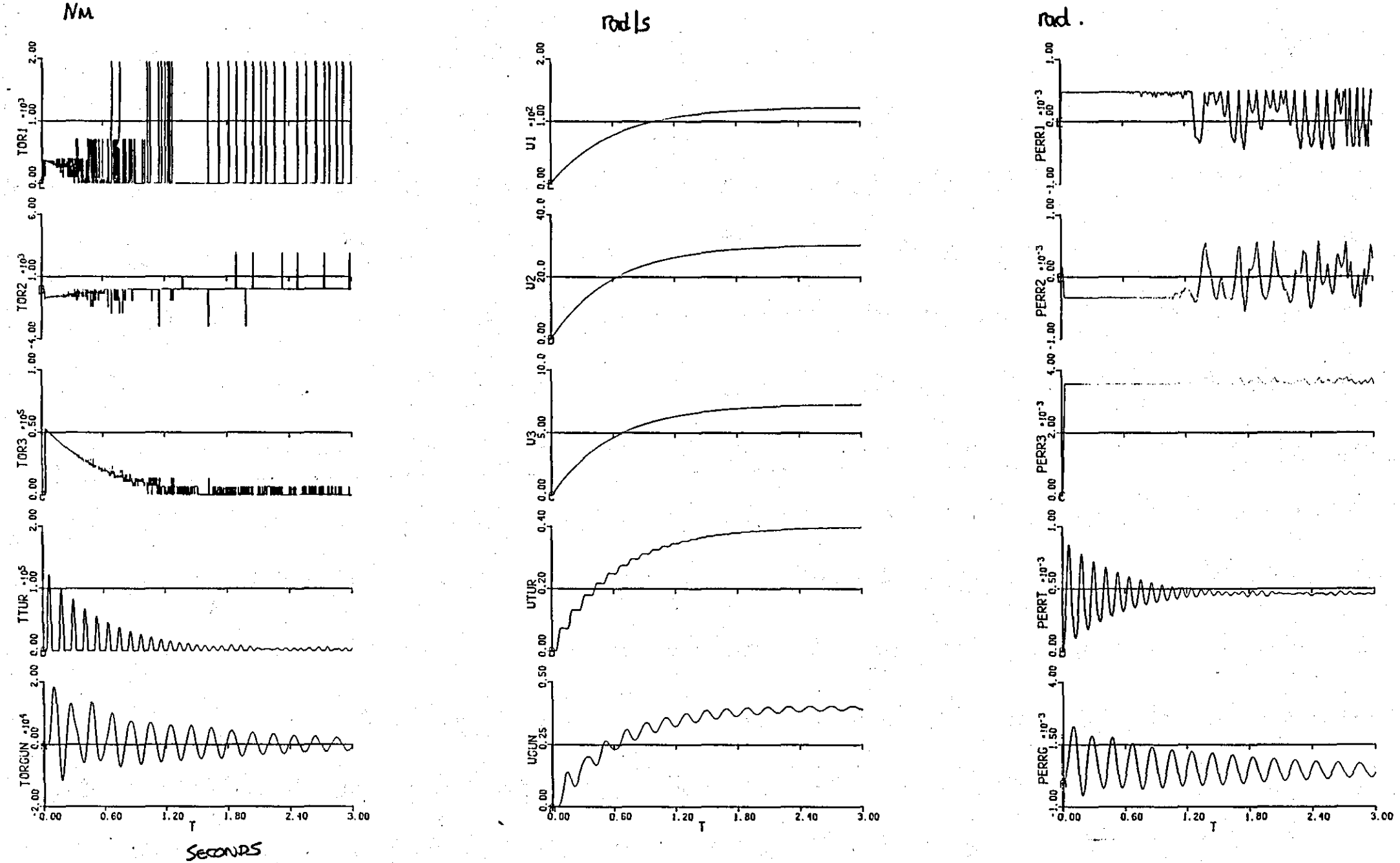
Nm
rad/s
rad.
TORJ
TOR2
TOR3
TTUR
TORGUN
U1
U2
U3
UTUR
UGUN
PERRJ
PERR2
PERR3
PERRT
PERRG
T
Seconds

Fig. 9·5: CASE E

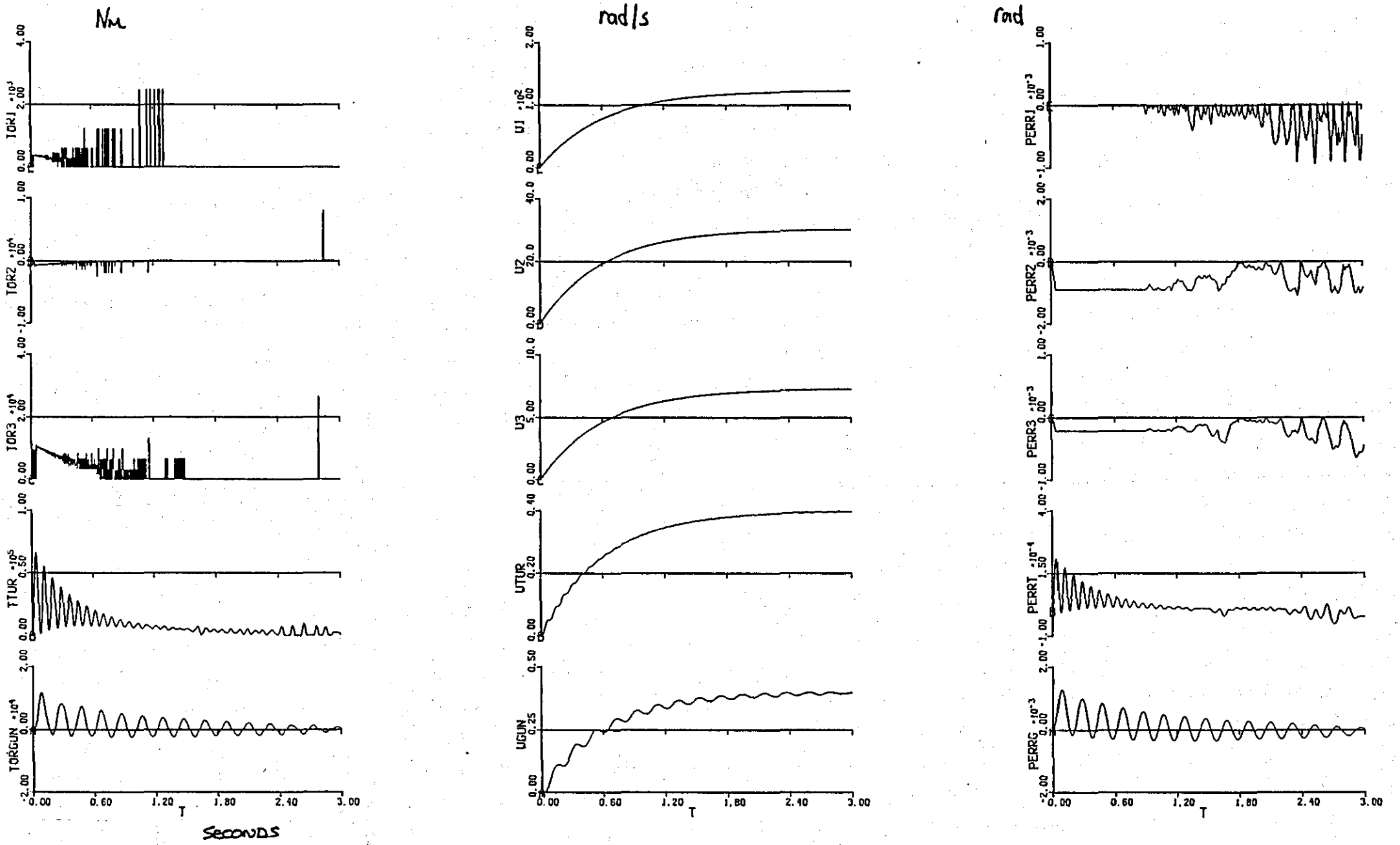
Nm
rad/s
rad
TOR1 ·10³
TOR2 ·10⁴
TOR3 ·10⁴
TTUR ·10⁵
TORGUN ·10⁴
U1 ·10²
U2
U3
UTUR
UGUN
PERR1 ·10⁻³
PERR2 ·10⁻³
PERR3 ·10⁻³
PERRT ·10⁻⁴
PERRG ·10⁻³
T
Seconds

Fig. 9.6. CASE F

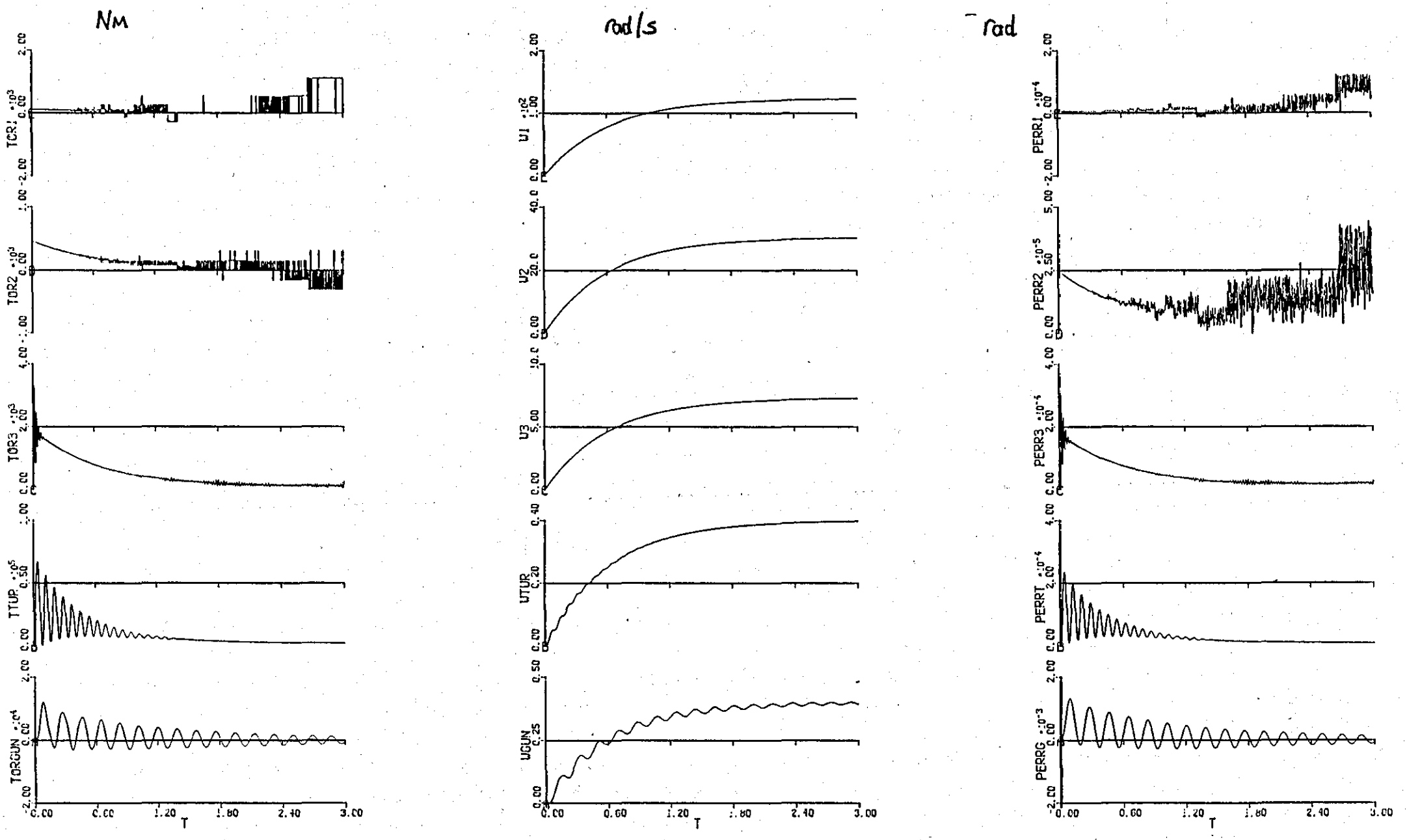
Nm
rad/s
rad
TCR1
TOR2
TOR3
TTUP
TORGUN
U1
U2
U3
UTUR
UGUN
PERR1
PERR2
PERR3
PERRT
PERRG
T
Seconds

Fig. 9·7 : CASE G

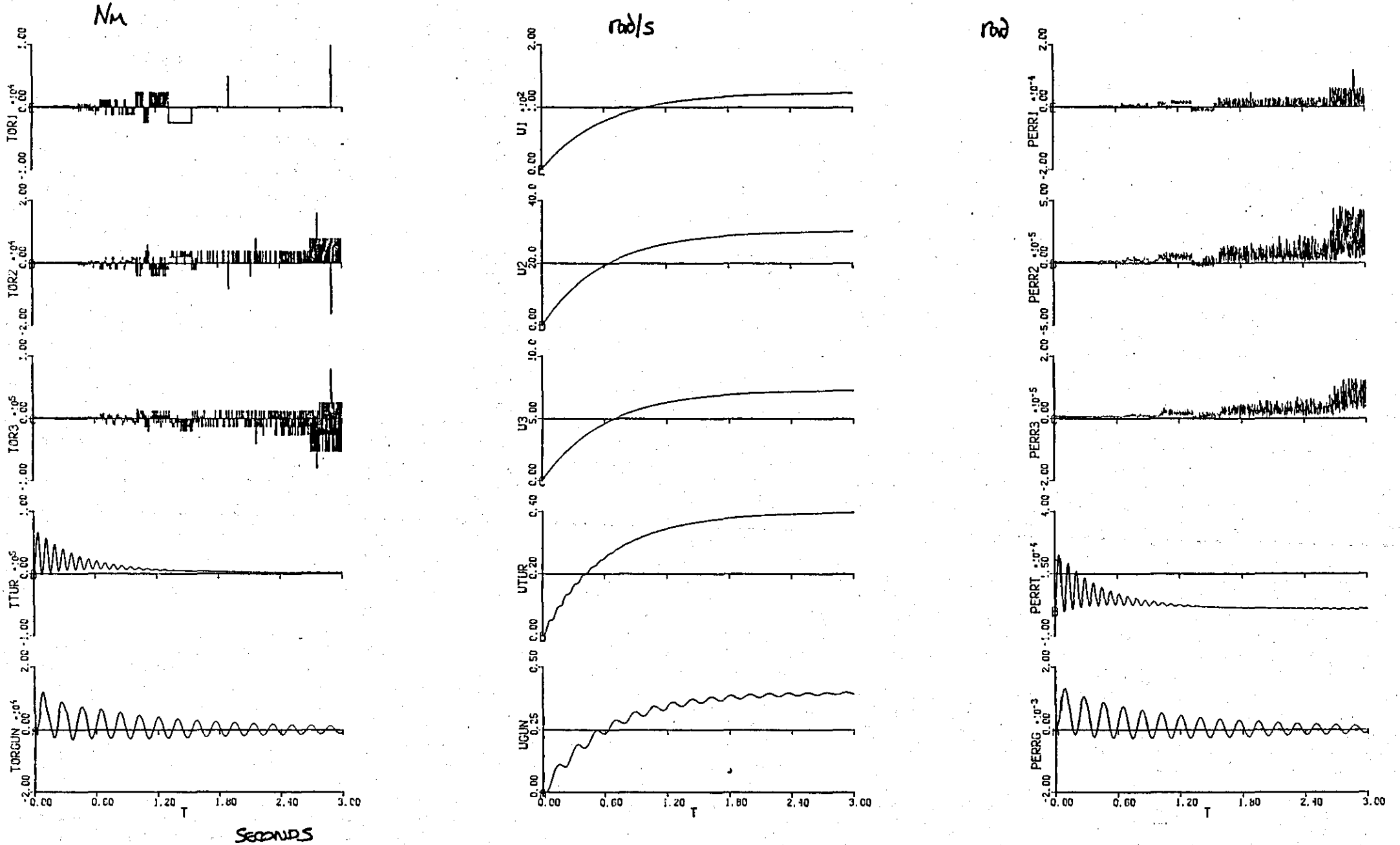
Nm
rad/s
rad
TORJ
TOR2
TOR3
TTUR
TORGUN
U1
U2
U3
UTUR
UGUN
PERRJ
PERR2
PERR3
PERRT
PERRG
T
SECONDS

Fig. 9·8 : CASE H

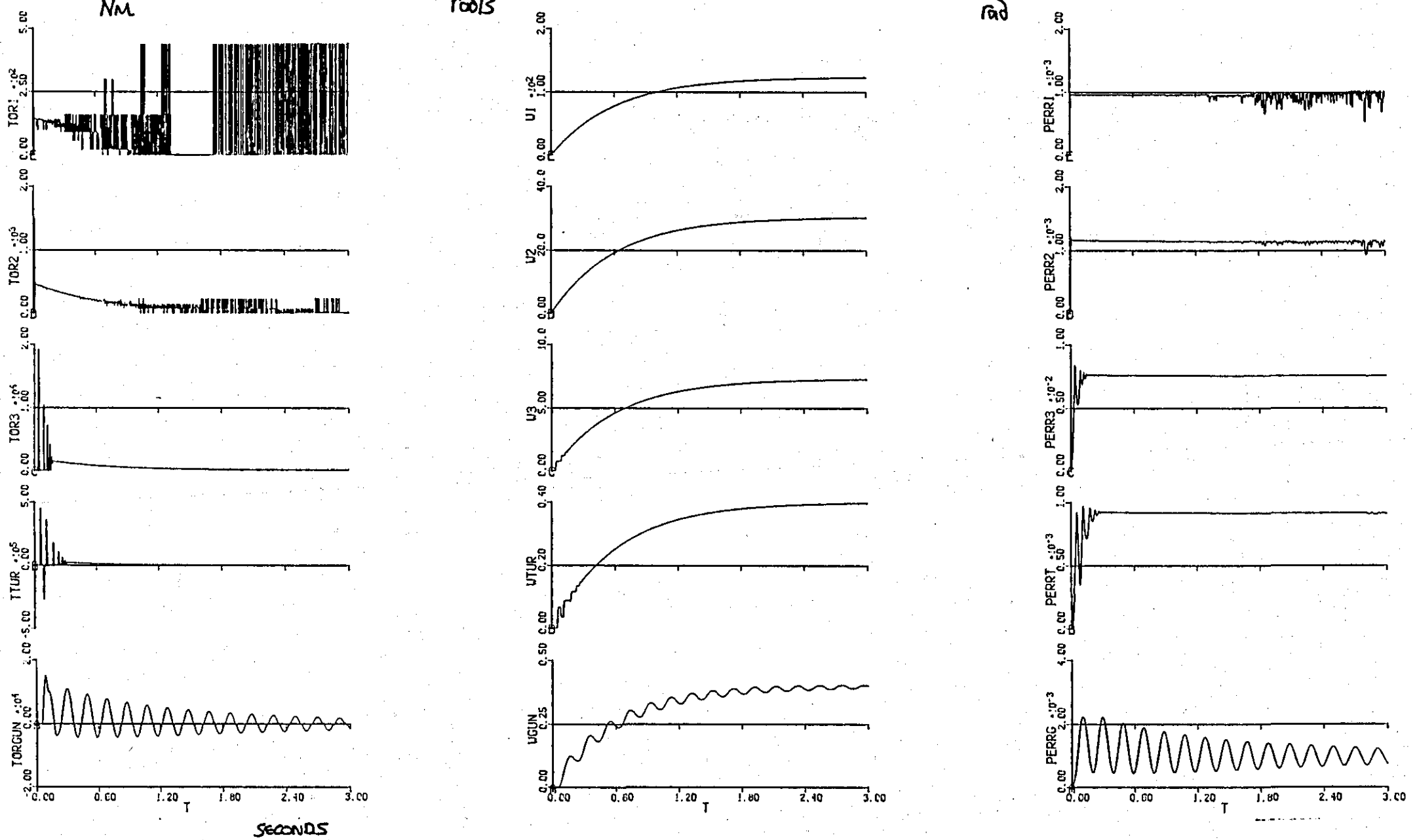
Nm
rad/s
rad
TOR1 *10^2
TOR2 *10^3
TOR3 *10^5
TTUR *10^5
TORGUN *10^4
U1 *10^2
U2
U3
UTUR
UGUN
PERR1 *10^-3
PERR2 *10^-3
PERR3 *10^-2
PERRT *10^-3
PERRG *10^-3
T
seconds

Fig. 9·9 : CASE I

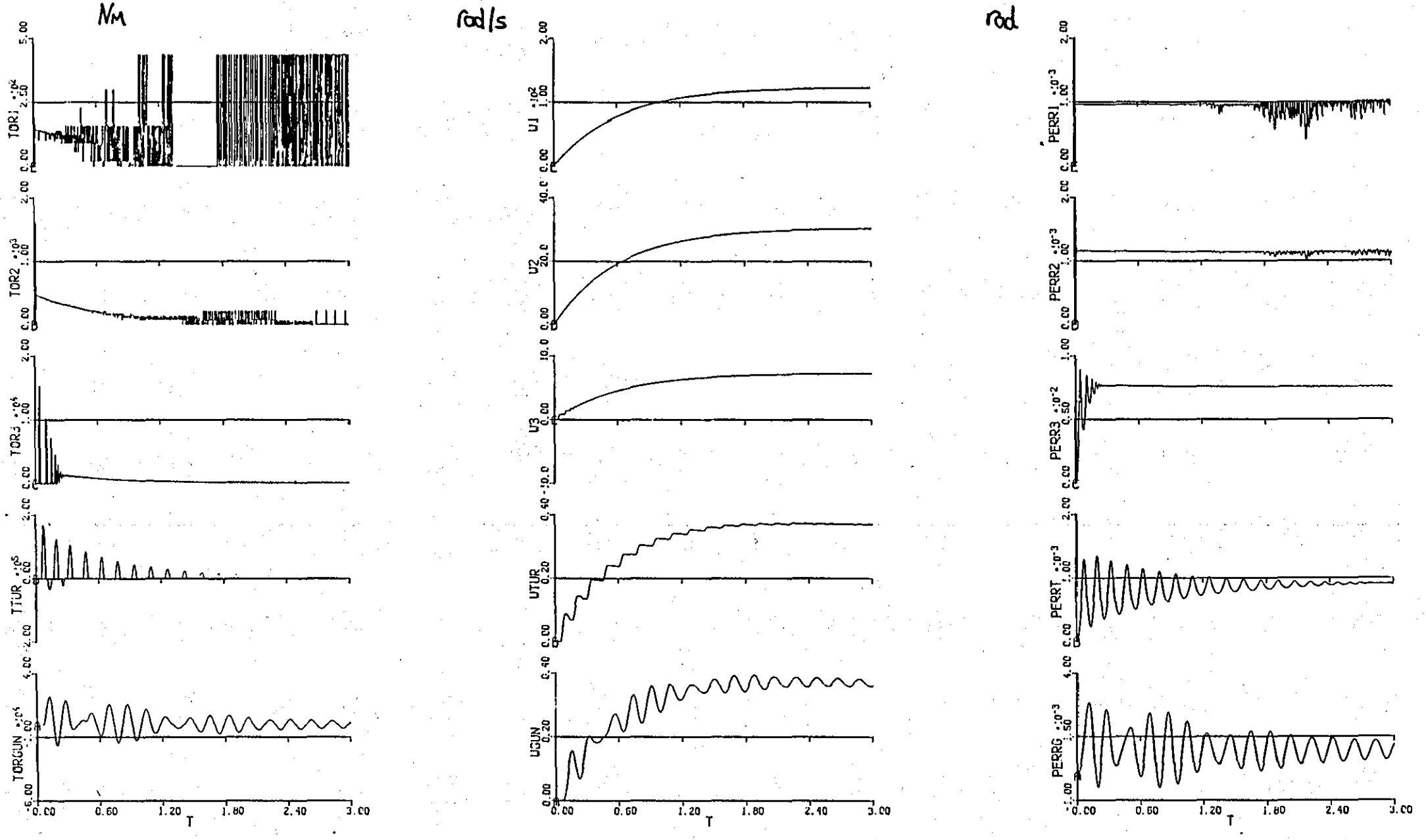

Fig. 9·10: CASE J

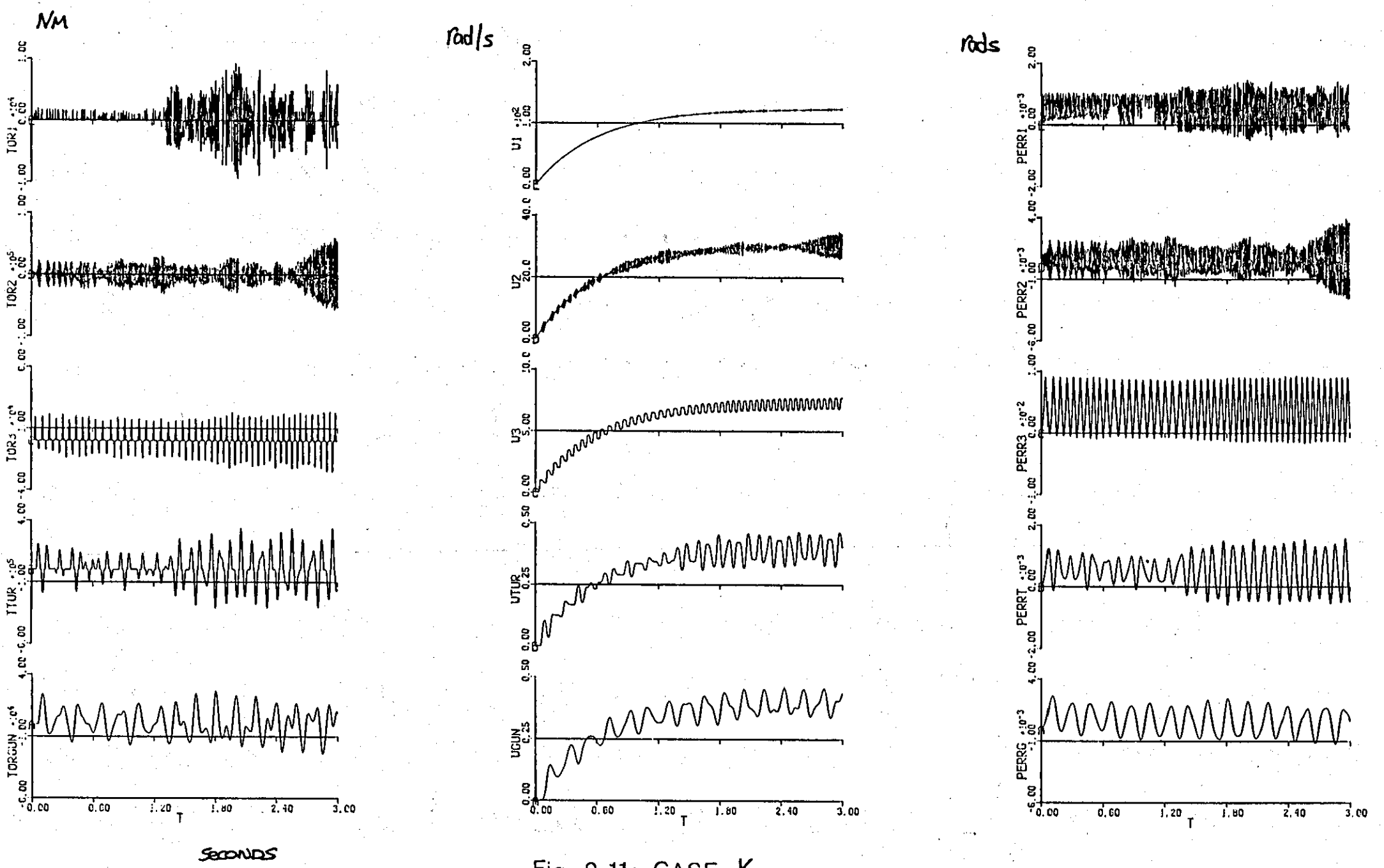

Fig. 9·11: CASE K

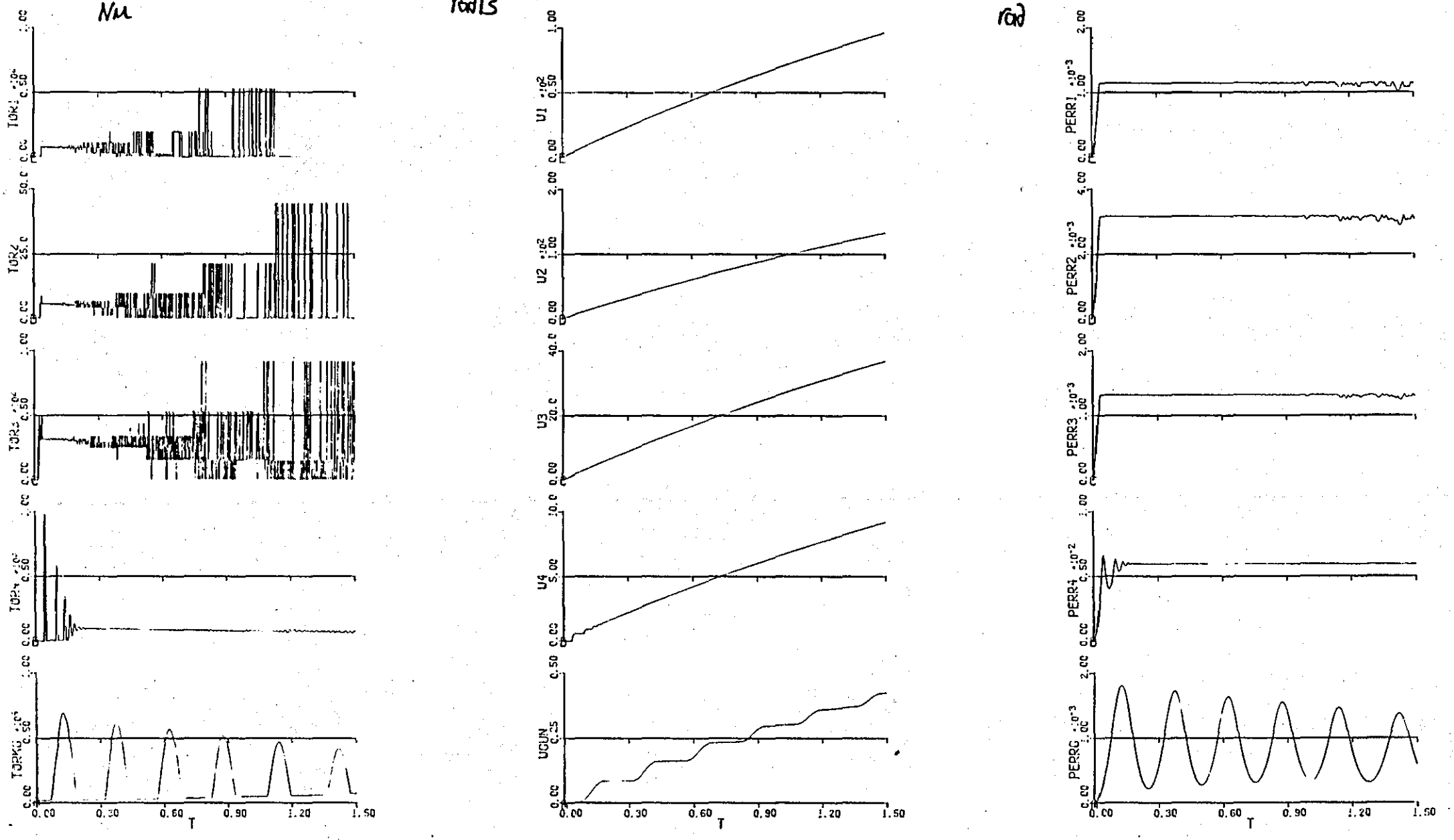

Fig. 9·12: CASE L

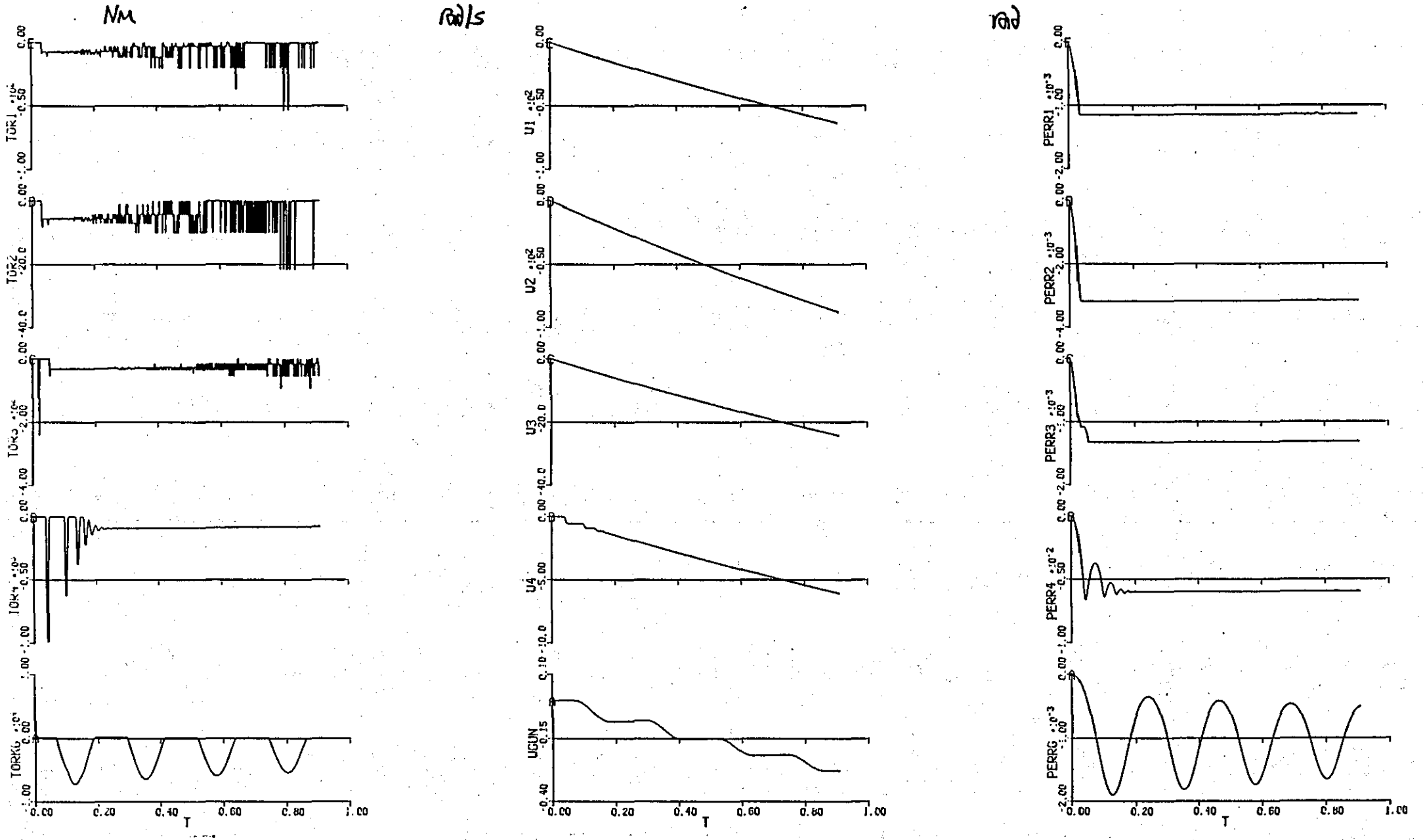

Fig. 9·13: CASE M

(a)

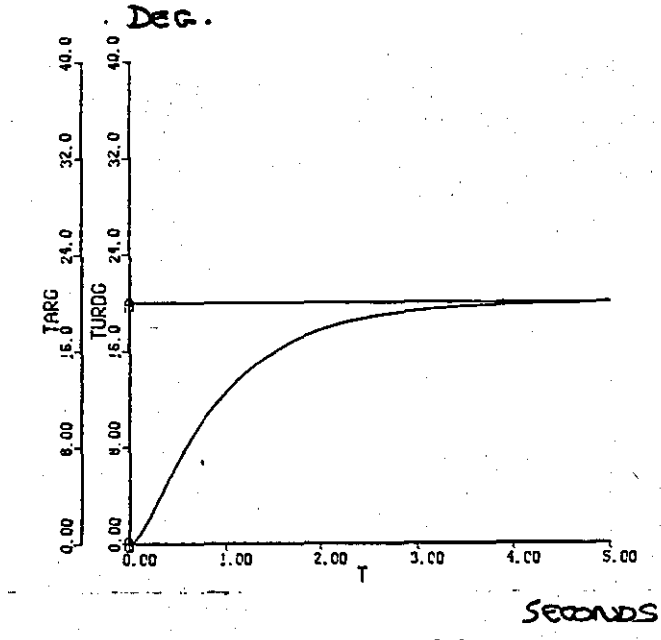

CASE N

(b)

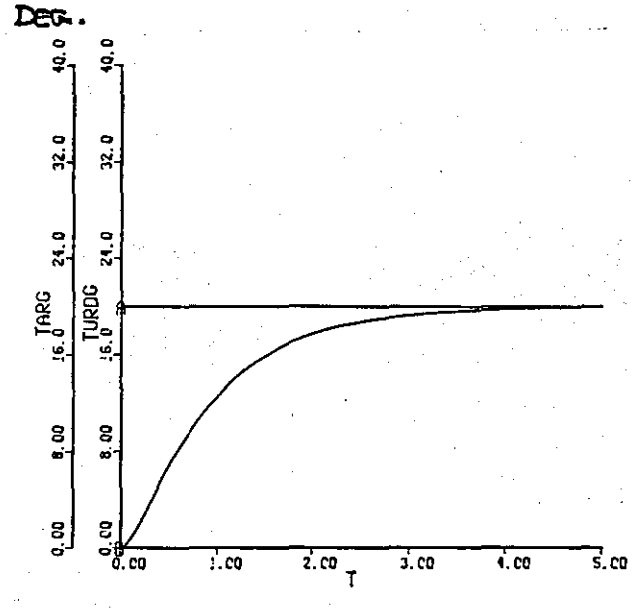

CASE O

Fig. 9·14

(c)

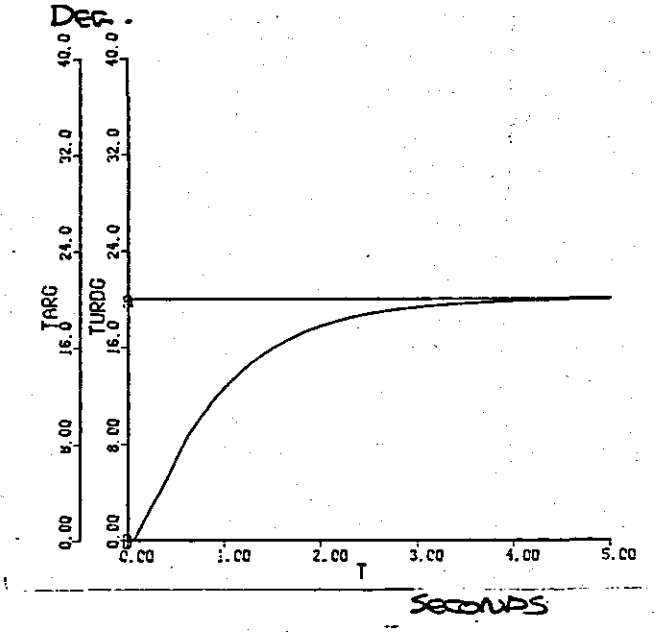

CASE P

(d)

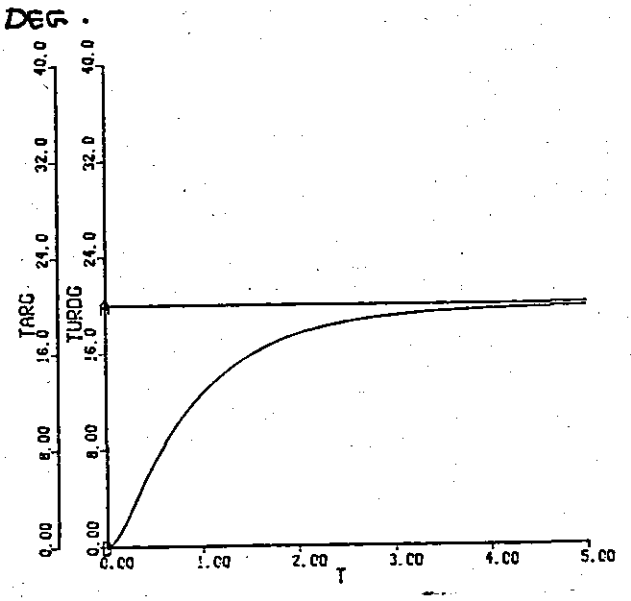

CASE Q

(e)

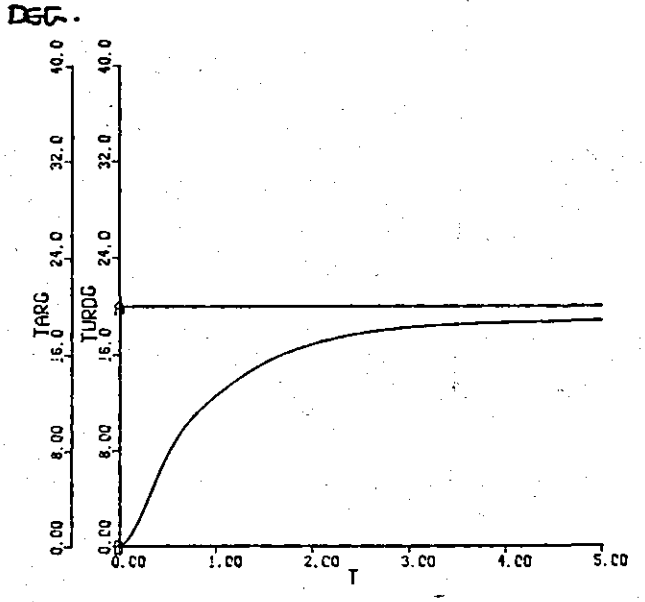

CASE R

Fig. 9·14 contd.

CHAPTER 10 CONCLUSIONS

10.1 Concluding summary

This research investigation was concerned with the mathematical modelling of the traverse and elevation gun drive systems of a modern main battle tank. The dynamic performance of the mathematical models was investigated, using digital simulation techniques, under open-loop conditions for a range of initial conditions.

The mathematical models presented were full system models based upon the generation of torque at each gear mesh through the collision-engagement of the mating gear teeth, and included the non-linear effects of backlash and friction at each mesh.

The necessary geometric relationships for the calculation of system inertia and stiffness were presented in Chapters 2 & 3, respectively. It was shown that inertia and stiffness are both referred parameters, and that the effective inertia and stiffness of a component is increased by the effect of all other components loadside. It was shown that inertia and stiffness are reflected back through the gear train by the square of the appropriate gear ratio.

A full description of friction was presented in Chapter 4, along with the appropriate mathematical relationships for its description in a digital simulation

study. Due to the nature of torque development in the models, it was found impossible to achieve the desired friction function at each gear mesh and thus a simplified version of the motor friction characteristic was used.

Rather than use a step input angle to the first gear mesh, a motor model was developed to provide the forcing inputs into each system. The description of the developed motor model was presented in Chapter 5, along with a linear analysis showing that the dynamic performance of the motor is dependent upon system inertia and friction.

A full description of backlash and the mathematical representation of torque generation was presented in Chapter 6. It was shown that the generation of torque at each mesh is dependent on the backlash at each mesh, and the associated initial condition. Linearisation of the equations, by removing the dependence of torque on the backlash condition, showed that the transfer function relating input angle to output angle could be considered as a linear second-order system multiplied by a scaling factor, which was the gear ratio. Under steady-state conditions this transfer function predicts that the output angular displacement is the product of the gear ratio and the input angular displacement.

As both gun drive systems contained a planetary gear train at the load end, the transformations necessary for representation of the planetary train as a single effective

mesh were presented in Chapter 7.

The implementation of the modelling equations in the digital simulation was presented in Chapter 8. In the course of the research study it became apparent that the effects of non-linear friction were not easily detected under open-loop conditions, and therefore a simple control law was developed to investigate the performance of the traverse system under closed-loop conditions.

The results from the digital simulation for the traverse system, under open-loop conditions, clearly showed the effects of backlash, and its initial condition, on torque generation. The levels of torque through the system were much higher than was expected from consideration of the gear ratios alone, due to the collision-engagement of the mating gears. These high impulse torques were particularly marked in the initial gear meshes, where the frequency of meshing was highest. The result was that the mating teeth came into and out-of-mesh with a frequency dictated by the effective stiffness of the mesh and the effective inertia of the output member. The achieved distribution of velocity through the system was seen to be very close to ideal, indicating that the gear mesh models were functioning correctly as speed converters. The form of velocity developed in the first three meshes was smooth, due to the high frequency meshing. The form of the developed turret velocity was seen to be dependent upon the initial backlash

condition, such that when the gears were assumed to be fully unmeshed in the direction of rotation as an initial condition, the turret velocity was stepped in nature, due to periods of non-engagement of the pinion with the turret ring. This effect became less pronounced when the gears were assumed to be 50% in mesh, and disappeared when the gears were assumed to be fully meshed. Thus, the initial collision-engagement of the gears results in a pulsing of torque into the turret and gun, the magnitude being dependent upon the initial backlash condition. The representation of the gun as a single lumped inertia resulted in low frequency vibrations as a result of its relatively low natural frequency (5 Hz).

The form of the pointing error at each mesh followed closely the form of the associated torque generation, ie higher frequencies in the earlier meshes, due to the torque being a function of relative gear angle. The steady-state pointing of the system, as indicated by the turret, was seen to be dependent upon the initial backlash condition such that the lowest error was achieved when the gears were assumed to be initially meshed. The pointing accuracy of the linearised model was identical to that of the non-linear model with the gears initially meshed, indicating that the bouncing back and forth of the gears, allowed by backlash, does not contribute to the pointing error, but rather the initial condition on backlash.

The effects of finite shaft stiffnesses on performance were clearly seen. The shafts were clearly not stiff enough for the levels of collision-engaged torque through the system, and there was evidence of the shaft dynamics coupling with the gun dynamics. The effects of finite shaft stiffness were not apparent in the elevation system as the assumed gun model is probably more representative in this axis. In addition, the levels of torque were lower in the elevation system, due to both the lower motor torque inputs and the lower overall gear ratio. The effect of the gun rack out-of-balance torque was clearly seen as an offset in the developed gun torque.

A preliminary investigation of the closed-loop traverse gun-drive system, although not initially one of the reasearch objectives, was carried out in order to ascertain the effects of the non-linearities upon system performance. This preliminary study showed that providing backlash is not excessive, and does not adversely affect the damping of the system, then the performance of the closed-loop gun drive system is dictated by the level of Coulomb friction in the system, resulting in a steady-state pointing error of the turret to step input demands on azimuth position.

10.2 Recommendations for further work

1. There remains a clear need for the investigation of gear meshing on the referred values of inertia, stiffness, and friction. This effect was not incorporated into the models as the problems associated with the integration were not sorted out to the complete satisfaction of the author by the completion of this work. The inclusion of the effect of gear meshing on referred parameters would result in a more realistic model. However, their inclusion may lead to an even more relaxed control on relative and absolute error bounds, which in turn may lead to problems with numerical accuracy.
2. A more complete investigation of gear mesh stiffness on dynamic performance is required for design purposes.
3. A more complete investigation of shaft stiffness is required, particularly the effects of the coupling of shaft and gun dynamics.
4. There is a need for a more realistic gun model, taking into account higher barrel frequencies than the fundamental, and the modes associated with these higher frequencies.
5. An investigation of the coupling between the traverse system and elevation system dynamics is

required, involving the linking of the two systems into one simulation program with the inclusion of the relevant coupling terms.

6. There is a need for the investigation of vehicle motions on system performance, particularly in relation to a coupled gun drive system model.

7. A more thorough investigation of the closed-loop dynamics of both systems is required, with the appropriate deisgn of the control law. This would require a more accurate description of the motor to include electrical phenomena, as well as mechanical phenomena, in the modelling equations.

8. An attempt should be made to confirm some of the findings of this research investigation by carrying out tests on the performance of a modern main battle tank. The required variables could be obtained by the positioning of the appropriate measurement sensors in the turret and gun.

REFERENCES

1.CHUBB, B.

Modern Analytical Design Of Instrument Servomechanisms.

Addison-Wesley Publishing Co., Reading, Massachusetts,1967.

2.GEAR, W.C.

Numerical Initial Value Problems in Ordinary Differential Equations.

Prentice-Hall, Inc., Englewood Cliffs, N.J.,1971.

3.KOCHENBURGER, R.J.

Computer Simulation Of Dynamic Systems.

Prentice-Hall, Inc., Englewood Cliffs, N.J.,1972.

4.DAHLQUIST, G.

A Special Stability Problem for Linear Multistep Methods.

BIT, 1963

5.ROSENBROCK, H.A.

Some General Implicit Processes for the Numerical Solution of Differential Equations.

Comp., Vol.5, 1963.

6.CALAHAN, D.A.

Computer-Aided Network Design.

McGraw-Hill Book Co., N.Y., 1972

7.KORN, G.A. AND J.V. WAIT

Digital Continuous-System Simulation.

Prentice-Hall, Inc., Englewood Cliffs, N.J., 1978.

APPENDIX 1 STIFF DIFFERENTIAL EQUATIONS

A major reason for problems with numerical integration is that the system to be simulated may have system-response time constants that are short compared to the solution time. This can be true even if the system response is not oscillatory. This may force one to use integration steps, DT, of the order of the smallest time-constant, causing not only slow computation but also serious round-off errors.

For the general non-linear vector equation

$$\frac{dX}{dT} = G(X,T) \qquad \ldots\ (A\text{-}1)$$

we speak of the system being locally stable if the eigenvalues $\lambda_i(X,T)$ of the local Jacobian matrix

$$J \equiv \frac{\partial G}{\partial X} \equiv \mathrm{Jac}(G) \qquad \ldots\ldots(A\text{-}2)$$

have negative real parts.

A differential-equation system (A-1) will be called stiff if the relative range of its local time constants is large, say, larger than 100, for any point (X,T). For example, the system

$$\frac{d^2X}{dT^2} + \frac{dX}{dT} + 100X = 0 \qquad \ldots\ldots(A\text{-}3)$$

is a stiff system with eigenvalues -100 and -1; the solution can contain a 'fast' component of a_1e^{-t} and a 'slow' component of a_2e^{-100t}. Note that the response is non-oscillatory

in this case.

Application of numerical-integration rules transforms a given differential-equation system into a system of difference equations. The latter may, however, be unstable, and thus amplify small numerical errors as the solution proceeds, even though the original differential-equation system is completely stable. Consider open Euler integration applied to the simple differential equation

$$\frac{dX}{dT} = \lambda X \qquad \text{.....(A-4)}$$

ie.,

$$^{k+1}X = {}^{k}X + \lambda {}^{k}X DT = (1+\lambda DT)\,{}^{k}X \qquad \text{....(A-5)}$$

This difference equation is completely stable if and only if

$$|1+\lambda DT| < 1 \qquad \text{.....(A-6)}$$

even though the original differential equation (A-4) is completely stable for

$$Re(\lambda) < 0 \qquad \text{.....(A-7)}$$

Note that integration stability can force the use of an inconveniently small DT even though the transients associated with the larger values λ_i contribute little to the particular solution.

One is, then, led to seek integration rules with large regions of stability. Dahlquist (ref.4) defined an integration rule as A-stable if and only if the numerical solution goes to 0 for all DT as $T_k \to \infty$ for any asymptotically stable differential-equation system, ie a

system with $Re(\lambda) < 0$.

Since stiff differential equations frequently arise from considerations of physical systems, practical digital simulation systems must include at least one stiff-system integration rule. The most successful rules, though not A-stable, are implicit methods. Unfortunately, they require substantial per-step computing effort, but this is often paid for by the possibility of using much larger integration steps. Implicit rules require solution of a possibly large system of Eq.(A-1) for the vector ${}^{k+1}X$ at each step. The typical approach to this problem is to use a form of Newton-Raphson iteration. This involves finding an approximation to the Jacobian of the derivative matrix,

$$J = \frac{\partial G}{\partial X} \qquad \text{.....(A-8)}$$

This is usually done by making n+1 calls to the derivative function and finding the local approximations to the elements of J:

$$K_{j_{ij}} \approx \frac{G_i({}^{k}X + \Delta X_j) - G_i({}^{k}X)}{\Delta X_j} \quad , \quad j = 1,2,3....n$$

where G_i is the ith element of the nth-order derivative vector. This time-consuming process is obviously only worth doing if DT can be greatly increased, which is often the case in many problems.

Rosenbrock (ref.5) proposed an extension to implicit forms of the Runge-Kutta process. A simple second-order

example is

$$K_1 = \left[I - \frac{DT^k J}{2}\right] DT^k G \qquad \ldots.(A\text{-}9)$$

$$^{k+1}X = {}^{k}X + K_1 \qquad \ldots.(A\text{-}10).$$

Calahan (Ref.6) presents similar methods. Note that such methods require not only the n+1 call of the derivative function to estimate J, but also the inversion of possibly large $n^{x}n$ matrices at each step. Clearly, a lot of per-step effort is required for a high-ordered set of differential equations.

Gear (ref.2) has developed his 'stiffly stable' strategies, which provide high accuracy for major system eigenvalues of small magnitude and retain stability for relatively unimportant short time-constants associated with eigenvalues of large magnitude. Moreover, his methods are variable-order, variable-step strategies. To further reduce average per-step computing effort, Gear recomputes the Jacobian only when tests indicate that the current approximation to J is no longer suitable.

APPENDIX 2

ACSL Simulation Program of Traverse Gun Drive System

```
"        ------------------------------------------------        "
"        THIS PROGRAM SIMULATES THE TRAVERSE DRIVE                "
"        ------------------------------------------------        "

"---------------                                                  "
 PROGRAM TRAVERSE
"---------------                                                  "


 INITIAL
"-------                                                          "


       CINTERVAL CINT=0.001
       NSTEPS NSTP=1000000
       ALGORITHM IALG=2

      MERROR THEMOT=0.1,THET1=0.1,THET2=0.1,THET3=0.1
      MERROR THETUR=0.1,THETG=0.1,WMOT=0.1,W1=0.1,W2=0.1,W3=0.1
      MERROR WTUR=0.1,WGUN=0.1
      XERROR THEMOT=0.1,THET1=0.1,THET2=0.1,THET3=0.1
      XERROR THETUR=0.1,THETG=0.1,WMOT=0.1,W1=0.1,W2=0.1,W3=0.1
      XERROR WTUR=0.1,WGUN=0.1

 "-------------------------------------                           "
 "REFERRED FRICTION TO GEARS AND MOTOR"
 "-----------------------------------                             "


 "ABSOLUTE VALUES OF FRICTION"
 "---------------------------                                     "

 " 1.STICTION"
 "-----------                                                     "

" FOFF IS SWITCH TO TURN OFF ALL NON-LINEAR FRICTION "
 "-------------------------------------------- "
CONSTANT FOFF=1
"----------------NOTE FRICTION REMOVED WHEN FOFF=0  "


" NONLIN IS SWITCH TO LINEARISE MODEL "
" ------------------------------------"
CONSTANT NONLIN=1.0
"     ----------NOTE TO LINEARISE MODEL NONLIN MUST BE SET TO ZERO.    "
"---------------HOWEVER FOFF MUST BE SET TO UNITY TO PREVENT THE "
"---------------REMOVAL OF VISCOUS FRICTION"

  FSTM=0.46*FOFF*NONLIN
  FST1=0.41964*FOFF*NONLIN
  FST2=0.41964*FOFF*NONLIN
  FST3=0.532062*FOFF*NONLIN
  FSTT=1520*FOFF*NONLIN

 "  2.COULOMB"
 "----------                                                     "
```

```
  FCOUM=Ø.26*FOFF*NONLIN
  FCOU1=Ø.24479*FOFF*NONLIN
  FCOU2=Ø.24479*FOFF*NONLIN
  FCOU3=Ø.31Ø37*FOFF*NONLIN
  FCOUT=1410*FOFF*NONLIN

 " 3.VISCOUS"
" ------------        "

  FVM=Ø.Ø46
  FV1=Ø.57259
  FV2=Ø.57259
  FV3=Ø.61369
  FVT=13ØØ


CONSTANT STOPM=5Ø
CONSTANT STOP1=5Ø
CONSTANT STOP2=5Ø
CONSTANT STOP3=5Ø
CONSTANT STOPT=1ØØØØ
 "-------------------------          "
 "DEFINITION OF GEAR RATIOS"
 "-------------------------          "

 CONSTANT N1=Ø.37Ø78
 CONSTANT N2=Ø.24691
CONSTANT N3=Ø.24
"--------------------NOTE N4 MAY VARY IF TURRET ECCENTRICITY INCLUDED "

 "INVERSE GEAR RATIOS"
"-------------------"

 N1A=1/N1
 N2A=1/N2
 N3A=1/N3

 "GEAR RATIO FUNCTIONS FOR REFERRAL OF INERTIA AND FRICTION"
 "-------------------------------------------------------------      "

 N1N1=N1*N1
 N2N2=N2*N2
 N3N3=N3*N3


"-----------------------------------"
"ABSOLUTE STIFFNESSES"
"-----------------------------------"
 CONSTANT K1=1.6974E+Ø7
 CONSTANT K2=1.9721E+Ø7
CONSTANT K3=1.Ø137E+Ø7
 CONSTANT KT=2.89E+Ø8 $ " TURRET STIFFNESS "
       CONSTANT KTG=9.22E+Ø6 $"GUN TO TURRET STIFFNESS   "
        KS1=1.13525E+Ø8*STOFF
        KS2=1.116E+Ø8*STOFF
       KS3=6.994E+Ø9*STOFF
      CONSTANT STOFF=1.Ø
END
```

```
DYNAMIC
"_________"
DERIVATIVE
"__________     "

CONSTANT MAJ=2,MIN=2
RTUR=((MAJ*SIN(THETUR))**2+(MIN*COS(THETUR))**2)**Ø.5
NOT=RTUR*256/2
N4=14/NOT
N4A=1/N4
N4N4=N4*N4
 "  CALCULATION OF REFERRED FRICTION"

 " 1 MOTOR SHAFT"

 STICMR=FSTM+(N1*FST1)+(N2*N1*FST2)+(N3*N2*N1*FST3)+...
 (N4*N3*N2*N1*FSTT)
 FCMREF=FCOUM+(N1*FCOU1)+(N2*N1*FCOU2)+(N3*N2*N1*FCOU3)+...
 (N4*N3*N2*N1*FCOUT)

 FVMREF=FVM+(N1N1*FV1)+(N2N2*N1N1*FV2)+(N3N3*N2N2*N1N1*FV3)...
 +(N4N4*N3N3*N2N2*N1N1*FVT)

 " 2.FIRST GEAR MESH"

 STIC1R=FST1+(N2*FST2)+(N3*N2*FST3)+(N4*N3*N2*FSTT)
 FC1REF=FCOU1+(N2*FCOU2)+(N3*N2*FCOU3)+(N4*...
 N3*N2*FCOUT)
 FV1REF=FV1+(N2N2*FV2)+(N3N3*N2N2*FV3)+...
 (N4N4*N3N3*N2N2*FVT)

 " 3.SECOND GEAR MESH"

 STIC2R=FST2+(N3*FST3)+(N4*N3*FSTT)
 FC2REF=FCOU2+(N3*FCOU3)+(N4*N3*FCOUT)
 FV2REF=FV2+(N3N3*FV3)+(N4N4*N3N3*FVT)

 " 4 THIRD GEAR MESH"
"PLANETRY SYSTEM , FRICTION ON EACH SIDE OF PLANET GEARS "

 STIC3R=FST3+(N4*FSTT)
 FC3REF=FCOU3+(N4*FCOUT)
 FV3REF=FV3+(N4N4*FVT)



 "ABSOLUTE INERTIAS"
 CONSTANT JMOT=Ø.ØØ5
 CONSTANT JA=1.9745E-Ø4
CONSTANT JB=4.879E-Ø3
CONSTANT JC=5.88431E-Ø5
CONSTANT JD=7.7126E-Ø3
CONSTANT JE=1.996E-Ø4
CONSTANT JF=1.47774E-Ø4
CONSTANT JP=1.Ø744E-Ø2
CONSTANT JS1=1.Ø4144E-Ø5
CONSTANT JS2=3.45413E-Ø4
CONSTANT JS3=5.95949E-Ø3
```

```
CONSTANT JS3=5.95949E-03
 .
"ADDITION OF INERTIAS ON COMMON SHAFTS "
 JM=JMOT+JA
J1=JB+JS1+JC
J2=JD+JS2+JE
J3=(3*JF)+JS3+JP  $ "THREE PLANETRY GEARS "
 CONSTANT JTUR=43000

 "BACKLASH CALCULATIONS"

"BOFF IS SWITCH TO TURN OFF ALL BACKLASH"
CONSTANT BOFF=1
 BACK1=9.525E-04*BOFF*NONLIN
 BACK2=9.0445E-04*BOFF*NONLIN
BACK3=0.007284*BOFF*NONLIN
  BACK4=0.0005015*BOFF*NONLIN
  BACK5=0.0001*BOFF*NONLIN

 " INITIAL CONDITIONS FOR MESHING"
 CONSTANT FRAC=50

 BK1=BACK1*FRAC/100
 BK2=BACK2*FRAC/100
 BK3=BACK3*FRAC/100
 BK4=BACK4*FRAC/100
 BK5=BACK5*FRAC/100

 "EFFECTIVE BACKLASH AT EACH MESH"

 DL1=(BK1)
 DL1A=(BACK1-BK1)
 DL2=(BK2)
 DL2A=(BACK2-BK2)
 DL3=(BK3)
 DL3A=(BACK3-BK3)
 DL4=BK4
DL4A=(BACK4-BK4)
DL5=BK5
 DL5A=(BACK5-BK5)

"EFFECTIVE BACKLASH AT PINNION - SPEC <12 THOU "
EBP=(DL1A*N2*N3)+(DL2A*N3)+DL3A

"EFFECTIVE BACKLASH AT LOAD "
" 1 . EFFECTIVE BACKLASH AT TURRET - EBT   "
EBT=(DL1A*N2*N3*N4)+(DL2A*N3*N4)*(DL3A*N4)+DL4A
" 2 . EFFECTIVE BACKLASH AT GUN -EBG  "
EBG=(DL1A*N2*N3*N4)+(DL2A*N3*N4)*(DL3A*N4)+DL4A+DL5A
 JMREF=JM+(J1*N1N1)+(J2*N2N2*N1N1)+(J3*N3N3*N2N2*N1N1)...
 +(JTUR+JGUN)*(N4N4*N3N3*N2N2*N1N1)
 J1REF=J1+(J2*N2N2)+(J3*N3N3*N2N2)+...
 (JTUR+JGUN)*(N4N4*N3N3*N2N2)
 J2REF=J2+(J3*N3N3)+(JTUR+JGUN)*(N4N4*N3N3)
 J3REF=J3+(JTUR+JGUN)*(N4N4)

"_____"
"CALCULATION OF EFFECTIVE STIFFNESS"
"_____"
K1EFF=K1+KS1+(K2+KS2)*N2N2+(K3+KS3)*N3N3*N2N2+(KT+KTG)...
```

```
K1EFF=K1+KS1+(K2+KS2)*N2N2+(K3+KS3)*N3N3*N2N2+(KT+KTG)...
*N4N4*N3N3*N2N2
KS1EFF=K1EFF-K1
K2EFF=K2+KS2+(K3+KS3)*N3N3+(KT+KTG)*N4N4*N3N3
KS2EFF=K2EFF-K2
K3EFF=K3+KS3+(KT+KTG)*N4N4
KS3EFF=K3EFF-K3
KTEFF=KT+KTG

"-----------------------------------INPUT PARAMETERS-----------------"
 "      MOTOR CHARACTERISTICS     "

 CONSTANT TARG=20
 CONSTANT GTHET=9.0
 CONSTANT GINT=0.001
CONSTANT GW=-7.0
 ERROR=(TARG-TURDG)
 INTERR=INTEG(ERROR,0.0)
CONSTANT LAG=0
CONSTANT TK=46
CONSTANT T1=0.1
PROCEDURAL(INPUT=TK,LAG,T1)
IF(LAG.EQ.0)INPUT=TK
IF(LAG.EQ.1)INPUT=INTEG((TK-INPUT)/T1,0.0)
END
 CONSTANT OPEN=1
PROCEDURAL(TMOT=INPUT,OPEN,ERROR,INTERR,GTHET,GINT,GW)
IF(OPEN.EQ.1)TMOT=INPUT
IF(OPEN.EQ.0)TMOT=GTHET*ERROR+GINT*INTERR+GW*WTURDG
END

"-------------------------------END OF INPUT SELECTION-------"
 WVM=0.42*NONLIN*FOFF
GRADM=(STICMR-FCMREF)*2.381
 PROCEDURAL(FM=TMOT,STICMR,GRADM,FCMREF,WVM,FVMREF,WMOT)
 IF(((TMOT-FM)*WMOT).GT.0.0.AND.ABS(WMOT).LT.WVM)FM=(STICMR*...
 SIGN(1.0,WMOT))-(GRADM*WMOT)
 IF(((TMOT-FM)*WMOT).LT.0.0.AND.ABS(WMOT).LT.WVM)FM=...
 FCMREF*SIGN(1.0,WMOT)
 IF(WMOT.EQ.0.0)FM=STICMR*SIGN(1.0,(TMOT-FM))
 IF(ABS(TMOT).LE.STICMR.AND.WMOT.EQ.0.0)FM=TMOT
 IF(ABS(WMOT).GE.WVM)FM=(ABS(FVMREF*(WMOT-WVM))+FCMREF)*SIGN(1.0,WMOT)
IF(ABS(TMOT).LE.FCMREF.AND.ABS(WMOT).LE.WVM)FM=STOPM*WMOT
 END
ACTMOT=TMOT-FM
 ACCMOT=ACTMOT/JMREF      $ " MOTOR ACCELERATION      "
       WMOT=INTEG(ACCMOT,ICWMOT)  $ " MOTOR VELOCITY "
      THEMOT=INTEG(WMOT,ICTHMO)
       WMOTDG=WMOT*180/3.1416
       CONSTANT ICWMOT=0.0
      CONSTANT ICTHMO=0.0
 " RELATIVE GEAR ANGLES FOR TORQUE GENERATION      "
       THETS1=DL1-((THET1)-THEMOT*N1)
       THETS2=DL1A+((THET1)-THEMOT*N1)
       THETS3=DL2-((THET2)-THET1A*N2)
       THETS4=DL2A+((THET2)-THET1A*N2)
      THET1A=THET1-((TOR1*STOFF)/KS1EFF)
            DELTA1=TOR1/K1
       THETS5=DL3-((THET3)-THET2A*N3)
       THETS6=DL3A+((THET3)-THET2A*N3)
```

```
        THETS6=DL3A+((THET3)-THET2A*N3)
       THET2A=THET2-((TOR2*STOFF)/KS2EFF)
  " GEAR MESH STIFFNESSES    "
       "EFFECTIVE STIFFNESSES"
 CONSTANT ETA=1.0  $" GEAR EFFICIENCY   "
  "    TORQUE CALCULATIONS     "
"DAMPING COEFFICIENTS"
CONSTANT BS1=0
CONSTANT BS2=0
CONSTANT BS3=0
CONSTANT BST=0
CONSTANT BSG=0
        PROCEDURAL(TOR1=THETS1,THETS2,K1EFF,ETA,BS1)
 IF(THETS2.LT.0.0)TOR1=-K1EFF*ETA*THETS2-BS1*(WMOT-W1)
 IF(THETS1.LT.0.0)TOR1=K1EFF*ETA*THETS1-BS1*(WMOT-W1)
        IF((THETS1.GE.0.0).AND.(THETS2.GE.0.0))TOR1=0.0
        END
CONSTANT WV1=0.0
CONSTANT GRAD1=0.0
 PROCEDURAL(F1=TOR1,STIC1R,GRAD1,FC1REF,WV1,FV1REF,W1)
 IF(((TOR1-F1)*W1).GT.0.0.AND.ABS(W1).LT.WV1)F1=(STIC1R*...
 SIGN(1.0,W1))-(GRAD1*W1)
 IF(((TOR1-F1)*W1).LT.0.0.AND.ABS(W1).LT.WV1)F1=...
 FC1REF*SIGN(1.0,W1)
 IF(W1.EQ.0.0)F1=STIC1R*SIGN(1.0,(TMOT-FM))
 IF(ABS(TOR1).LE.STIC1R.AND.W1.EQ.0.0)F1=STIC1R*SIGN(1.0,TMOT)
 IF(ABS(W1).GT.WV1)F1=(ABS(FV1REF*(W1-WV1))+FC1REF)*SIGN(1.0,W1)
IF(ABS(TOR1).LE.FC1REF.AND.ABS(W1).LE.WV1)F1=STOP1*W1
 END
ACC1=(TOR1-F1)/J1REF
        W1=INTEG(ACC1,ICW1)
        THET1=INTEG(W1,ICTH1)
       NTHET1=THET1*N1A
        CONSTANT ICW1=0.0
        CONSTANT ICTH1=0.0
        PROCEDURAL(TOR2=THETS3,THETS4,K2EFF,ETA,BS2)
 IF(THETS4.LT.0.0)TOR2=-K2EFF*ETA*THETS4-BS2*(W1-W2)
  IF(THETS3.LT.0.0)TOR2=K2EFF*ETA*THETS3-BS2*(W1-W2)
        IF((THETS3.GE.0.0).AND.(THETS4.GE.0.0))TOR2=0.0
        END
CONSTANT WV2=0.0
CONSTANT GRAD2=0.0
 PROCEDURAL(F2=TOR2,STIC2R,GRAD2,FC2REF,WV2,FV2REF,W2)
 IF(((TOR2-F2)*W2).GT.0.0.AND.ABS(W2).LT.WV2)F2=(STIC2R*...
 SIGN(1.0,W2))-(GRAD2*W2)
 IF(((TOR2-F2)*W2).LT.0.0.AND.ABS(W2).LT.WV2)F2=...
 FC2REF*SIGN(1.0,W2)
 IF(W2.EQ.0.0)F2=STIC2R*SIGN(1.0,(TMOT-FM))
 IF(ABS(TOR2).LE.STIC2R.AND.W2.EQ.0.0)F2=STIC2R*SIGN(1.0,TMOT)
 IF(ABS(W2).GT.WV2)F2=(ABS(FV2REF*(W2-WV2))+FC2REF)*SIGN(1.0,W2)
IF(ABS(TOR2).LE.FC2REF.AND.ABS(W2).LE.WV2)F2=STOP2*W2
 END
ACC2=(TOR2-F2)/J2REF
        W2=INTEG(ACC2,ICW2)
        THET2=INTEG(W2,ICTH2)
       NTHET2=THET2*N1A*N2A
        CONSTANT ICW2=0.0
        CONSTANT ICTH2=0.0
        PROCEDURAL(TOR3=THETS5,THETS6,K3EFF,ETA,BS3)
 IF(THETS6.LT.0.0)TOR3=-K3EFF*ETA*THETS6-BS3*(W2-W3)
```

```
 IF(THETS6.LT.Ø.Ø)TOR3=-K3EFF*ETA*THETS6-BS3*(W2-W3)
.IF(THETS5.LT.Ø.Ø)TOR3=K3EFF*ETA*THETS5-BS3*(W2-W3)
       IF((THETS5.GE.Ø.Ø).AND.(THETS6.GE.Ø.Ø))TOR3=Ø.Ø
       END
CONSTANT GRAD3=Ø.Ø
CONSTANT WV3=Ø.Ø
 PROCEDURAL(F3=TOR3,STIC3R,GRAD3,FC3REF,WV3,FV3REF,W3)
 IF(((TOR3-F3)*W3).GT.Ø.Ø.AND.ABS(W3).LT.WV3)F3=(STIC3R*...
 SIGN(1.Ø,W3))-(GRAD3*W3)
 IF(((TOR3-F3)*W3).LT.Ø.Ø.AND.ABS(W3).LT.WV3)F3=...
 FC3REF*SIGN(1.Ø,W3)
 IF(W3.EQ.Ø.Ø)F3=STIC3R*SIGN(1.Ø,(TMOT-FM))
 IF(ABS(TOR3).LE.STIC3R.AND.W3.EQ.Ø.Ø)F3=STIC3R*SIGN(1.Ø,TMOT)
 IF(ABS(W3).GT.WV3)F3=(ABS(FV3REF*(W3-WV3))+FC3REF)*SIGN(1.Ø,W3)
IF(ABS(TOR3).LE.FC3REF.AND.ABS(W3).LE.WV3)F3=STOP3*W3
 END
ACC3=(TOR3-F3)/J3REF
       W3=INTEG(ACC3,ICW3)
       THET3=INTEG(W3,ICTH3)
      NTHET3=THET3*N1A*N2A*N3A
       CONSTANT ICW3=Ø.Ø
       CONSTANT ICTH3=Ø.Ø

     " TOTAL REFERRED DEADSPACE IN TRAVERSE DRIVE   "

 THETS7=DL4-((THETUR)-THET3A*N4)
 THETS8=DL4A+((THETUR)-THET3A*N4)
      THET3A=THET3-((TOR3*STOFF)/KS3EFF)
 PROCEDURAL(TTUR=THETS7,THETS8,KTEFF,ETA,BST,TORLIM)
 IF(THETS8.LT.Ø.Ø)TTUR=(-KTEFF*ETA*THETS8)-BST*(W3-WTUR)
 IF(THETS7.LT.Ø.Ø)TTUR=(KTEFF*ETA*THETS7)-BST*(W3-WTUR)
       IF((THETS7.GE.Ø.Ø).AND.(THETS8.GE.Ø.Ø))TTUR=Ø.Ø
       IF((ABS(TTUR).GE.TORLIM))TTUR=TORLIM*SIGN(1.Ø,TTUR)
       CONSTANT TORLIM=1.ØE+3Ø $" CLUTCH SETTING "
       END
CONSTANT WVT=Ø.Ø
CONSTANT GRADT=Ø.Ø
 PROCEDURAL(FTUR=TTUR,FSTT,GRADT,FCOUT,WVT,FVT,WTUR)
 IF(((TTUR-FTUR)*WTUR).GT.Ø.Ø.AND.ABS(WTUR).LT.WVT)FTUR=(FSTT*...
 SIGN(1.Ø,WTUR))-(GRADT*WTUR)
 IF(((TTUR-FTUR)*WTUR).LT.Ø.Ø.AND.ABS(WTUR).LT.WVT)FTUR=...
 FCOUT*SIGN(1.Ø,WTUR)
 IF(WTUR.EQ.Ø.Ø)FTUR=FSTT*SIGN(1.Ø,(TMOT-FM))
 IF(ABS(TTUR).LE.FSTT.AND.WTUR.EQ.Ø.Ø)FTUR=FSTT*SIGN(1.Ø,TMOT)
 IF(ABS(WTUR).GT.WVT)FTUR=(ABS(FVT*(WTUR-WVT))+FCOUT)*SIGN(1.Ø,WTUR)
IF(ABS(TTUR).LE.FCOUT.AND.ABS(WTUR).LE.WVT)FTUR=STOPT*WTUR
 END
ACCTUR=(TTUR-FTUR)/(JTUR+JGUN)
       WTUR=INTEG(ACCTUR,ICWT)
       WTURDG=WTUR*18Ø/3.1416
       THETUR=INTEG(WTUR,ICTHT)
      NTHETT=THETUR*N1A*N2A*N3A*N4A
       TURDG=THETUR*18Ø/3.1416
       CONSTANT ICWT=Ø.Ø
       CONSTANT ICTHT=Ø.Ø
       PERRT=(THEMOT*N1*N2*N3*N4)-THETUR
      PERR1=(THEMOT*N1)-THET1
      PERR2=(THEMOT*N1*N2)-THET2
      PERR3=(THEMOT*N1*N2*N3)-THET3
 "    GUN DYNAMICS   "
```

```
 "    GUN DYNAMICS    "
      THETS9=DL5-(THETG-THETUR)
      THES1Ø=DL5A+(THETG-THETUR)
      PROCEDURAL(TORGUN=THETS9,THES1Ø,KTG,BSG)
      IF(THES1Ø.LT.Ø.Ø)TORGUN=-KTG*THES1Ø-BSG*(WTUR-WGUN)
      IF(THETS9.LT.Ø.Ø)TORGUN=KTG*THETS9-BSG*(WTUR-WGUN)
      IF((THETS9.GE.Ø.Ø).AND.(THES1Ø.GE.Ø.Ø))TORGUN=Ø.Ø
      END


 CONSTANT MGUN=267
 CONSTANT RT=1.Ø6
 CONSTANT RGUN=1.77
 "ABSOLUTE INERTIA OF GUN ABOUT C.G. "
 CONSTANT JGABS=5913.52

"INERTIA OF GUN ABOUT CENTRE OF ROTATION"
JGUN=JGABS+((RGUN+RT)**2)*MGUN
      ACCGUN=TORGUN/JGUN
      WGUN=INTEG(ACCGUN,ICWG)
      THETG=INTEG(WGUN,ICTHG)
      CONSTANT ICWG=Ø.Ø
      CONSTANT ICTHG=Ø.Ø
      PERRG=(THEMOT*N1*N2*N3*N4)-THETG
PROCEDURAL (MESH1=THETS2,BACK1,DL1A)
IF (THETS2.LE.Ø.Ø)MESH1=1ØØ
IF(THETS2.GE.BACK1)MESH1=Ø.Ø
IF(THETS2.GT.Ø.Ø.AND.THETS2.LT.BACK1) MESH1=1-(THETS2/DL1A)
END
PROCEDURAL (MESH2=THETS4,BACK2,DL2A)
IF (THETS4.LE.Ø.Ø)MESH2=1ØØ
IF(THETS4.GE.BACK2)MESH2=Ø.Ø
IF(THETS4.GT.Ø.Ø.AND.THETS4.LT.BACK2) MESH2=1-(THETS4/DL2A)
END
PROCEDURAL (MESH3=THETS6,BACK3,DL3A)
IF (THETS6.LE.Ø.Ø)MESH3=1ØØ
IF(THETS6.GE.BACK3)MESH3=Ø.Ø
IF(THETS6.GT.Ø.Ø.AND.THETS6.LT.BACK3) MESH3=1-(THETS2/DL3A)
END
PROCEDURAL (MESHT=THETS8,BACK4,DL4A)
IF (THETS8.LE.Ø.Ø)MESHT=1ØØ
IF(THETS8.GE.BACK4)MESHT=Ø.Ø
IF(THETS8.GT.Ø.Ø.AND.THETS8.LT.BACK4) MESHT=1-(THETS8/DL4A)
END
PROCEDURAL (MESHG=THES1Ø,BACK5,DL5A)
IF (THES1Ø.LE.Ø.Ø)MESHG=1ØØ
IF(THES1Ø.GE.BACK5)MESHG=Ø.Ø
IF(THES1Ø.GT.Ø.Ø.AND.THES1Ø.LT.BACK5) MESHG=1-(THES1Ø/DL5A)
END


 " TERMINATION CONDITION    "
 TERMT(T.GE.TF)
 CONSTANT TF=3.Ø  $ " SECONDS  "
 END
 END
 END

BOTTOM
```

APPENDIX 3

ACSL Simulation Program of Elevation Gun Drive System

```
"       THIS PROGRAM SIMULATES THE ELEVATION DRIVE       "
PROGRAM ELEVATION
INITIAL
      CINTERVAL CINT=Ø.ØØ1
      NSTEPS NSTP=1ØØØØØØ
      ALGORITHM IALG=2
      MERROR THEMOT=Ø.1,THET1=Ø.1,THET2=Ø.1,THET3=Ø.1,THET4=Ø.1
      MERROR THET5=Ø.1,THETG=Ø.1,WMOT=Ø.1,W1=Ø.1,W2=1,W3=1
      MERROR W4=1,W5=Ø.1,WGUN=Ø.1
      XERROR THEMOT=Ø.1,THET1=Ø.1,THET2=Ø.1,THET3=Ø.1,THET4=Ø.1
      XERROR THET5=Ø.1,THETG=Ø.1,WMOT=Ø.1,W1=Ø.1,W2=1,W3=1
      XERROR W4=1,W5=Ø.1,WGUN=Ø.1

"REFERRED FRICTION TO GEARS AND MOTOR"

"ABSOLUTE VALUES OF FRICTION"

" 1.STICTION"

" FOFF IS SWITCH TO TURN OFF ALL NON-LINEAR FRICTION"
CONSTANT FOFF=1
"————————————————NOTE FRICTION REMOVED WHEN FOFF=Ø  "

" NONLIN IS SWITCH TO LINEARISE MODEL"
CONSTANT NONLIN=1.Ø
FSTM=Ø.423875*FOFF*NONLIN
FST1=Ø.1151*FOFF*NONLIN
FST2=Ø.1151*FOFF*NONLIN
FST3=Ø.1151*FOFF*NONLIN
FST4=Ø.143875*FOFF*NONLIN
FSTG=125.76*FOFF*NONLIN

"  2.COULOMB"

FCOUM=Ø.254325*FOFF*NONLIN
FCOU1=Ø.Ø8855*FOFF*NONLIN
FCOU2=Ø.Ø8855*FOFF*NONLIN
FCOU3=Ø.Ø8855*FOFF*NONLIN
FCOU4=Ø.11Ø69*FOFF*NONLIN
FCOUG=1Ø2.64*FOFF*NONLIN

" 3.VISCOUS"

FVM=Ø.Ø6475
FV1=Ø.ØØ23178
FV2=Ø.ØØ23178
FV3=Ø.ØØ23178
FV4=Ø.ØØ2463
FVG=99.Ø196

"DEFINITION OF GEAR RATIOS"

CONSTANT N1=1.4728
CONSTANT N2=1.385
CONSTANT N3=Ø.27624
CONSTANT N4=Ø.25
CONSTANT N5=Ø.Ø45455

"INVERSE GEAR RATIOS"
```

```
"INVERSE GEAR RATIOS"

N1A=1/N1
N2A=1/N2
N3A=1/N3
N4A=1/N4
N5A=1/N5

"GEAR RATIO FUNCTIONS FOR REFERRAL OF INERTIA AND FRICTION"

N1N1=N1*N1
N2N2=N2*N2
N3N3=N3*N3
N4N4=N4*N4
N5N5=N5*N5

"  CALCULATION OF REFERRED FRICTION"

" 1 MOTOR SHAFT"

STICMR=FSTM+(N1*FST1)+(N2*N1*FST2)+(N3*N2*N1*FST3)+(N4*N3*N2*N1*FST4)...
+(N5*N4*N3*N2*N1*FSTG)
FCMREF=FCOUM+(N1*FCOU1)+(N2*N1*FCOU2)+(N3*N2*N1*FCOU3)+(N4*N3*N2*...
N1*FCOU4)+(N5*N4*N3*N2*N2*FCOUG)

FVMREF=FVM+(N1N1*FV1)+(N2N2*N1N1*FV2)+(N3N3*N2N2*N1N1*FV3)...
+(N4N4*N3N3*N2N2*N1N1*FV4)*(N5N5*N4N4*N3N3*N2N2*N1N1*FVG)

" 2.FIRST GEAR MESH"

STIC1R=FST1+(N2*FST2)+(N3*N2*FST3)+(N4*N3*N2*FST4)+(N5*N4*N3*N2*FSTG)
FC1REF=FCOU1+(N2*FCOU2)+(N3*N2*FCOU3)+(N4*N3*N2*FCOU4)+(N5*N4*...
N3*N2*FCOUG)
FV1REF=FV1+(N2N2*FV2)+(N3N3*N2N2*FV3)+(N4N4*N3N3*N2N2*FV4)...
+(N5N5*N4N4*N3N3*N2N2*FVG)

" 3.SECOND GEAR MESH"

STIC2R=FST2+(N3*FST3)+(N4*N3*FST4)+(N5*N4*N3*FSTG)
FC2REF=FCOU2+(N3*FCOU3)+(N4*N3*FCOU4)+(N5*N4*N3*FCOUG)
FV2REF=FV2+(N3N3*FV3)+(N4N4*N3N3*FV4)+(N5N5*N4N4*N3N3*FVG)

" 4 THIRD GEAR MESH"

STIC3R=FST3+(N4*FST4)+(N5*N4*FSTG)
FC3REF=FCOU3+(N4*FCOU4)+(N5*N4*FCOUG)
FV3REF=FV3+(N4N4*FV4)+(N5N5*N4N4*FVG)


 "5 FOURTH GEAR MESH"

STIC4R=FST4+(N5*FSTG)
FC4REF=FCOU4+(N5*FCOUG)
FV4REF=FV4+(N5N5*FVG)


"ABSOLUTE INERTIAS"
CONSTANT JMOT=0.005
CONSTANT JA=1.1998E-03
CONSTANT J1=1.9772E-04
```

```
CONSTANT J1=1.9772E-Ø4
CONSTANT J2=2.223E-Ø4
CONSTANT J3=4.882E-Ø3
CONSTANT J4=4.65E-Ø3
JM=JMOT+JA
CONSTANT JGUN=5913.52

"BACKLASH CALCULATIONS"
" BOFF IS SWITCH TO TURN OFF ALL BACKLASH"
CONSTANT BOFF=1.Ø
 BACK1=2.292E-Ø3*BOFF*NONLIN
 BACK2=3.175E-Ø3*BOFF*NONLIN
 BACK3=Ø.8835E-Ø3*BOFF*NONLIN
 BACK4=Ø.Ø111Ø6*BOFF*NONLIN
 BACK5=1.232E-Ø3*BOFF*NONLIN

" INITIAL CONDITIONS FOR MESHING"
CONSTANT FRAC=Ø.5

BK1=BACK1*FRAC
BK2=BACK2*FRAC
BK3=BACK3*FRAC
BK4=BACK4*FRAC
BK5=BACK5*FRAC

"EFFECTIVE BACKLASH AT EACH MESH"

DL1=(BK1)
DL1A=(BACK1-BK1)
DL2=(BK2)
DL2A=(BACK2-BK2)
DL3=(BK3)
DL3A=(BACK3-BK3)
DL4=BK4
DL4A=(BACK4-BK4)
DL5=BK5
DL5A=(BACK5-BK5)

"CALCULATION OF REFERRED INERTIA"

JMREF=JM+(J1*N1N1)+(J2*N2N2*N1N1)+(J3*N3N3*N2N2*N1N1)...
+(J4*N4N4*N3N3*N2N2*N1N1)+(JGUN*N5N5*N4N4*N3N3*N2N2*N1N1)
J1REF=J1+(J2*N2N2)+(J3*N3N3*N2N2)+(J4*N4N4*N3N3*N2N2)...
+(JGUN*N5N5*N4N4*N3N3*N2N2)
J2REF=J2+(J3*N3N3)+(J4*N4N4*N3N3)+(JGUN*N5N5*N4N4*N3N3)
J3REF=J3+(J4*N4N4)+(JGUN*N5N5*N4N4)
J4REF=J4+(JGUN*N5N5)

"ABSOLUTE STIFFNESS"
CONSTANT K1=3.119E+Ø6
CONSTANT K2=1.6Ø1E+Ø6
CONSTANT K3=2.1Ø4E+Ø7
CONSTANT K4=1.3Ø2E+Ø6
CONSTANT KG=7.48E+Ø6
       KS1=9.5E+Ø4*STOFF
       KS2=9.6537E+Ø4*STOFF
       KS3=2.234E+Ø5*STOFF
      CONSTANT STOFF=Ø.Ø

"CALCULATION OF EFFECTIVE STIFFNESS"
```

```
"CALCULATION OF EFFECTIVE STIFFNESS"
K1EFF=K1+(K2+KS1)*N2N2+(K3+KS2)*N3N3*N2N2+(K4+KS3)*N4N4*N3N3*N2N2...
+(KG)*N5N5*N4N4*N3N3*N2N2
K2EFF=K2+KS1+(K3+KS2)*N3N3+(K4+KS3)*N4N4*N3N3+(KG)*N5N5*N4N4*N3N3
KS1EFF=K2EFF-K2
K3EFF=K3+KS2+(K4+KS3)*N4N4+(KG)*N5N5*N4N4
KS2EFF=K3EFF-K3
K4EFF=K4+KS3+(KG)*N5N5
KS3EFF=K4EFF-K4
END

DYNAMIC
DERIVATIVE
 "      MOTOR CHARACTERISTICS     "

      CONSTANT INPUT=15
PROCEDURAL(TMOT=GUNDG)
IF(GUNDG.GE.20)TMOT=0
IF(GUNDG.LE.-8)TMOT=0
IF(GUNDG.LT.20.AND.GUNDG.GT.-8)TMOT=INPUT
END
GRADM=(STICMR-FCMREF)*2.381
CONSTANT STOPM=0
CONSTANT STOP1=0
CONSTANT STOP2=0
CONSTANT STOP3=0
CONSTANT STOP4=0
CONSTANT STOPG=0
WVM=0.42*FOFF*NONLIN
 PROCEDURAL(FM=TMOT,STICMR,GRADM,FCMREF,WVM,FVMREF,WMOT)
 IF(((TMOT-FM)*WMOT).GT.0.0.AND.ABS(WMOT).LT.WVM)FM=(STICMR*...
 SIGN(1.0,WMOT))-(GRADM*WMOT)
 IF(((TMOT-FM)*WMOT).LT.0.0.AND.ABS(WMOT).LT.WVM)FM=...
 FCMREF*SIGN(1.0,WMOT)
 IF(WMOT.EQ.0.0)FM=STICMR*SIGN(1.0,(TMOT-FM))
 IF(ABS(TMOT).LE.STICMR.AND.WMOT.EQ.0.0)FM=TMOT
 IF(ABS(WMOT).GE.WVM)FM=(ABS(FVMREF*(WMOT-WVM))+FCMREF)*SIGN(1.0,WMOT)
IF(ABS(TMOT).LE.FCMREF.AND.ABS(WMOT).LE.WVM)FM=STOPM*WMOT
 END
ACTMOT=TMOT-FM
ACCMOT=ACTMOT/JMREF     $ " MOTOR ACCELERATION     "
      WMOT=INTEG(ACCMOT,ICWMOT)  $ " MOTOR VELOCITY "
      WMOTDG=WMOT*180/3.1416
      CONSTANT ICWMOT=0.0
      THEMOT=INTEG(WMOT,ICTHMO) $ " MOTOR ANGLE  (RADIANS)     "
      CONSTANT ICTHMO=0.0
" RELATIVE GEAR ANGLES FOR TORQUE GENERATION     "
      THETS1=DL1-((THET1)-THEMOT*N1)
      THETS2=DL1A+((THET1)-THEMOT*N1)
      THETS3=DL2-((THET2)-THET1*N2)
      THETS4=DL2A+((THET2)-THET1*N2)
      THET2A=THET2-((TOR2*STOFF)/KS1EFF)
      THETS5=DL3-((THET3)-THET2A*N3)
      THETS6=DL3A+((THET3)-THET2A*N3)
      THET3A=THET3-((TOR3*STOFF)/KS2EFF)
      THETS7=DL4-((THET4)-THET3A*N4)
      THETS8=DL4A+((THET4)-THET3A*N4)
      THET4A=THET4-((TOR4*STOFF)/KS3EFF)
      THETS9=DL5-((THETG)-THET4A*N5)
      THES10=DL5A+((THETG)-THET4A*N5)
```

```
      THES10=DL5A+((THETG)-THET4A*N5)
" GEAR MESH STIFFNESSES   "
CONSTANT ETA=0.95  $" GEAR EFFICIENCY  "
"   TORQUE CALCULATIONS    "
      PROCEDURAL(TOR1=THETS1,THETS2,K1EFF,ETA)
IF(THETS2.LT.0.0)TOR1=-K1EFF*ETA*THETS2
IF(THETS1.LT.0.0)TOR1=K1EFF*ETA*THETS1
      IF((THETS1.GE.0.0).AND.(THETS2.GE.0.0))TOR1=0.0
      END
CONSTANT GRAD1=0
CONSTANT WV1=0
 PROCEDURAL(F1=TOR1,STIC1R,GRAD1,FC1REF,WV1,FV1REF,W1)
 IF(((TOR1-F1)*W1).GT.0.0.AND.ABS(W1).LT.WV1)F1=(STIC1R*...
 SIGN(1.0,W1))-(GRAD1*W1)
 IF(((TOR1-F1)*W1).LT.0.0.AND.ABS(W1).LT.WV1)F1=...
 FC1REF*SIGN(1.0,W1)
 IF(W1.EQ.0.0)F1=STIC1R*SIGN(1.0,(TMOT-FM))
 IF(ABS(TOR1).LE.STIC1R.AND.W1.EQ.0.0)F1=STIC1R*SIGN(1.0,TMOT)
 IF(ABS(W1).GT.WV1)F1=(ABS(FV1REF*(W1-WV1))+FC1REF)*SIGN(1.0,W1)
IF(ABS(TOR1).LE.FC1REF.AND.ABS(W1).LE.WV1)F1=STOP1*W1
 END
      ACC1=(TOR1-F1)/J1REF
      W1=INTEG(ACC1,ICW1)
      THET1=INTEG(W1,ICTH1)
      CONSTANT ICW1=0.0
      CONSTANT ICTH1=0.0
      PROCEDURAL(TOR2=THETS3,THETS4,K2EFF,ETA)
IF(THETS4.LT.0.0)TOR2=-K2EFF*ETA*THETS4
 IF(THETS3.LT.0.0)TOR2=K2EFF*ETA*THETS3
      IF((THETS3.GE.0.0).AND.(THETS4.GE.0.0))TOR2=0.0
      END
CONSTANT GRAD2=0
CONSTANT WV2=0
 PROCEDURAL(F2=TOR2,STIC2R,GRAD2,FC2REF,WV2,FV2REF,W2)
 IF(((TOR2-F2)*W2).GT.0.0.AND.ABS(W2).LT.WV2)F2=(STIC2R*...
 SIGN(1.0,W2))-(GRAD2*W2)
 IF(((TOR2-F2)*W2).LT.0.0.AND.ABS(W2).LT.WV2)F2=...
 FC2REF*SIGN(1.0,W2)
 IF(W2.EQ.0.0)F2=STIC2R*SIGN(1.0,(TMOT-FM))
 IF(ABS(TOR2).LE.STIC2R.AND.W2.EQ.0.0)F2=STIC2R*SIGN(1.0,TMOT)
 IF(ABS(W2).GT.WV2)F2=(ABS(FV2REF*(W2-WV2))+FC2REF)*SIGN(1.0,W2)
IF(ABS(TOR2).LE.FC2REF.AND.ABS(W2).LE.WV2)F2=STOP2*W2
 END
      ACC2=(TOR2-F2)/J2REF
      W2=INTEG(ACC2,ICW2)
      THET2=INTEG(W2,ICTH2)
      CONSTANT ICW2=0.0
      CONSTANT ICTH2=0.0
      PROCEDURAL(TOR3=THETS5,THETS6,K3EFF,ETA)
IF(THETS6.LT.0.0)TOR3=-K3EFF*ETA*THETS6
IF(THETS5.LT.0.0)TOR3=K3EFF*ETA*THETS5
      IF((THETS5.GE.0.0).AND.(THETS6.GE.0.0))TOR3=0.0
      END
CONSTANT GRAD3=0
CONSTANT WV3=0
 PROCEDURAL(F3=TOR3,STIC3R,GRAD3,FC3REF,WV3,FV3REF,W3)
 IF(((TOR3-F3)*W3).GT.0.0.AND.ABS(W3).LT.WV3)F3=(STIC3R*...
 SIGN(1.0,W3))-(GRAD3*W3)
 IF(((TOR3-F3)*W3).LT.0.0.AND.ABS(W3).LT.WV3)F3=...
 FC3REF*SIGN(1.0,W3)
```

```
 FC3REF*SIGN(1.0,W3)
 IF(W3.EQ.0.0)F3=STIC3R*SIGN(1.0,(TMOT-FM))
 IF(ABS(TOR3).LE.STIC3R.AND.W3.EQ.0.0)F3=STIC3R*SIGN(1.0,TMOT)
 IF(ABS(W3).GT.WV3)F3=(ABS(FV3REF*(W3-WV3))+FC3REF)*SIGN(1.0,W3)
IF(ABS(TOR3).LE.FC3REF.AND.ABS(W3).LE.WV3)F3=STOP3*W3
 END
      ACC3=(TOR3-F3)/J3REF
      W3=INTEG(ACC3,ICW3)
      THET3=INTEG(W3,ICTH3)
      CONSTANT ICW3=0.0
      CONSTANT ICTH3=0.0

      PROCEDURAL(TOR4=THETS7,THETS8,K4EFF,ETA)
IF(THETS8.LT.0.0)TOR4=-K4EFF*ETA*THETS8
 IF(THETS7.LT.0.0)TOR4=K4EFF*ETA*THETS7
      IF((THETS7.GE.0.0).AND.(THETS8.GE.0.0))TOR4=0.0
      END
CONSTANT GRAD4=0
CONSTANT WV4=0
 PROCEDURAL(F4=TOR4,STIC4R,GRAD4,FC4REF,WV4,FV4REF,W4)
 IF(((TOR4-F4)*W4).GT.0.0.AND.ABS(W4).LT.WV4)F4=(STIC4R*...
 SIGN(1.0,W4))-(GRAD4*W4)
 IF(((TOR4-F4)*W4).LT.0.0.AND.ABS(W4).LT.WV4)F4=...
 FC4REF*SIGN(1.0,W4)
 IF(W4.EQ.0.0)F4=STIC4R*SIGN(1.0,(TMOT-FM))
 IF(ABS(TOR4).LE.STIC4R.AND.W4.EQ.0.0)F4=STIC4R*SIGN(1.0,TMOT)
 IF(ABS(W4).GT.WV4)F4=(ABS(FV4REF*(W4-WV4))+FC4REF)*SIGN(1.0,W4)
IF(ABS(TOR4).LE.FC4REF.AND.ABS(W4).LE.WV4)F4=STOP4*W4
 END
      ACC4=(TOR4-F4)/J4REF
      W4=INTEG(ACC4,ICW4)
      THET4=INTEG(W4,ICTH4)
      CONSTANT ICW4=0.0
      CONSTANT ICTH4=0.0

    " TOTAL REFERRED DEADSPACE IN TRAVERSE DRIVE   "


" GUN OUT OF BALANCE TORQUE"
CONSTANT OOB=1.0
TOB=RSW(ABS(TMOT).GT.STICMR,((1494.1*THETG)+208.62)*OOB,0.0)
TORKG=TORGUN+TOB
PROCEDURAL(TORGUN=THETS9,THES10,KG,ETA)
IF(THES10.LT.0.0)TORGUN=-KG*THES10*ETA
IF(THETS9.LT.0.0)TORGUN=KG*THETS9*ETA
IF((THETS9.GE.0.0).AND.(THES10.GE.0.0))TORGUN=0.0
END
CONSTANT GRADG=0
CONSTANT WVG=0
 PROCEDURAL(FG=TORKG,FSTG,GRADG,FCOUG,WVG,FVG,WGUN)
 IF(((TORKG-FG)*WGUN).GT.0.0.AND.ABS(WGUN).LT.WVG)FG=(FSTG*...
 SIGN(1.0,WGUN))-(GRADG*WGUN)
 IF(((TORKG-FG)*WGUN).LT.0.0.AND.ABS(WGUN).LT.WVG)FG=...
 FCOUG*SIGN(1.0,WGUN)
 IF(WGUN.EQ.0.0)FG=FSTG*SIGN(1.0,(TMOT-FM))
 IF(ABS(TORKG).LE.FSTG.AND.WGUN.EQ.0.0)FG=FSTG*SIGN(1.0,TMOT)
 IF(ABS(WGUN).GT.WVG)FG=(ABS(FVG*(WGUN-WVG))+FCOUG)*SIGN(1.0,WGUN)
IF(ABS(TORKG).LE.FCOUG.AND.ABS(WGUN).LE.WVG)FG=STOPG*WGUN
 END
      ACCGUN=(TORKG-FG)/JGUN
```

```
      ACCGUN=(TORKG-FG)/JGUN
      WGUN=INTEG(ACCGUN,ICWG)
      WGUNDG=WGUN*180/3.1416
      THETG=INTEG(WGUN,ICTHG)
      GUNDG=THETG*180/3.1416
      CONSTANT ICWG=0.0
      CONSTANT ICTHG=0.0
PERR1=(THEMOT*N1)-THET1
PERR2=(THEMOT*N1*N2)-THET2
PERR3=(THEMOT*N1*N2*N3)-THET3
PERR4=(THEMOT*N1*N2*N3*N4)-THET4
      PERRG=(THEMOT*N1*N2*N3*N4*N5)-THETG


" TERMINATION CONDITION    "
PROCEDURAL(FINISH=GUNDG)
IF(GUNDG.GE.20)FINISH=1
IF(GUNDG.LE.-7.5)FINISH=1
END
TERMT(FINISH.GE.1)
CONSTANT TF=3.0  $ " SECONDS  "
END
END
END
BOTTOM
```